Ternary Si-Metal-N Ceramics: Single-Source-Precursor Synthesis, Nanostructure and Properties Characterization

A dissertation approved by the Department of Materials and Earth Sciences

In fulfillment of the requirements for the degree of Doctor rerum naturalium (Dr.rer.nat.)

M. Sci. Cong Zhou

The City of Wuhu, Anhui Province, China

Matrikel-Nr. 1834660

TECHNISCHE UNIVERSITÄT DARMSTADT

Berichterstatter: Prof. Dr. Ralf Riedel

Mitberichterstatter: Prof. Dr. Zhaoju Yu

Fachbereich Material- und Geowissenschaften

Technischen Universität Darmstadt

Date of submission: 10. January.2017

Date of oral examination: 23. February.2017

Darmstadt 2017

D 17

Dedicated to My Parents

TABLE OF CONTENTS

List of Figures

List of Tables

ABSTRACT

Si-M-N (M=metal) ceramic nanocomposites are novel materials that combine the advantages of both ceramics and metals. Additionally, a variety of intriguing functional properties are observed in the metal-modified ceramics due to the formation of a second phase, which reveals promising applications in the fields of optics (*e.g.*, light-emitting diodes), semiconductors, catalysis and energy technology. Until now, most of the metal-modified nanocomposites are fabricated by using traditional powder techniques, but the grain sizes of the composites are limited to the micrometer range, and the dispersion of metal particles is not homogeneous. Polymer-derived ceramics route is widely considered as a promising approach in the synthesis of novel nanocomposites, where the nanocomposites are derived from the corresponding single-source precursors and exhibit improved structural and functional properties due to the unique nanostructures. This Ph.D. thesis is focused on the synthesis of ternary Si-M-N ceramics derived from single-source precursors with tailored compositions and structures, which were synthesized via the chemical modification of polysilazane with metallic compounds. The main objective of this research is to study the chemical modification of the precursors and nanostructures of Si-M-N ceramics and to gain a better understanding of the effect caused by the modification with different metallic compounds on the structures and properties of resultant ceramic nanocomposites.

In the present research, single-source precursors with varied compositions and structures were synthesized by chemical modification of perhydropolysilazane (PHPS) with transition-metal compounds. Si-Hf-N, Si-V-N(O) and Si-Fe-N(O) single-source precursors were synthesized by using TDMAH, $VO(acac)_2$ and $Fe(acac)_2$, respectively. Amorphous single-phase Si-M-N ceramics were prepared via the subsequent cross-linking and pyrolysis under an ammonia atmosphere. The syntheses of these preceramic polymers were investigated by means of spectroscopic techniques including FT-IR, Raman and solid MAS NMR spectroscopy, and the results indicated the formation of expected transition-metal-modified precursors. Then, the structural evolution during the polymer-to-ceramic conversion of the precursors was monitored with FT-IR measurements. The prepared materials were investigated with respect to their crystallization behaviors and phase compositions using spectroscopic techniques together with X-ray diffraction (XRD), elemental analysis (EA) and scanning/transmission electron microscopy (SEM/TEM). Annealing experiments on the Si-M-N ceramics were performed in a nitrogen atmosphere at temperatures ranging from 1100 to 1800 ℃, leading to the conversion of the amorphous materials into crystalline nanocomposites. It was found that α- and β-Si_3N_4 were obtained in the Si-M-N composites during the high-temperature treatment and built a matrix, while the transition-metals formed different crystallites such as metal nitrides (HfN, VN and Fe_2N), pure metal (α-Fe) and metal silicide (Fe_3Si) depending on the intrinsic characteristics of transition-metals and sintering temperatures, and these metal-containing crystallites homogeneously dispersed in the silicon nitride matrix. The high-temperature phase separation and crystallization behaviors of the Si-M-N ceramics were intensively investigated.

The focus was firstly placed on the synthesis of novel polymer-derived SiHfN ceramics. They were prepared via the pyrolysis of a single-source precursor which was synthesized by the chemical reaction between perhydropolysilazane (PHPS) and tetrakis(dimethylamido) hafnium(IV) (TDMAH). The hafnium-modified PHPS precursor convert upon heat treatment in an ammonia atmosphere at 1000 ℃ into an XRD amorphous single-phase $Si_1Hf_{0.056}N_{1.32}$ ceramic and remained amorphous even after annealing at 1400 ℃ in a nitrogen atmosphere. The PHPS-derived ceramic without modification showed a composition of $Si_1N_{0.71}$ at 1000 ℃ and started to crystallize at 1300 ℃. The electron microscopy investigation exhibited that the annealing of the highly homogeneous single-phase SiHfN ceramic induced a local enrichment (clustering) of hafnium, leading to amorphous HfN/SiN_x nanocomposites. The modification with TDMAH not only increases the nitrogen content of the ceramic materials but also efficiently improves the high-temperature stability of the Si_3N_4 against crystallization greatly. Annealing in nitrogen at 1600 ℃ resulted in a phase separation, and crystallized HfN/Si_3N_4 nanocomposite was obtained. The α- to β-Si_3N_4 phase transformation was greatly inhibited in the SiHfN ceramics at 1800 ℃. Extensive STEM characterizations of the polycrystalline nanocomposites indicated further substitutional and interstitial doping of hafnium in Si_3N_4.

An amorphous single-phase SiVN(O) ceramic was prepared via the ammonolysis of the corresponding single-source precursor, which was synthesized by the chemical modification of PHPS with vanadyl acetylacetonate ($VO(acac)_2$). The as-obtained SiVN(O) ceramic exhibited high-temperature resistance against crystallization up to 1400 ℃. Annealing at 1600 ℃ caused a phase separation and intensive crystallization. As a result, the nanocomposite composed of VN, α- and β-Si_3N_4 was obtained. Further investigation suggested that the introduction of $VO(acac)_2$ promoted the α- to β-Si_3N_4 phase transformation at 1600 ℃, and a VN/β-Si_3N_4 nanocomposite was obtained when the sample was annealed at 1600 ℃. Furthermore, mesoporous SiVN(O) ceramics with high specific surface area (SSA) were successfully prepared by using polystyrene (PS) as self-sacrificial templates via a one-pot synthesis. After cross-linking and pyrolysis in an ammonia atmosphere at 1000 ℃, a mesoporous SiVN(O) ceramic with a SSA of 506 m^2/g was produced. Both the specific surface area and pore size distribution of the mesoporous ceramics can be adjusted by changing the amount of PS templates in the feed. Moreover, the mesoporous SiVN(O) ceramics exhibited good structural stability up to 1400 ℃ (SSA maintained *ca.* 200 m^2/g), but a total collapse of the mesoporous structures was observed at 1600 ℃.

A SiFeN(O) precursor was synthesized by the reaction of PHPS with iron(II) acetylacetonate ($Fe(acac)_2$) via the formation of Si-O-Fe bonds. The pyrolysis of SiFeN(O) precursor in ammonia induced a phase separation with the formation of Fe_2N at 600 ℃, and then the Fe_2N decomposed into α-Fe by increasing the temperature to 1000 ℃. Crystalline Fe_3Si was obtained when the temperature was over 1200 ℃. The observations demonstrated that the modification with $Fe(acac)_2$ had a considerable influence on the phase separation and crystallization behaviors of the ceramics. Subsequently, a SiFeN(O)-based ceramic paper with in-situ generated hierarchical micro/nano-morphology was prepared by pyrolyzing a filter paper template that was modified with a SiFeN(O) precursor. After ammonolysis at 1000 ℃, the obtained SiFeN(O)-based ceramic paper decorated with crystalline α-Fe had the same morphology as that of the used paper template. Ultra-long silicon nitride

nanowires with great aspect ratios (~200 nm in diameter and several millimeters in length) were *in-situ* formed in a large quantity both on the surface and in the pores of the ceramic paper, when the ceramic paper was further annealed in nitrogen at temperatures from 1200 to 1400 ℃. The nanowires exhibited a round Fe_3Si tip at the end, indicating that the growth of one-dimensional nanostructures occurred via an iron-catalyzed VLS (vapor-liquid-solid) mechanism, and the length and yield of nanowires can be controlled by adjusting the experimental conditions, including temperatures and the addition of $Fe(acac)_2$. Therefore, the combination of the single-source precursor, catalyst-assisted pyrolysis and template method provides a convenient one-pot route for the fabrication of ceramic paper and one-dimensional structures with high yields.

In summary, the present Ph.D work proved that Si-M-N single-source precursors can be synthesized via the PDC route by modifying PHPS with different metallic compounds, and amorphous Si-M-N single-phase ceramics can be obtained via pyrolysis of the corresponding precursors. Polymer-derived ceramic nanocomposites composed of X/Si_3N_4 (X = metal, metal nitride or metal silicide) with a homogenous microstructure can be prepared by further annealing at higher temperatures. This thesis provides some new insights into the design and synthesis of metal-modified precursors and enables the production of Si-M-N ceramic nanocomposites via the PDC approach.

ZUSAMMENFASSUNG

Keramische Si-M-N (M = Metall) Nanokomposite sind eine neue Materialklasse, welche die positiven Eigenschaften von keramischen und metallischen Materialien kombinieren. Es wurden eine Reihe faszinierender funktioneller Eigenschaften in solchen Materialien entdeckt, die auf die Bildung einer zweiten Phase zurückzuführen sind. Diese Eigenschaften ermöglichen die potentielle Nutzung dieser Materialien in Bereichen der Optik-, Halbleiter-, Katalysator- und Energietechnologie. Bisher wurden die meisten metallmodifizierten Nanokomposite mit traditionellen Pulver-Sinterverfahren hergestellt, was zu Korngrößen im Mikrometerbereich führt und zu keiner homogenen Verteilung der Metallpartikel in der keramischen Matrix führt. Die Synthese von Keramiken durch polymerische Präkursoren (polymer derived ceramics, PDC) ist ein allgemein anerkanntes Verfahren für die Synthese neuer Materialien. Die Nanokomposite werden direkt aus Einkomponentpräkursoren hergestellt und besitzen dank deren besonderen Nanostruktur verbesserte strukturelle und funktionelle Eigenschaften. Diese Dissertation befasst sich überwiegend mit der Synthese ternärer keramischer Si-M-N Nanokomposite, die aus Einkomponentpräkursoren mit maßgeschnittener Zusammensetzung und Struktur abgeleitet sind. Die Präkursoren wurden durch chemische Modifikationen an Polysilazanen mit metallischen Verbindungen synthetisiert. Der Schwerpunkt dieser Arbeit liegt auf der Untersuchung der chemischen Modifikationen der Präkursoren und den damit einhergehenden Mikrostrukturen der keramischen Si-M-N Nanokomposite. Mit dem Ziel mehr Verständnis über die Einflüsse der Modifikationen mit unterschiedlichen metallischen Verbindungen auf die Strukturen und Eigenschaften der hergestellten keramischen Komposite zu erhalten.

In der vorliegenden Arbeit wurden Einkomponentenpräkursoren mit variierenden Zusammensetzungen und Strukturen durch chemische Modifikationsreaktionen zwischen Perhydropolysilazan (PHPS) und Übergangsmetallverbindungen hergestellt. Si-Hf-N, Si-V-N(O) und Si-Fe-N(O) Einkomponentenpräkursoren wurden jeweils mit TDMAH, $VO(acac)_2$ und $Fe(acac)_2$ synthetisiert. Amorphe einphasige Si-M-N Keramiken wurden durch Vernetzung und Pyrolyse unter Ammoniak Atmosphäre erhalten. Die Synthese der prekeramischen Polymere wurde mit Hilfe von spektroskopischen Techniken wie FT-IR, Raman und Festkörper MAS NMR untersucht. Die Ergebnisse deuten auf die Bildung gewünschter Übergangsmetall-modifizierten Präkursoren hin. Die strukturelle Entwicklung der Präkursoren in der Polymer-zu-Keramik Umwandlung wurde mit FT-IR Messungen überwacht. Die erhaltenen Si-M-N Keramiken wurden auf deren Kristallisationsverhalten und Phasenzusammensetzungen hin mit spektroskopischen Techniken, Röntgenbeugung (XRD), Elementaranalyse (EA) und Raster- und Transmissionselektronenmikroskopie (REM und TEM) untersucht. Temperversuche wurden bei den hergestellten Si-M-N Keramiken bei Temperaturen von 1100 °C bis 1800 °C in Stickstoff Atmosphäre durchgeführt, was zu einer Umwandlung der amorphen einphasigen Keramiken in kristalline Nanokomposite führte. Es wird gezeigt, dass α- und β-Si_3N_4 Phasen durch Hochtemperaturbehandlungen entstanden sind und sich als Matrix in den Nanokompsiten eingebettet haben. Die Übergangsmetalle bilden in Abhängigkeit von den intrinsischen Eigenschaften der Übergangsmetalle und

Behandlungstemperaturen verschiedene Kristallite wie Metallnitride (HfN, VN und Fe_2N), reines Metall (α-Fe) und Metallsilicide (Fe_3Si), die in der Siliziumnitridmatrix homogen verteilt sind. Die Hochtemperaturphasentrennung und das Kristallizationsverhalten der Si-M-N Keramiken wurden intensiv untersucht.

Der Schwerpunkt bildet die Untersuchung und Synthese der neuartigen polymerabgeleiteten SiHfN Keramiken, welche durch Pyrolyse der Einkomponentenpräkursoren entstanden. Die hierfür verwendeten Einkomponentenpräkursoren ergaben sich aus der chemischen Reaktion zwischen Perhydropolysilazan (PHPS) und Tetrakis(dimethylamido)hafnium(IV) (TDMAH). Die hafniummodifizierten PHPS-Präkursoren wurden bei 1000 °C in Ammoniak Atmosphäre pyrolysiert und zu einer amorphen einphasigen $Si_1Hf_{0.056}N_{1.32}$ Keramik verwandelt. Anschließend wurde Phasentrennung während des Temperns bei 1400 °C beobachtet, wobei ihre amorphe Struktur erhalten blieb. Polymerabgeleitete Keramiken aus reinem PHPS wiesen eine Zusammensetzung von $Si_1N_{0.71}$ bei 1000 °C auf, wobei deren Kristallisation bei 1300 °C begann. Die elektronenmikroskopische Untersuchung zeigt, dass sich während des Temperns von homogenen, einphasigen SiHfN lokale Anreicherung (Clustering) von Hafnium bildeten, welche dann zur weiteren Transformation in einen amorphen HfN/SiNx Nanokomposit führten. Die Modifikation mit TDMAH erhöht nicht nur den Stickstoff Anteil in den Materialien, sondern auch die Hochtemperaturstabilität von Si_3N_4 gegen die Kristallisation. Tempern von SiHfN in Stickstoff bei 1600 °C führte zur Phasentrennung und Bildung von kristallisierten HfN/Si_3N_4. Auch die Phasentransformation von α- Si_3N_4 zu β-Si_3N_4 ist in den SiHfN Keramiken bei 1800 °C stark unterdrückt. Umfangreiche RTEM Charakterisierungen der polykristallinen Nanokomposite deuten auf Substitutionsdotierung und interstitielle Dotierung vom Hafnium in Si_3N_4 hin.

Eine amorphe einphasige SiVN(O) Keramik wurde per Ammonolyse des entsprechenden Einkomponentenpräkursors, der durch chemische Modifikation von PHPS mit Vanadylacetylacetonat ($VO(acac)_2$) hergestellt wurde, synthetisiert. Die erhaltene SiVN(O) Keramik zeigte einen Widerstand gegen Kristallisation bis zu 1400 °C. Tempern bei 1600 °C führte zu einer Phasentrennung und intensiver Kristallisation. Als Folge davon, wurde ein Nanokomposit, das sich aus VN, α- und β-Si_3N_4 zusammensetzt, erhalten. Weitere Untersuchungen zeigten, dass die Modifikation mit $VO(acac)_2$ die Phasentransformation von α-Si_3N_4 zu β-Si_3N_4 bei 1600 °C verstärkt und VN/β-Si_3N_4 Nanokomposite aus SiVN(O) erhalten wurden. Des Weiteren wurden mesoporöse SiVN(O) Keramiken mit hoher spezifischer Oberfläche mit Polystyrol (PS) als Opfertemplat durch Eintopfreaktionen erfolgreich hergestellt. Nach der Vernetzung und Pyrolyse in Ammoniak Atmosphäre bei 1000 °C wurde eine mesoporöse SiVN(O) Keramik mit einer spezifischen Oberfläche von 506 m^2/g hergestellt. Sowohl die spezifische Oberfläche als auch die Porengrößenverteilung sind durch den Anteil der eingesetzten PS Schablone einstellbar. Außerdem zeigte die mesoporöse SiVN(O) Keramik gute strukturelle Stabilität bis 1400 °C (Die spezifische Oberfläche blieb bei ca. 200 m^2/g), allerdings wurde der Zusammenbruch der mesoporösen Strukturen bei 1600 °C beobachtet.

Ein SiFeN(O) Präkursor wurde durch die chemische Modifikation von PHPS mit Eisen(II)acetylacetonat ($Fe(acac)_2$) durch die Bildung von Si-O-Fe Bindungen synthetisiert. Durch Pyrolyse des SiFeN(O) Präkursors in Ammoniak wurde eine Phasentrennung mit der Bildung vom Fe_2N bei 600 °C induziert. Bei der Erhöhung der Temperatur auf 1000 °C zersetzte sich das Fe_2N zu α-Fe. Weiteres Erhöhen der Temperatur auf 1200 °C leitete die Bildung von kristallinen Fe_3Si ein. Diese Beobachtung zeigt, dass die Einführung von $Fe(acac)_2$ einen beträchtlichen Einfluss auf die Phasentrennung und das Kristallisationsverhalten der Keramik ausübt. Anschließend wurde ein SiFeN(O)-basiertes Keramikpapier mit in-situ generierter hierarchischer Mikro-/Nanomorphologie durch Pyrolyse einer mit einem SiFeN(O) Präkursor modifizierten Filterpapierschablone hergestellt. Nach einer Ammonolyse bei 1000 °C besitzte das SiFeN(O)-basierte Keramikpapier, das mit kristallinen α-Fe dekoriert wurde, dieselbe Morphologie wie die der Papierschablone. Ultra-lange Siliziumnitrid Nanofasern mit hohen Aspektverhältnis (~200 nm im Durchmesser und mehrere Millmeter in der Länge) wurden in einer großen Menge in-situ auf der Oberfläche und in den Poren des Keramikpapiers geformt, wenn das Keramikpapier in Stickstoff Atomsphäre von 1200 °C auf 1400 °C weiter geheizt wurde. Die Nanofasern haben runde Fe_3Si Spitzen an einem Ende, was darauf hinweist, dass das Wachstum der eindimensionalen Nanostruktur durch einen Eisen-katalysierten Dampf-Flüssigkeit-Feststoff Mechanismus herbeigeführt wurde. Die Länge und der Ertrag der Nanofasern sind durch die Einstellung der Versuchsparameter wie Temperatur und der Fe(acac)2 Menge kontrollierbar. Deswegen bietet sich eine Kombination von Einkomponentenpräkursoren, katalysatorunterstützte Pyrolyse und Templatmethode als eine passende Eintopf-Route für die Herstellung von Keramikpapieren und eindimensionalen Nanostrukturen mit hohen Erträgen an.

Zusammenfassend beweist die vorliegende Dissertation, dass Si-M-N Einkomponentenpräkursoren per chemische Modifikation von PHPS mit verschiedenen metallischen Verbindungen herstellbar sind und amorphe einphasige Si-M-N Keramiken durch deren Pyrolyseerhalten werden können. Außerdem sind Polymer abgeleitete keramische Nanokomposite, bestehend aus X/Si_3N_4 (X = Metall, Metallnitrid, Metallsilicid, usw.), mit einer homogenen Mikrostruktur durch weiteres Sintern bei hohen Temperaturen hergestellt. Diese Arbeit wirft neue Einblicke in das Design und die Synthese von metallmodifizierten Präkursoren und ermöglicht die Herstellung von keramischen Si-M-N Nanokompositen durch die PDC Route.

LIST OF ABBREVIATIONS

Abbreviation	Definition
ATR	Attenuated total reflectance
BET	Brunauer, Emmett and Teller
CP	Cross polarization
EA	Elemental analysis
EDS	Energy dispersive spectrometer
EDX	Energy dispersive X-ray
$Fe(acac)_2$	Iron(II) acetylacetonate
FT-IR	Fourier transform infrared
FWHM	Full width at half maximum
HAADF	High angle annular dark field
HP	High pressure
HT	High temperature
MAS	Magic angle spinning
NMR	Nuclear magnetic resonance
PDCs	Polymer-derived ceramics
PHPS	Perhydropolysilazane
RT	Room temperature
SAED	Selected area electron diffraction
SEM	Scanning electron microscope
SSA	Specific surface area
SSPs	Single-source precursors
TDMAH	Tetrakis(dimethylamido) hafnium(IV)
TEM	Transmission electron microscope
$VO(acac)_2$	Vanadium(IV)oxy acetylacetonate
XRD	X-ray diffraction

1. INTRODUCTION AND MOTIVATION

Ternary Si-M-N (M = metal) materials have attracted the attention of researchers in recent years, since they exhibit excellent stability against decomposition and crystallization as well as good mechanical and interesting electrical properties[1, 2]. Si-M-N ceramics such as SiTaN[3, 4], SiMoN[5], SiTiN[6, 7] and SiCrN[8] have been highly evaluated for their physical properties in terms of hardness and wear resistance, high-temperature stability and oxidation resistance[8, 9], and they are used as protective coatings against wear and as diffusion barriers in metallizations; moreover, effective work function values spanning 4.16 to 4.8 eV and high-k dielectrics are also observed for these materials[10], making them attractive candidates for next generation nano/micro electro mechanical systems (NEMS/MEMS).

However, Si-M-N single-phase ceramics and multiphase nanocomposites with an uniform distribution of elements is difficult to achieve, owing to the low diffusion coefficient of O, C, N and metals in SiC and Si_3N_4. This obstacle is difficult to overcome by traditional powder techniques, and many attempts have been made to produce Si-M-N ceramics with homogeneous distribution. CVD (chemical vapor deposition), ALD (atomic layer deposition) and reactive magnetron sputtering methods are reported to be applied in the fabrication of Si-M-N materials[3-5]; however, these methods are mostly used to prepare films and coatings but are not suitable for producing monoliths or components with complex structures. Therefore, Polymer-derived ceramics (PDCs) route exhibits its particular advantages in the fabrication of metal-modified single-phase ceramics and corresponding ceramic nanocomposites. PDCs have been studied and developed for decades, and substantial achievements have been made in understanding the nature of the approach as well as the relationship between the precursors and ceramics. Some PDCs have realized large-scale production, and many PDCs with high performance have been adopted in the aerospace industry, automobile industry and MEMS. PDCs display many excellent properties like high strength, excellent oxidation and corrosion resistance. PDCs exhibit some particular properties, which are difficult to be acquired by conventional approaches, such as the outstanding stability with respect to crystallization and decomposition, designable ability of preceramic polymers, easy processing and the existence of well-distributed chemical components.

The best advantages of PDCs are the easy processability and the designable ability of polymer molecules: the easy processability makes it a promising candidate for the fabrication of ceramic fibers, coatings and components with complex shapes or microscopic dimensions; while the molecular designability makes it easy to synthesize the preceramic precursor with tunable chemical compositions to create ceramics with different structures. Based on the molecular designability and abundant reactive functional groups, metal elements can be transferred to the preceramic polymer skeleton by the chemical reaction of Si-based precursors with organometallic compounds, and the metal elements can disperse in the precursors homogeneously at the molecular level. By following pyrolysis, amorphous single-phase ceramics can be produced. Ceramic nanocomposites with refined nanostructures can be easily obtained by annealing the sample at high temperature,

because the single-phase ceramics are thermodynamically unstable, while metal oxides, nitrides and silicides are relative stable at high temperature [11].

Transition metals and their derivatives (*e.g.*, oxides, nitrides and silicides) are materials with not only excellent physical and mechanical performance but also attractive functional properties because of their partially filled *d* sub-shell. Most of the transition metal nitrides have extremely high melting points (2000-4000 ℃) and they are frequently referred to as refractory nitrides; in addition, they have important commercial value, stemming from their extreme hardness. The transition metal nitrides have been increasingly used in the micro-electronic field such as integrated circuitry based on their electrical properties. Transition metals-modified PDCs have attracted researchers' attentions because of their excellent properties, and some interesting results have been published. Recently, the synthesis of hafnium alkoxide-modified polysiloxane have been reported[12, 13]: the obtained Si-Hf-C-O ceramics with nanocrystalline hafnia homogeneously dispersed in the matrix are found to possess better thermal stability with respect to decomposition at high temperature. In addition, the hafnium-modified polymer-derived SiCN(O) is also achieved via chemical modification of a polysilazane and of a cyclotrisilazane with hafnium(IV) n-butoxide[14, 15]; the hafnium compound reacts with the both precursors, and its influence on the microstructure evolution and crystallization behavior of the materials were fully studied. Dense monolithic SiC/HfC_xN_{1-x}-based ceramic nanocomposites are prepared via the single-source precursor, which is synthesized by the reaction of polycarbosilane and TDMAH, and the hafnium-modified ceramics show enhanced microwave absorption capability and potential application in electromagnetic interference [16]. Bulk nanocomposites with amorphous Si_3N_4 matrix homogeneously embedded with TiN crystallites have been achieved via the PDCs route, and they display a Vickers hardness as high as 25.1 GPa [17]. New hybrid materials were made by a reaction of polydimethylsiloxane and vanadium tert-amyloxide, and the hybrid is metastable and showed a strong phosphorescence at low temperature[18, 19]. A novel type of periodic mesoporous organosilica (PMO) embedded with vanadyl acetylacetonate has been synthesized, and it exhibits a remarkable catalyst for selective hydroxylation of benzene to phenol[20]. A variety of Si-based precursors have been modified with iron-compounds, and the resultant iron-containing ceramics exhibit interesting magnetic properties[21] and enhanced catalysis properties[22]; moreover, the iron could act as a catalyst and promote the generation of one-dimensional nanostructures[23].

All of the above mentioned results exhibit the intriguing properties and promising prospect of transition metal-modified PDCs. Depending on the transition metal, different ceramic phases can be formed. It is obvious that the constitution and nanostructures of the final ceramics are controlled by the design of metal-containing precursors, and these transition metals crystallites endow the materials novel properties.

In the present Ph.D work, different transition metals (hafnium, vanadium and iron) are introduced into perhydropolysilazane (PHPS) via chemical modification, with the purpose of synthesizing the metal-modified single-source precursors and the corresponding ceramic nanocomposites. In a study of Si-Hf-N ternary system, a novel oxygen-free metallic compound named tetrakis(dimethylamido) hafnium(IV) (TDMAH) is adopted.

Vanadyl acetylacetonate ($VO(acac)_2$) was used as the vanadium source for the synthesis of SiVN(O) precursor because it has suitable reactivity with PHPS, and vanadium was easy to be reduced under ammonia. Iron(II) acetylacetonate ($Fe(acac)_2$) was used to synthesize SiFeN(O) preceramic polymer. Hence, this thesis is mainly focused on the following topics.

● (1) The essential key aspect in the present thesis is to develop novel Si-M-N ceramic nanocomposites with refined structure via the PDC method, starting from the synthesis of Si-M-N single-source precursors by chemical modification of the commercially available precursor perhydropolysilazane with different metallic compounds including TDMAH, $VO(acac)_2$ and $Fe(acac)_2$.

● (2) Investigation of the chemical reaction between perhydropolysilazane and metallic compounds.

● (3) Investigation of the polymer-to-ceramic conversion of the single-source precursors and the as-obtained single-phase ceramics.

● (4) Processing of Si-M-N ceramic nanocomposites, investigating the phase separation, crystallization behavior and nanostructure of the nanocomposites and studying the influences on the structures of the final nanocomposites caused by the introduction with different transition metals.

2. LITERATURE REVIEW

2.1 Terms and definitions

2.1.1 Polymer-derived ceramics (PDCs)

The processing of polymer-derived ceramics (PDCs) is a method using preceramic polymers as precursors for the production of advanced ceramics. The PDC route is a relatively young technology for the manufacturing of ceramic materials, and it has brought significant technological breakthroughs for ceramic science and technology and offered a verity of advantages for the ceramic materials over conventional routes.

In the 1960s, a kind of Si-based nonoxide ceramic derived from a precursor was firstly reported by Ainger and Herbert[24], Chantrell and Popper[25]; this is usually considered to be the pioneer work in the field of PDCs. Then, Verbeek and colleagues[26] reported the fabrication of a series of Si_3N_4 or SiC fibers derived from pyrolyzing different precursors such as polysilazanes, polysiloxanes and polycarbosilanes. The successful preparation of SiC ceramics via the pyrolysis of polycarbosilanes precursors, which was published by Yajima[27], Fritz and Raabe[28], brought significant developments and initiated a new stage in the field of PDCs. Nowadays, the PDC route is a promising chemical process as attested by the massive research results reported and increasingly commercial development of different precursors to produce near-net shapes in a way not known from other techniques. A large number of material components with complex structures which are difficult to achieve by traditional methods, such as ceramic fibers, coatings, ceramic adhesives and ceramic matrix composites, are successfully prepared via the PDC route. The polymer precursors provide ceramics with a tailored chemical composition and a closely defined nanostructure. The chemical and physical properties of the preceramic precursors, as well as the derived ceramics, can be easily designed and tailored at the molecular level by using different reactions. Moreover, the active functional groups of polymer precursors enable a further modification of the precursors, and then new ceramic materials with high purity and homogeneous distribution of the elements at the nanoscale could be prepared. In addition, the precursors can be cross-linked to a three-dimensional unmeltable green body, which is the precondition for the fabrication of monolithic ceramic components with complicated structures. The polymer-to-ceramic transformation can be decreased to relatively low temperatures (< 1000 ℃), which is much lower than that of traditional powder sintering methods (1700 - 2000 ℃); therefore, the PDC method has lower energy consumption.

The properties of PDCs strongly depend on the chemical composition and polymer structures. Appropriate chemical modification and optimal processing routes also play important roles on the final structures of the ceramics, and then the performance and functional properties of the ceramics. The covalent bonds in the PDCs such as Si-C, Si-N and Si-C-N bonds endow excellent chemical, physical and mechanical properties, and PDCs usually exhibit outstanding stability in terms of crystallization, phase separation, creep and oxidation at high temperatures and in harsh environments. Another advantage presented by PDCs is that they can be used to

manufacture ternary systems such as SiCN and SiOC as well as the quaternary systems such as SiBCN, SiAlCN, SiBCO and SiCNO ceramics. This is because carbon and nitrogen cannot dissolve in Si_3N_4 and SiC, respectively, (similarly, carbon and oxygen cannot dissolve in SiO_2 and SiC), while boron and metal have low diffusion coefficients in SiC and Si_3N_4, and even the blend of nano-powders cannot achieve the ideal result due to the aggregation of nano-particles. Therefore, these ternary and quaternary ceramics can only be achieved using PDC route. Hitherto, countless polymer precursors and derived ceramics have been synthesized and studied in detail. There are many kinds of classification methods for these preceramics according to different standards such as constitutes and functions, and usually, they are classified on the basis of the element linked to silicon in the backbone of the polymer molecular; the main types are shown in Figure 2-1.

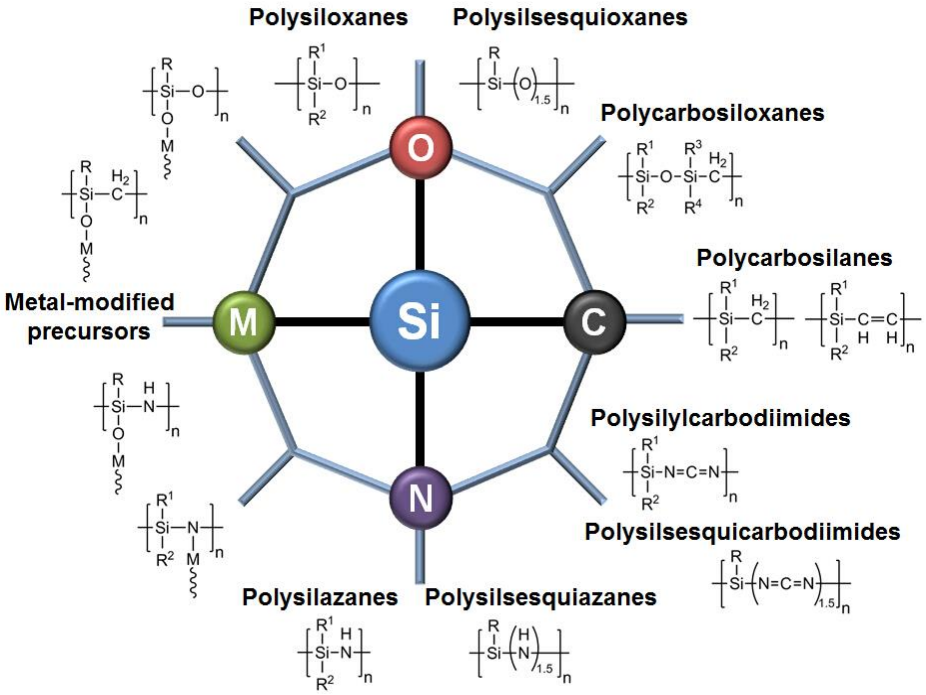

Figure 2-1. Main types of Si-based precursors for PDCs (M=metals).

A large amount of materials with excellent properties that are made from PDCs are already derived from the numerous Si-based precursors mentioned above. For instance, polymer-derived SiCN ceramics exhibited creep and oxidation resistance in the high temperature range from 1000 to 1500 ℃[29]; SiBCN ceramics show extremely high temperature stability with respect to decomposition, even up to 2000 - 2200 ℃ in an inert atmosphere[30]; the silicon oxycarbide (SiOC) ceramic synthesized at 1400 ℃ exhibits uniquely high piezoresistivity, leading to strain sensitivities (k factors) of ~145[31, 32]. It can be expected that, in the near future, PDCs will have much wider prospect and promising application in the field of structural components for high-temperature, functional materials, nano/micro electro mechanical systems (NEMS/ MEMS), energy and biomedical science.

2.1.2 Polymer-derived ceramic nanocomposites (PDC-NCs)

Nanocomposites are one type of material that consists of at least two Gibbsian phases with different properties, and one of them is at the nano-scale. They exhibit a homogeneous structure on macro-scope, but they have a heterogeneous microstructure and possess improved properties with respect to their components. The concept of nanocomposite was firstly proposed by Roy and Komarneni[33], and then it obtained considerable development and achievement due to the contribution of H. Gleiter on nanocrystalline materials[34]. A large amount of nanocomposite materials have been produced and intensively studied in last decades because of the remarkable improvement in their properties by reducing the size of the components towards the nanoscale, and the materials with anticipated-and even exceptional-properties can be obtained via the design and synthesis of nanocomposite materials. Based on the micro/nano-structure, nanocomposite materials can be classified with connectivity, which is a classic concept proposed by Newnham[35]. The connectivity within a composite material is the critical factor affecting the properties of multiphase materials; by controlling the connectivity present in the materials, the properties can change in several orders of magnitude.

By combining the PDCs and nanocomposites, a new class of ceramic nanocomposites named polymer-derived ceramic nanocomposites (PDC-NCs) has been suggested and received increased attention in recent years. Similar to PDC materials, PDC-NCs can also be produced via polymer-to-ceramic transformation of suitable polymeric precursors, resulting in amorphous single-phase ceramics by preliminary pyrolysis at relatively low temperature; after being phase separated, binary or multiphase ceramic nanocomposites could be obtained by subsequent heat-treatment at higher temperatures. The internal nanostructures endow PDC-NCs that are more interesting and exhibit excellent properties compared to conventional ceramics that enable them to be promising candidates as structural and functional materials. Meanwhile, one of the most significant advancements of the precursor method is the design ability of the polymer molecules, where the chemical and physical properties of the PDC-NCs can be controlled and adjusted as required by the modification of the preceramic polymers.

In general, the single-source precursors for PDC-NCs materials can be synthesized by the chemical modification of Si-based preceramic polymers with inorganic/organic compounds, such as metal alkoxides, metal amido complexes as well as boron-containing compounds. In another way, PDC-NCs can also be prepared via an active filler controlled pyrolysis (AFCOP) process by blending the precursors with active fillers (*i.e.*, Metallic: B, Ti, Cr, V or intermetallic: $MoSi_2$, $CrSi_2$), and then a near-net-shape monolith with low porosity can be prepared via the pyrolytic conversion. PDCs modified with metals are an important way for the preparation of PDC-NCs with novel functional properties. This has been extensively investigated in recent years, and many nanocomposite materials with improved thermomechanical and intriguing functional properties have been obtained.

2.1.3 Polymer-derived ceramics (PDCs) modified with metals

Ceramics and metals are two kinds of the oldest materials with very different natural properties, performance and applications. For a long time, numerous ways have been tried to mix these two materials together in the hope of preparing a novel ceramic-metal composite material in order to combine the properties of two. The PDC route is a novel technology that produces ceramics by thermolysis of polymer precursors, and it offers a new perspective and method for the manufacture of ceramic-metal composites. In this system, a ceramic matrix can be obtained from the Si-based polymer during pyrolysis, and metallic particles or phases structured on a nanoscale can be achieved due to the reductive conditions and noble character. Due to the designed ceramic matrix disturbed within the homogeneous metallic nanophase, intriguing functional properties were observed in the metal-modified PDCs, which reveal great potential and exhibit promising applications in the fields of optics (light-emitting diodes), semiconductors, catalysis and energy technology. Based on published studies, the pathway for preparation of metal-modified PDCs can be roughly classified into three types.

- (a) Precursors are simply physically blended with metal, metal oxides, metal nitrides, metal carbides or metal silicides, which are chemically inert to the raw precursors.

- (b) Metal-containing organic precursors are synthesized from original metallopolymers.

- (c) The existing precursors are chemically modified with metallic organic compounds.

In route (a), metal (or metal oxide, nitrides, silicides) are physically mixed with polymer precursors without forming any chemical bonding; here, metal-contained PDCs are produced by the subsequent cross-linking and ceramization. However, the inorganic metallic compounds are hardly uniformly dispersed in the ceramic matrix, and the particles (or metallic phase) are difficult to reach the nano-size due to the agglomeration, even when metallic nano-particles are used; consequently, the properties and performance are restricted. In route (b), the metal atoms are chemically bonded to the monomer units from the beginning, and the desired nanoparticles can be designed in the precursors and subsequently obtained after the pyrolysis. Nevertheless, the synthesis of metallopolymers required complex steps and high cost, which limits the development of this approach.

Compared with the former two, route (c) is a versatile and economic approach, in which the metal atoms would transfer from the organic metallic complex to the polymer precursor chain via chemical reactions, giving rise to the so-called metal-modified SSP, then metal-enhanced PDCs are yielded by pyrolysis. This precursor modification approach is considered advantageous, owing to the homogeneous distribution of the metal at an atomic level, its ease of structural design, wide applicability, employment of commercially available precursors and that the obtained ceramics exhibit outstanding performance. Therefore, route (c) has gradually become the focus in recent studies, and many achievements have been made.

2.2 Silicon nitride

Silicon nitride (Si_3N_4) is one of the major structural ceramics with several properties, such as high flexural strength, good fracture resistance, great creep resistance and ultrahigh hardness. Originally, studies focus primarily to the challenge to manufacture a suitable material for gas turbine engines which can serve as structural components at high temperature. The Si_3N_4 ceramic engine programs had only partial success, but they led to a better understanding of Si_3N_4 and of its processing and properties. To this day, many advanced and versatile properties of Si_3N_4 have been discovered, and numerous research have been reported: Si_3N_4 with different structures and morphologies such as films, membranes, nanowires and porous ceramics have been fabricated; also, Si_3N_4 was also developed to be applied in the fields of battery, catalysis, gas absorption and filtration, and these explorations have achieved good results. Based on the previous studies, it can be suggested that Si_3N_4 is an advanced material and has huge potential in the future.

2.2.1 Development history of silicon nitride

As one of the oldest chemical materials, the existence of Si_3N_4 can be traced back to the prehistory of the earth[36]. Additionally, evidence for the natural existence of Si_3N_4 in the galaxy was also discovered[37, 38]. As a versatile structural material, Si_3N_4 exhibits outstanding chemical, physical and mechanical properties. The first research concerning a synthetic S_3N_4 was reported by Deville and Wöhler in 1859[39]; later, the production of Si_3N_4 by the carbothermal reduction of SiO_2 under nitrogen was published in a Germen patent in 1896[40]. Simultaneously, the studies on the chemical formula and atomic structure of Si_3N_4 was carried out, and the silicon and nitrogen of stoichiometry close to 3 : 4 was reviewed by Weiss and Engelhardt[41] and by Wöhler[42], respectively. Since the 1950s, Si_3N_4 was accepted as a refractory material and began to be applied as a bonding phase for SiC and oxide refractories, crucibles for molten metals, rocket nozzles and thermocouple tubes that worked over 1371 ℃[43]. Because of the excellent high-temperature properties and resistance to thermal shock, the further development of Si_3N_4 ceramics was promoted and resulted in the successful fabrication of a wide range of commercial Si_3N_4 components for internal combustion engines[44]. Thereafter, intensive works were focused on the applications of Si_3N_4 at temperatures over 1371 ℃ as atomic energy jets and rockets as well as the manufacture of famous reaction bonded silicon nitride (RBSN), which was formed by nitriding silicon powder compacts in the temperature range 1100 - 1450 ℃.

The high strength and hardness of Si_3N_4 are the intrinsic properties that stem from the high-energy covalent chemical bonds, which provided the material excellent physical and mechanical performances; on the contrary, they were disadvantages in sintering processes. As is well-known, the self-diffusivity in Si_3N_4 is quite low, and atomic species become sufficiently mobile for densification at ultrahigh temperatures over 1850 ℃, where the Si_3N_4 begins to decompose. A significant breakthrough was achieved in 1961, where fully dense Si_3N_4 ceramics with improved strength were obtained by hot-pressing (HPSN, for short) with the help of sintering additives,

such as Mg_3N_2, MgO and Al_2O_3[45, 46]. Later, with the improvements of powder manufacture and ceramic forming techniques, a series of silicon nitride ceramics were developed, such as sintered silicon nitride (SSN), hot isostatically pressed silicon nitride (HIPSN) and the well-known solid solution SiAlONs (Sialon).

2.2.2 Structures and properties of silicon nitride

2.2.2.1 α-silicon nitride and β-silicon nitride

With the help of detailed X-ray diffractometry examinations, two major crystallographic modifications of silicon nitride were discovered, they were α- and β-phases, and both appeared to be hexagonal with the same chemical compositions (have 3:4 stoichiometry) and similar measured densities (approximately 3.2 g cm^{-3}). The c-axis dimension of the unit cell of the α-Si_3N_4 was approximately twice that of the β-Si_3N_4. As shown in Figure 2-2, the crystal structure is based on the phenacite (Be_2SiO_4) type, in which the O atoms are replaced by N and the Be atoms by Si. Each Si atom is at the center of a tetrahedron, while the nitrogen is in trigonal and approximately planar coordination by three silicon atoms, to link three SiN_4 trtrahedra. The unit cell of β-Si_3N_4 is consisted of Si_6N_8, and was assigned to the space group $P6_3/m$ by Hardie and Jack[47]. The structure of α-Si_3N_4 was later determined to be closely related to that of β-Si_3N_4; it had a unit cell composition of $Si_{12}N_{16}$ and was assigned to the space group $P3_1c$.

Usually, it is considered that β-Si_3N_4 is the steady phase at elevated temperatures, and α-Si_3N_4 can be converted to β-Si_3N_4 with prolonged annealing at high temperatures. This transformation contains the breakage and reformation of Si-N bonds in each unit cell, with a change in one nitrogen position and a small displacement of neighboring atoms. Some studies indicated that the α- to β-Si_3N_4 transformation is impurity controlled, such as oxygen[48]; they play an important role in this process and lead to the formation of a liquid phase through the reconstructive transformation. However, the reverse transformation from β- to α-Si_3N_4 has never been observed to date. With the protection of inert atmosphere, silicon nitride can keep stable to at least 1400 ℃. By further increasing the temperatures, Si_3N_4 does not melt but dissociates into silicon and nitrogen.

$$Si_3N_4\ (s) \rightarrow 3Si\ (g,l) + 2N_2\ (g)$$

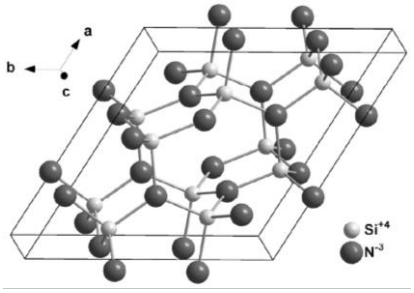

Figure 2-2. Schematic crystal structures of ambient-pressure hexagonal β-Si_3N_4 (space group $P6_3/m$, No. 176) with all Si-atoms in tetrahedral (4-fold) coordinations.

2.2.2.2 γ-silicon nitride with spinel structure

In 1999, Zerr and Riedel reported the synthesis of a third polymorph of silicon nitride with a cubic spinel structure[49]. This new phase was termed as γ-Si_3N_4 (or c -Si_3N_4), which was prepared at pressures above 15 GPa and temperatures exceeding 2000 K by utilizing the technique of laser heating in a diamond cell (LH-DAC). This γ-Si_3N_4 can persist metastably in air at ambient pressure to at least 700 K, and the first-principle calculations suggested that the bulk and shear c_{44} moduli of γ-Si_3N_4 could be as high as 300 GPa and 340 GPa, respectively. These results were comparable to those of the hardest known oxide, stishovite (a high-pressure phase of SiO_2)[50], and much higher than those of α- and β-Si_3N_4, making γ-Si_3N_4 become the third hardest material after diamond and cubic BN. A bulk modulus of B_0 = 290(5) GPa and shear modulus of $G_0 \geq$ 148(16) GPa were obtained by experiment measurement later[51], and they were both higher than those of α- and β-Si_3N_4 [52, 53]. In the unit cell shown in Figure 2-3, one third of the Si atoms are tetrahedrally coordinated to nitrogen and two thirds of the Si atoms are octahedrally coordinated to nitrogen, which are firstly observed in the nitride spinel. The high coordination results in a high density, with a 25% increase, over 4 g cm^{-3}.

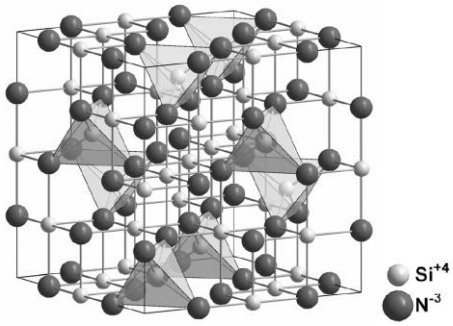

Figure 2-3. Schematic crystal structures of high-pressure cubic spinel γ-Si_3N_4 (space group *Fd* 3*m* , No. 227) with Si-atoms in both octahedral (light-grey spheres) and tetrahedral (grey tetrahedrons) coordinations.

The high-pressure and high-temperature conditions are essential for the synthesis of γ-Si_3N_4, and three approaches have been developed: (i) the first method was carried out in the LH-DAC devices[49, 54], but the yield was limited. Some other approaches were developed in order to efficiently synthesize γ-Si_3N_4 with large scale; (ii) Schwarz et al.[55] reported that γ-Si_3N_4 with dimensions up to 2 mm × 3.5 mm (mass=6.4 mg) was prepared by means of multi-anvil presses; (iii) cubic Si_3N_4 was also obtained by a shock wave synthesis[56, 57], and powdered γ-Si_3N_4 can be fabricated by a shock wave (above 20 GPa) carried on the mixture of α- or β-Si_3N_4 and copper powders catalyst[58, 59]. γ-Si_3N_4 was reported to show particular optical performance[60]. The mainly direct electronic band gaps with values could span the whole visible wavelength region, and the measured electronic band gap value and the calculated exciton binding energy value of γ-Si_3N_4 were 4.8±0.2 eV and 333 meV, respectively[61], indicating that the spinel silicon nitrides and their solid solutions were prospective candidates for optoelectronic devices such as lighting applications with chemical and mechanical stabilities.

2.2.3 Properties and applications of silicon nitride

Si_3N_4 received a lot of attention and exhibited versatile applications in many different fields. In the 1950s, Si_3N_4 became commercially available for the first time and was developed as a refractory bonding phase[62]. Nowadays, nitride-bonded SiC components have become one of the most important applications for Si_3N_4, and the annual output of Si_3N_4 powder was estimated to be between 300-350 tonnes. Reaction-bonded silicon nitride (RBSN) is one of the classic and representative applications. By the nitridation reaction of loosely packed silicon powders, a monolithic Si_3N_4 replica of the original shape with considerable strength was obtained[63]. Subsequently, RBSN was selected as a major material for service in the hottest zones of a ceramic gas-turbine engine. The porosity of as-obtained RBSN was 25-35%, but the strength could still be as high as 200-300 MPa, combined with the high creep resistance, high thermal shock resistance as well as the low cost of starting materials. All the mentioned advantages made the RBSN ceramics an attractive candidate for the thermocouple sheaths and crucibles[43]. The main drawbacks of RBSN are the difficulties of controllable microstructure and the high energy cost due to the slow reaction-bonding process at high temperature[64].

Nowadays, due to the more excellent wear resistance, higher modulus, lower friction and lower density with respect to metal materials, dense silicon nitride ceramic materials have been exploited for turbocharger rotors, turbine blades and in various wear parts for engines. Because the friction and rolling contact fatigue rates of Si_3N_4 are low[65, 66], coupled with high wear resistance, high stiffness and low density, Si_3N_4 bearings can serve much longer than conventional higher-density steel and hard-metal bearings. Because of the low lattice mobility of silicon and nitrogen as well as the high temperature decomposition of Si_3N_4, dense material was difficult to achieve with increasing temperature and resulted in microstructural coarsening[67]. Hot pressing and hot isostatic pressing are the common ways to produce dense ceramics by pressure-assisted sintering, and Si_3N_4 made in these approaches gains improvements in density and strength. Usually, oxides and nitrides sintering additives such as Y_2O_3, Al_2O_3, MgO and Mg_3N_2 were introduced into Si_3N_4 in order to prepare dense materials, and MgO was considered as the most effective one [45].

Thin amorphous silicon nitride films are regarded as one of the most important manufacturing accomplishments, because of its wide applications in the semiconductor device field[68, 69]. Amorphous Si_3N_4 films exhibited a variety of outstanding properties, such as high electrical resistivity (10^{12} Ω·m), hardness, chemical inertness and low permeability toward sodium, oxygen and hydrogen[70, 71]. Amorphous Si_3N_4 films with thickness of 100-200 nm were widely employed in the silicon-based integrated circuits, as a substitute or supplement for SiO_2 films, and Si_3N_4 films made it possible for the fabrication of integrated circuits components with controlled doped layers. Later, amorphous Si_3N_4 films are further developed as a passivation layer to alkali or moisture diffusion, a masking layer to prevent oxidation, and so on[69]. After years of intensive researches, Si_3N_4 ceramic films were successfully prepared with the support of chemical vapor deposition (CVD) technique [70]. By adopting advanced techniques such as plasma enhancement CVD (PECVD) and low pressure CVD (LPCVD)[72-74], large-

scale production of Si_3N_4 films can be easily prepared on silicon and other substrates at a relatively low temperature and in a high-speed.

In recent years, more and more attention has been concentrated on the nonlinear optics and electronic performance of Si_3N_4. The silicon nitride platform exhibits great competence and potential in nonlinear optics applications owing to their low linear loss, relatively large nonlinearities compared to those of typical fibers and their negligible nonlinear loss at telecommunication wavelengths. The first nonlinear optical study of SiN waveguides was reported by Ikeda *et al.*[75, 76]. Later, a sizeable second-order nonlinearity at optical wavelengths was reported to be prepared in a Si waveguide with a stressing silicon nitride overlayer[77]. Moreover, stoichiometric silicon nitride resonators have been reported to exhibit considerable quality factor (Q) exceeding one million, which is the key feature for a good resonator, owing to its intrinsic high tensile stress. But the insulating nature of Si_3N_4 has blocked development. Electrical integration is usually composed of capacitive coupled with conducting resonators; therefore, a massive effort has been made to metallize Si_3N_4 resonators by deposition of metals such as chromium[78], aluminum[79] and gold[80], and the results indicated that the electrical properties were significantly enhanced, but the quality factor was degraded dramatically. Other studies put their attention on the fabrication of Si_3N_4-graphene/carbon nanotube (CNT) hybrid heterostructure materials[81, 82], in which the excellent electrical and thermal properties of graphene/CNT as well as the mechanical capacity of Si_3N_4 are integrated together [83, 84]. At last, based on the high strength and fracture resistance of Si_3N_4 in extreme conditions, combined with its biocompatibility and visibility on plain radiographs as a partially radiolucent material[85, 86], Si_3N_4 was expected to show its capability in the biomedical field. It has been employed in spinal fusion implants and has been developed for bearing components of prosthetic hip and knee joints. Cervical spacers and spinal fusion devices made of Si_3N_4 composites have already come into use and achieved good short-term clinical results[87]; surgical screws and plates made of Si_3N_4 are also being tested[88].

In conclusion, silicon nitride is an important material with diverse properties that can be applied to many aspects. With further research on the chemistry and microstructures of silicon nitride materials, a deeper understanding of the relationship between the structures and properties can be established, and then this traditional ceramic material can regenerate and make a greater contribution.

2.2.4 Synthesis of silicon nitride

With the rapid development of materials, silicon nitride with high purity was urgently demanded because the significant influence of impurity for the high temperature properties of sintered Si_3N_4 was recognized. Oxygen is one of the most critical factors that affects the performances of Si_3N_4. Oxygen can exist in each particle as either internal oxygen or as a nanometer surface layer of SiO_2/Si_2ON_2, and this phenomenon becomes more apparent on the nanopowder with high surface area, resulting in Si_3N_4 with a much higher oxygen content and a greater proportion of surface oxygen. Carbon is another important factor in the Si_3N_4 materials. Carbon can be

present as amorphous carbon or graphite-like carbon and reacts with Si_3N_4 to form SiC at high temperature via a carbothermal reaction. Except for the RBSN and silicon nitride films discussed above, quite a large amount of silicon nitride have been produced in the form of powders every year. In the next section, the common methods of manufacturing silicon nitride will be introduced.

2.2.4.1 Conventional routes

The carbothermal reduction of SiO_2 powder under nitrogen is considered to be the earliest route for Si_3N_4 production, and now it is the most cost-effective industrial procedure for the fabrication of high purity α-Si_3N_4 powder because of the simple technology process and low-cost of, non-toxic and environmentally safe raw materials [89, 90]. The reactants are usually required to be processed into fine powders in order to obtain a high surface area for an increased reaction rate. The temperature of reaction should be controlled between 1450 and 1500 ℃ strictly, because the reaction kinetic is extremely slow below 1450 ℃. While thermodynamically stable, SiC will be the main product when the temperature is over 1500 ℃. In addition to temperature control, the partial pressure of oxygen and CO played important roles in the carbothermal reduction. If the oxygen partial pressure is too high, carbon reactant will react with oxygen rather than SiO_2 to form CO, while the high partial pressure of CO will suppress the reduction reaction[90]. At last, products are annealed in air at 600-850 ℃ to remove the residual carbon.

$$3\ SiO_2 + 6\ C + 2\ N_2 = \alpha\text{-}Si_3N_4 + 6\ CO\ (g) \quad (\text{at } 1450\text{-}1500\ ℃)$$

The synthesis method of Si_3N_4 powder via the nitridation of silicon powder was achieved in the 1960s, and it was the first large-scale method for the preparation of Si_3N_4 powder[91]. The direct nitridation reaction is exothermic, while silicon melts at 1414 ℃; hence, temperature control becomes the key factor in this approach. Higher temperature will cause the fast melt of silicon particles, and then the liquid silicon will fuse together into larger globules instead of wetting the partial coating of silicon nitride, resulting in a decrease of the effective surface area for the direct nitridation reaction[63]. By adopting an appropriate catalyst such as iron, the kinetics of the direct nitridation reaction can be improved [92].

$$3\ Si + 2\ N_2 = \alpha\text{-}Si_3N_4 \quad (\text{at } 1300\text{-}1400\ ℃)$$

Silicon diimide could decompose by heat treatment and initially lead to the production of amorphous Si_3N_4, which can be further converted to an α-Si_3N_4 crystal by sintering at 1400-1500 ℃ under a nitrogen atmosphere[93, 94]. Because amorphous Si_3N_4 with high purity can be obtained, this synthesis route has become the second most important way for commercial Si_3N_4 production. In this approach, the critical factor is the synthesis of the starting diimide reactant, which is synthesized by the reaction between $SiCl_4$ and ammonia at approximately 0 ℃. Subsequently, by heat-treatment at 1000 ℃ in a N_2 atmosphere, $Si(NH)_2$ can decompose into amorphous Si_3N_4.

$$SiCl_4\ (l) + 6\ NH_3 \rightarrow Si(NH)_2\ (s) + 4\ NH_4Cl\ (s) \quad (\text{at } 0\ ℃)$$

$$3\ Si(NH)_2 \rightarrow (amorphous)\ Si_3N_4 + N_2\ (g) + 3\ H_2\ (g) \quad (at\ 1000\ ℃)$$

By means of the reactions of vapor phase raw chemical materials, Si_3N_4 powders in a very pure state can be obtained with homogeneous size at the nano scale. Cannon *et al.* reported the successful preparation of nanosized Si_3N_4 powders by using CO_2 laser and plasma energized reactions of silane and ammonia. The sizes of the Si_3N_4 nanoparticles are typically in the range from 10 to 25 nm. Subsequently, equiaxed α-Si_3N_4 can be produced by further sintering[95, 96].

$$3\ SiH_4\ (g) + 4\ NH_3\ (g) \rightarrow (amorphous)\ Si_3N_4 + 12\ H_2\ (g)$$

2.2.4.2 Polymer-derived ceramics (PDCs) route

Polymer-derived ceramics (PDCs) processing is a kind of method using preceramic polymers as precursors for the production of silicon-based advanced ceramics. As discussed in section 2.1.1, the PDC route is a relatively young technology for the manufacturing of ceramic materials; it brings significant breakthroughs for the ceramic science and technology and offers a variety of advantages for ceramic materials over conventional routes.

Polysilazane is an important precursor for the fabrication of SiCN or Si_3N_4 ceramics. They are usually inexpensive, and a great variety of derivatives are commercially available. Polysilazanes are a kind of organic Si-based polymer in the general formula $[SiR_1R_2\text{-}N]_n$. The synthesis and characterization of polysilazanes can be traced back to 1885[97], then some more related reports garnered attention 60 years later[98]. Polysilazane precursors are mostly synthesized by ammonolysis reactions of chlorosilanes with ammonia or by aminolysis with different primary amines[99]. This synthesis route was firstly reported by Krüger and Rochow in 1964[100], followed with the successful production of small diameter ceramic fibers derived from polymeric carbosilazanes by Verbeek[101]. These series of pioneering work opens the way and lays the foundation for the synthesis and application of high-performance polysilazane precursors. Nowadays, extensive activities have been devoted to the preparation and optimization of high-molecular-weight polysilazanes, and many different synthesis routes for polysilazanes have been discovered and reported. The most classical and common methods among them are ammonolysis, aminolysis[102, 103], hydrazinolysis[104], dehydrogenation coupling[105] and ring-opening polymerization[106, 107]. Due to the proper reactivity of chlorosilanes, the low cost of ammonia (amine) and the ease of industrialization, ammonolysis and aminolysis have become the major approaches for producing polysilazanes. The basic synthesis reaction equations of polysilazanes is shown in Figure 2-4, N-H reacts with Si-Cl and forms a Si-N bond. Further condensation may occur between two N-H groups[108], and the Si-H group assigned to silanes could further react with N-H groups[109] to enhance the degree of cross-linking and molecular weight.

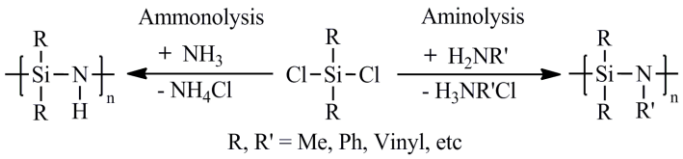

Figure 2-4. Brief synthesis routes to polysilazanes via ammonolysis and aminolysis.

Presently, various polysilazanes with tailored structure and constituents are synthesized by ammonolysis of the mixture of different chlorosilanes, which is also known as co-ammonolysis. Linear and branched polysilazanes can be easily produced by using monochlorosilane (as terminator), dichlorosilane (as chain extender) and trichlorosilane (as branching agent), and functional groups such as C=C, C≡C and phenyl can also be simply introduced (see Figure 2-5).

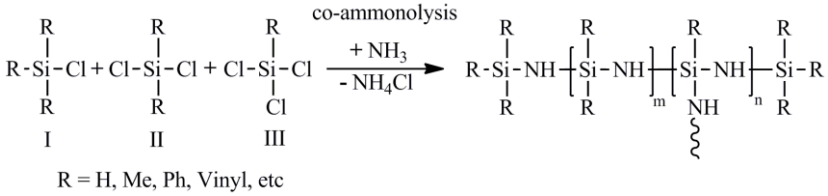

Figure 2-5. Co-ammonolysis reaction of different chlorosilanes, I = monochlorosilane, II = dichlorosilane, III = trichlorosilane.

2.3 Preparation of polymer-derived ceramic nanocomposites (PDC-NCs)

2.3.1 Synthesis of silicon-based polymer precursor

The molecular structure and elementary composition of preceramic polymers are two determining factors for the microstructure and properties of the final ceramics produced. In other words, by designing the precursors, the PDCs with expected chemical and physical properties can be achieved. A simplified general formula of Si-based precursors can be presented as $[Si(R_1R_2)\text{-}X]_n$[110]. In the formula, the X group is located in the backbone of the polymer molecular, and there is a strong covalent bonding between Si and X, therefore, the change of X has primary and critical influence on the nature of the precursors, and numerous precursors can be basically categorized according to different X groups, for instance, polysilanes with X=Si, polycarbosilanes with X=alkyl, polysilazanes with X=amido, polysiloxanes with X=O, and polysilylcarbodiimides with X = [N=C=N], they are also the most representative Si-based precursors. While the side groups R_1 and R_2 have a secondary impact on the properties of precursors, they can be freely replaced by many different kinds of functional groups, and the thermal stability, solubility, rheological property and chemical reactivity can be tailored and modified as well as the ceramic yield and functional properties of the as-received ceramics. The polymer precursors can be modified and designed on the molecular level, which is also the key point for the formation of ceramics with novel composition and extraordinary and singular performance. As shown in Figure 2-6, R_xSiCl_{4-x} (x = 0-3, R = organic group) are the most important raw materials for the synthesis of precursors due to their high reactivity,

commercial ability and low cost. Then, the synthesis of silicon-based precursors are usually achieved by the reaction between organic chlorosilanes and alkali metal such as lithium/ sodium/ potassium or ammonia/amines or water to yield polysilanes, polycarbosilanes, polysilazanes and polysiloxanes, respectively.

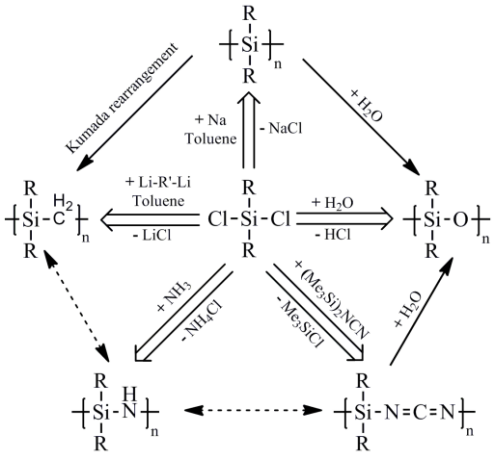

Figure 2-6. Synthesis routes of common organosilicon polymer precursors.

2.3.2 Synthesis of metal-modified single-source precursors

The emphasis of this section is related to the preparation of single-source precursors by chemical modification of Si-based precursors with metal organic compounds and their resulting PDC-NCs. In order to improve the performance of PDCs, a series of metals were doped into precursors, and Si-M-C-N-(O) ceramic nanocomposites were prepared by subsequent heat-treatment. Si-based polymer precursors such as polycarbosilanes and polysilazanes can be chemically modified with various metal alkoxide, metal acetyl acetonates and metal amido complexes. Therefore, three reaction pathways of precursors with metal-organic are briefly reviewed.

(a) The reaction between Si-based precursors with oxygen-containing metal compounds such as metal alkoxides, metal acetyl acetonates and metal carbonyls occur, and Si-M, Si-O-M or N-M bonds could be formed with the release of alkanes or acetyl acetonates by-products.

(b) Polymer precursors react with traditional oxygen-free metal compounds such as metal halides and metallocene as well as metal hydrides, and metal-modified precursors can be obtained with the formation of Si-M or N-M bonds.

(c) Precursors can be modified by novel metal amido complexes, and then the amine ligand is released. Different from the two former methods, this is a more advanced and convenient chemical approach and non-oxide nanocomposites can be obtained simply.

2.4.2.1 Chemical modification of precursors with oxygen-containing metal compounds

As a kind of commercial and widely applicable precursor, PCS has been researched and modified with different metallic compounds. It is reported to be modified with metal alkoxides with the formation of Si-O-M bonds[111]; however, no obvious and clear evidence for the chemical reaction mechanism has been provided, and metal alkoxide was even considered to be physically doped into the PCS matrix[112]. For the reaction of PCS modified with metal acetylacetonates, only the decrease of the intensity of Si-H bonds and the release of acetylacetonate were observed[113, 114]. From above all, the reactions between PCS and metal alkoxides and acetylacetonates are ambiguous due to the relative low reactivity.

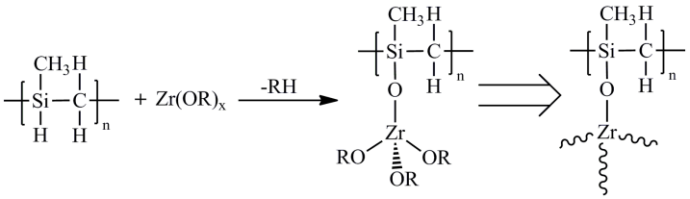

Figure 2-7. Chemical modification of PCS with zirconium alkoxides[113].

Polysiloxanes, which are preceramic polymers for the fabrication of silicon oxycarbide ceramics, can also be chemically modified with metal alkoxides such as zirconium n-propoxide or hafnium n-butoxide because of the reactive functional groups, such as the hydroxyl and alkoxy groups[12, 115]. In the reaction between polysiloxanes and metal alkoxides, not only the strong decrease of the amount of Si-OH bonds and the high cross-linking degree of precursors were observed, but also the formation of Si-O-M units was detected by FT-IR measurements. This is strong evidence for the chemical reaction of polysiloxanes and metal alkoxides, and it further demonstrates that the metal homogeneously dispersed in the polymeric network in an atomic scale.

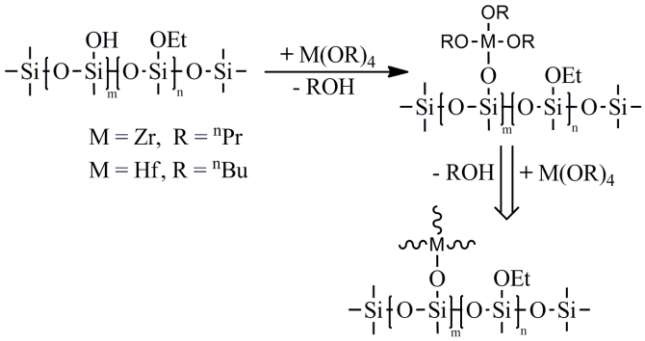

Figure 2-8. Chemical modification of a polysilsesquioxane with zirconium or hafnium alkoxides[12, 115].

Polysilazanes are another kind of precursors that are frequently modified by metallic compounds. Based on the availability of reactive Si-H, N-H and vinyl functionalities contained in these precursors, they show a very good cross-linking behavior and allow the introduction of metal atoms into the polymer chains. The ligands assigned to the metallic compounds may be released or become a part of the as-synthesized precursors. The covalent bonds between the metal ions and the precursors may be built up by the chemical reaction, and it is the

necessary stage for the preparation of metal-ceramic composites in order to avoid the loss of metal via sublimation during the following pyrolysis.

Perhydropolysilazanes are reported to react with titanium n-butoxide, but the chemical reaction was observed to occur only at the N-H groups[116]. While HTT 1800 (a methyl- and vinyl-substituted polysilazanes) can be also modified with $M(OR)_4$ (such as hafnium n-butoxide), and the Raman and NMR investigation confirmed that the reaction can take place at both Si-H and N-H groups of HTT 1800[14]. By comparing these studies above mentioned, it can be concluded that different reactivities of the polymeric precursors result in the metal-modified SSP with different structures, and the corresponding ceramics with various microstructures and functional properties may be acquired.

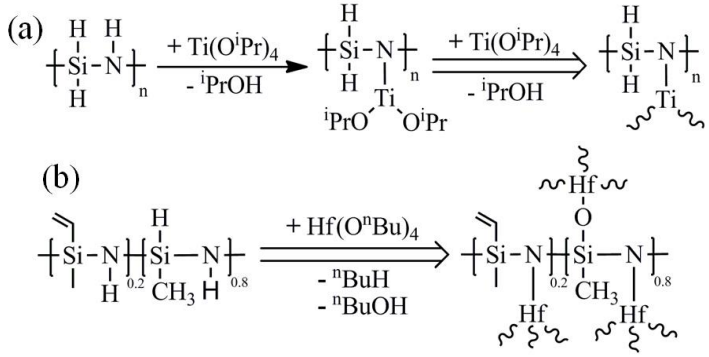

Figure 2-9. Chemical reaction of polysilazanes with titanium and hafnium alkoxides: (a) PHPS reacts with $Ti(O^iPr)_4$[116]; (b) HTT1800 reacts with $Hf(O^nBu)_4$[14].

The usage of metal carbonyls was also proposed on account of their advantageous reactivity that they can initiate hydrosilylation and dehydro-coupling reactions even at room temperature. The reaction of preceramic polymers with metal carbonyls was initially investigated by Seyferth and coworkers on the metallocenes modified polysilazanes and polycarbosilanes[117, 118]. Due to the active Si-H groups assigned to polycarbosilanes, an opportunity is provided to react with polynuclear metal carbonyls such as $Fe(CO)_5$, $Fe_3(CO)_{12}$, $Co_2(CO)_8$ and $Ru_3(CO)_{12}$. As a result, the cross-linking degree and ceramic yield are improved. The formation of ceramics doped with intermetallic compounds such as Fe_3Si or Co_2Si were achieved and confirmed by XRD and TEM[119, 120]. SiC fibers containing nanosized α-Fe crystallites were fabricated via the modification of PCS with $Fe(CO)_5$[121]. Soft magnetic properties of all the samples mentioned above were also investigated and the value of magnetization is determined by the amount of the metallic particles as well as their crystallinity. Unfortunately, metal carbonyls are extremely volatile and poisonous, and they may vaporize in the process of the ceramic formation at high temperature, leading to the uncontrollable content of additional metals; besides, a large number of the CO ligands are incorporated into the precursors, leading to an oxide ceramic matrix.

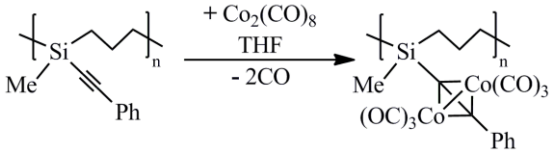

Figure 2-10. Synthesis reaction between acetylide-substituted polycarbosilane and Co carbonyl[120].

In addition, some novel oxygen-containing metallic complexes have also been attempted to be used in the chemical modification of preceramic precursors. For example, novel Ni-polysilazane precursors were reported to be synthesized using polysilazane and trans[bis(2-aminoetanol-N,O) diacetato-nickel(II)][122]. Interestingly, the Ni atoms did not directly connect to the Si or N of the polysilazane backbone; on the contrary, the nickel nanoparticles formed *in situ* during the synthesis of Ni-containing precursors. By subsequent heat-treatment, a nanoporous silicon oxycarbonitride ceramic was obtained, and a construction of turbostratic carbon was also formed due to the reactions catalyzed by nickel nanoparticles, which were homogeneously dispersed in the SiCN(O) matrix.

2.4.2.2 Chemical modification of precursors with oxygen-free metal compounds

As a result of using alkoxides or acetyl acetonates, oxygen is also introduced into the resultant ceramics, and sometimes oxide phases have an adverse effect on the high temperature performance of ceramics. Therefore, the oxygen-free metal compounds have caught researchers' concern. A new type of oxygen-free hyperbranched polysilazane containing iron precursor was reported to by synthesized by the polycondensation of $FeCl_3$ and silazane lithium salts, which were produced from the reaction of silazane with n-BuLi (Figure 2-11)[123].After pyrolysis, SiCNFe ceramic with controlling electrical and magnetic properties was prepared. Similarly, another non-oxide iron-containing liquid precursor was synthesized. By reacting polyvinylsilazane with $FeCl_3$ in the absence of a catalyst, the iron-containing precursor was cured at 130 ℃, and a ferromagnetic ceramic with α-Fe was obtained at only 500 ℃[124]. $TiCl_4$ was also employed in the modification of Si-based polymer precursors via this approach in order to prepare TiC/SiC and TiN/Si_3N_4 ceramic composites with excellent thermo-mechanical properties and ultra-high temperature resistance. However, the development of this approach is restricted by one obvious disadvantage, that is, it is difficult to remove the unreacted $FeCl_3$/$TiCl_4$ and formed LiCl by-product completely due to their poor solubility in organic solvents.

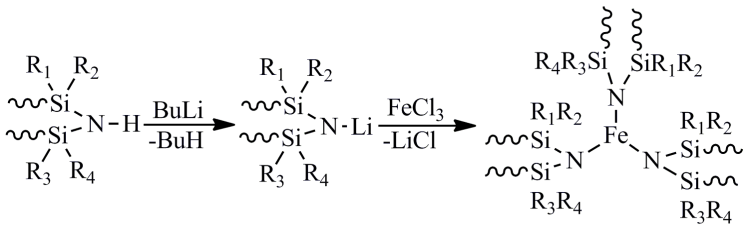

Figure 2-11. Chemical modification of polysilazanes with $FeCl_3$[123].

Bis(cyclopentadienyl)M dichloride (Cp_2MCl_2, M = transition metal) can be used as catalytic agents on the dehydrogenative polycondensation of Si-H groups of Si-based precursors. Tsirlin[125] took Cp_2ZrCl_2 and PCS as raw materials to prepare non-oxide ZrPCS polymer fiber. Afterwards, a series of SiC/MC (M = Ti, Zr and Hf) ceramic composites were fabricated through the reaction of precursors with corresponding Cp_2MCl_2 complexes[126]. The absence of oxygen in the composition of the polymers is an advantage for the fabrication of high performance ceramic materials. The cross-linking reaction is catalyzed by the Cp_2MCl_2, and final products with high ceramic yield are acquired. Yu's group published the synthesis of SiC/ZrC/C ceramic composites derived from PCS/Cp_2ZrCl_2 hybrid precursors[127], and the results suggested that dehydrocoupling, hydrosilylation and dehydrochlorication are involved in the cross-linking and responsible for the high ceramic yield. Moreover, they synthesized a novel processable hyperbranched polyferrocenylcarbosilanes using PCS and vinyl ferrocene with Pt-catalysis[128], a self-catalytic effect of ferrocenyl units on dehydrocoupling was observed in the curing process, and the as-obtained SiC/C/Fe nanocomposite demonstrated an interesting microstructure that α-Fe nanoparticles dispersed in the SiC/C matrix homogeneously. The α-Fe nanoparticles were separated by the turbostratic carbon layers located at crystal boundary. Thus, bis(cyclopentadienyl) metal complexes can be incorporated to the Si-based polymer in addition to the catalytic action. It can also act as a suitable alternative source of metal and open a new synthetic route toward the fabrication of Si-C-(N)-M ceramics nanocomposites. Finally, a poly(aluminasilazane)s precursor[129] was reported to be prepared via the modification of PHPS with aluminum hydride (trimethylamine-alane). The introduction of aluminum hydride could improve the cross-link degree of the precursor via dehydrocoupling, and the pyrolyzed residues from the precursors were composed of silicon nitride and 2*H* wurtzite-type compound.

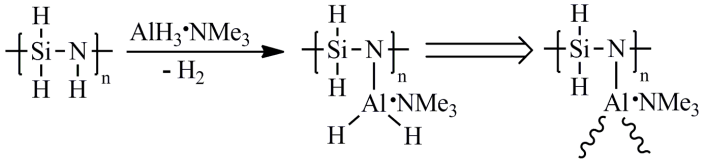

Figure 2-12. Chemical reaction between PHPS and trimethylamine-alane[129].

2.4.2.3 Chemical modification of precursors with metal amido complexes

Recently, amido metal complexes have been used as a new source of metal to modify precursors. Amido complexes have the following advantages: (i) they can be synthesized in high yields on a large scale and demonstrate good solubility in common organic solvents; (ii) they are oxygen-free chemicals, and they contain the similar elementary compositions as that of Si-based precursors, which can avoid the addition of any alien element into the resultant ceramics; and (iii) almost all of the transition metals are addressable, meaning the coordination compounds of many transition metals can be prepared and used for doping, showing a promising applicability.

In the mid-1990s, the metal amido complexes garnered attention and were used to chemically modify precursors. Solid metal-containing single-source precursors $[N(Si(NMe_2)_3)(Ti(NMe_2)_2)]_2$ and $N(SiMe_3)[Si(NMe_2)_3][Ti(NMe_2)_3]$ for SiTiCN ceramics have been synthesized by Wagner and Jansen[130]. Later, Hapke and Ziegler reported novel liquid organometallic precursors that were prepared by the chemical reaction of $Ti(NMe_2)_4$ with three types of polysilazanes precursors with different side groups[131]. After pyrolysis in argon, SiTiCN ceramics were successfully achieved, and the pyrolysis yield depended strongly on the Si/Ti ratio of the precursors. This approach provides the possibility of creating new controllable nanostructural hybrid composites and exhibits the potential applications in ceramic coatings and fibers by adjusting the precursor's viscosity.

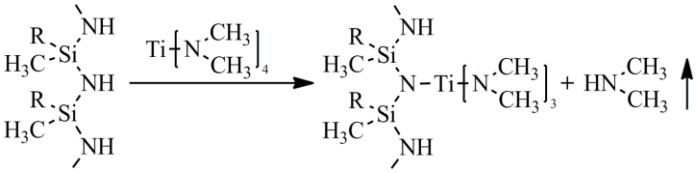

Figure 2-13. The proposed reaction pathway of polysilazanes with $Ti(NMe_2)_4$[131].

A simultaneous research work was performed by modifying PHPS with $Ti(NMe_2)_4$[17], and then a Ti-containing precursor was generated with the chemical formula $[Si_{1.1}Ti_{0.4}C_{2.2}N_{1.1}H_{6.2}]_n$ and a molecular weight of 4200 g·mol^{-1}; this precursor was warm-pressed and pyrolyzed under ammonia and then annealed under nitrogen. Finally, a monolithic nanocomposite was produced with a Vickers hardness as high as 25.1 GPa. In a recent study, it is reported that the polysilazane HTT 1800 can be chemically modified by tetrakis(diethylamido)hafnium (TDEAH)[132]: the chemical modification took place at both N-H and Si-H groups, but the vinyl groups (C=C) were not found to be affected by the reaction with TDEAH. By further modification with $BH_3 \cdot SMe_2$ and subsequent polymer-to-ceramic conversion, amorphous SiHfBCN ceramics were successfully fabricated. The SiHfBCN ceramics showed different phase separation and crystal behavior according to the annealing atmosphere, that is, $HfC/HfB_2/SiC$ (annealing in Ar) or $HfN/Si_3N_4/SiBCN$ (annealing in N_2) nanocomposites, which confirms that the phase separation progresses are thermodynamically controlled and lays the foundation for preparing UHTC-NCs with suitable structures.

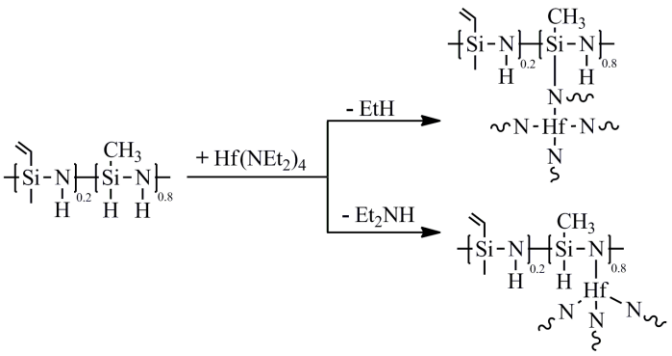

Figure 2-14. The proposed reaction pathway of HTT1800 with $Hf(NEt_2)_4$[132].

Other novel and promising non-oxygen metallic compounds introduced here are aminopyridinato metal complexes. Because of their unique nature and reaction activities, they have been applied in the fabrication of hybrid materials with nanostructures. Glatz et al. reported an easy and inexpensive strategy for the preparation of Cu-SiCN ceramic nanocomposite shown in Figure 2-15[133]. Due to the availability of more coordination sites supplied by the HTT 1800 backbone and the intrinsic reactivity of the amido complex, the metal transfers from the complex to the precursor, and it is assumed that covalent bonding between the copper atoms and the HTT 1800 formed with the liberation of protonated ligand $Ap^{TMS}H$. The copper loading content is adjustable over a broad range of precursors and result in SiCN ceramics with uniformly dispersed Cu nanoparticles with different sizes, which can be a potential material to be used as recyclable heterogeneous catalysts for the selective oxidation of cycloalkanes under mild conditions.

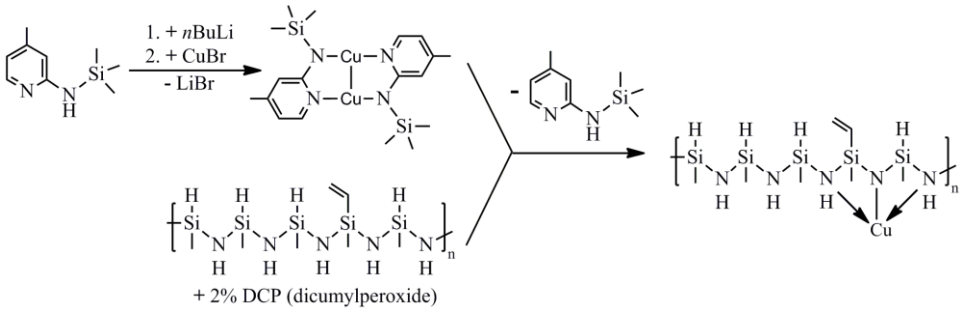

Figure 2-15. The approach to Cu-SiCN precursor by molecular design[133].

Similar chemical modification was also performed on HTT 1800 polymer by using aminopyridinato palladium complexes[134]. As with the previous case, palladium was transferred to the polymer framework by forming a N-Pd bond. Whereas, in contrast to the Cu-SiCN ceramics, a different behavior was observed for its crystal and phase separation behavior during the heat-treatment, amorphous SiCN matrix with the presence of homogeneously distributed hexagonal Pd_2Si crystallites was achieved, and the crystalline Pd_2Si provide catalytic activity for the selective hydrogenation of aromatic ketones. In other studies, the coordination compound [(cod)$PtMe_2$] (COD = 1,5 cyclooctadiene) was used as a platinum source, together with the poly(ureamethylvinyl)silazane (PUMVS) precursor, structure directing agent and self-assembly template of polystyrene spheres in order to fabricate hierarchically structured porous ceramics functionalized with Pt nanoparticles[135]. This approach has been further applied on the family of aminopyridinato complexes coordinated with different transition metals such as Fe, Co, Pt, Cu, Ag and Au[136], and then porous metal-SiCN ceramics were fabricated with the simultaneous *in situ* generation of catalytic active metal nanoparticles from the metal modified polysilazane precursors. On the account of the availability of metal aminopyridinato complexes, this bottom-up strategy can be extended to other transition metals to be regarded as suitable candidates for the modification of polymer precursors.

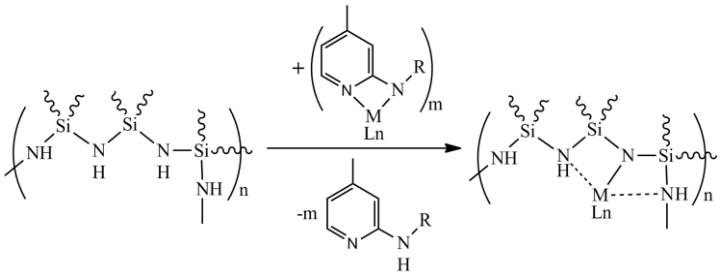

Figure 2-16. The metal transfer reaction between polysilazane and metal aminopyridinato complexes[136].

2.4 Porous ceramics

In recent years, micro- and mesoporous materials with a high effective surface area and a narrow pore size distribution has become an important research focus, because they are key enabling components for potential applications that require fast and efficient transport in, out of or within a high surface area, such as catalyst supports, gas filters and sensors. Porosity is the critical factor for the performance of porous materials, and macropores are ideal for providing access to internal sites, while micro- and mesopores are beneficial to increase the surface area and improve selectivity[137]. In order to meet different needs, tunable porous materials with tailored systems of large or small pores are required.

PDCs are diversely used materials because they are easy to manufacture, and the as-obtained porous non-oxide ceramics such as SiC, SiCN and Si_3N_4 have attracted growing attention due to their ability to bear high mechanical stresses, high temperatures and harsh operating environments. The fabrication of porous ceramics via PDC methods offers a series of advantages in terms of simple processing methodology, low cost and adjustability of porosity. As a result, porous PDCs have become promising candidates for the applications in the support structures for catalysis, energy storage and gas separation. Porous PDCs can be produced via a combination of the precursor pyrolysis with a variety of pore-forming techniques, for instance: replica forming[138, 139], direct foaming[140, 141] and using sacrificial fillers[142, 143]. Additionally, by selecting the appropriate pore-foaming reagent, the pore size and shape as well as its arrangement can be tailored.

The preparation of microporous silicon imido nitrides by pyrolysis of polysilazanes was reported for the first time by Bradley *et al.*[144, 145]. Later, silicon imido nitrides with high surface areas were also successfully synthesized by ammonolysis of silicon tetrachloride in organic solvents[146]. Furthermore, mesoporous silicon nitride materials with narrow pore size distributions were prepared by the reaction of silicon halides and ammonia in organic solvents at room temperature with subsequent dehalogenation at high temperature[147]. In addition, novel porous ceramics including Si_3N_4, Si_3N_4-BN and Si_3N_4-AlN were produced based on sol-gel processes. The use of a sacrificial template is another method for pore generation. It can be further divided into hard and soft templates. The hard template is usually a kind of inorganic material with porous or nano-sized structures, which does not react with the precursor. Final porous materials can be obtained by removing the template. Mesoporous silica and carbon are the two well-known hard templates. Mesoporous SiC ceramic were

prepared via a carbothermal reduction reaction with using mesoporous silica MCM-48[148] or SBA-15[149] as a solid template; however, the negative aspects of this method are that it requires a harmful etching step using strong acid to remove the template. Majoulet *et al.*[150] reported the first example of periodic mesoporous SiAlCN ceramic, it was prepared by a solvent nanocasting route using mesoporous carbon (CMK-3) as the hard template which was removed by annealing the sample in ammonia later.

The use of polyolefin as soft sacrificial templates is considered as one of the most promising strategies. A series of conventional polymers with high molecular weight such as polymethyl methacrylate (PMMA)[142], polystyrene (PS)[151] and polyethylene (PE)[152] can be applied as sacrificial fillers. They act as place holder substances and could be removed by thermal decomposition together with the ceramization process of precursor polymers to create open pore networks during the heat-treatment[153, 154], leading to the production of porous structure with high tailorability and reproducibility without additional steps. It was reported that mesoporous BN ceramics was synthesized using a hybrid organic-inorganic block copolymer[155]. As a conventional polymer, polystyrene has a simple composition and can be completely decomposed at temperatures of *ca.* 400 ℃[156], making it a promising self-sacrificial template. Nghiem *et al.* reported the application of PSZ-block-PS[157] and PCS-block-PS[158] diblock copolymer as precursors for the preparation of a mesoporous SiC and SiCN ceramics, respectively. Sung and colleagues[151] established a self-sacrificial template method by using polystyrene spheres, a packed bed of PS spheres was assembled and infiltrated by polysilazane precursor, then macroporous SiCN monoliths were obtained after the pyrolysis. Afterwards, Ewert *et al.*[159] reported the generation of mesoporous structured SiCN nanocomposite by using PS the self-sacrificial template in a simple one-pot synthesis.

Based on the specificity of polymeric precursors including solubility, ease of processability and the designability of molecules, ceramic components with high amounts of designed porosity can be produced by various processing methods, and the porous PDCs with a wide range of pore size and morphology can be useful for many specific applications.

2.5 Fabrication of one-dimensional nanostructures from polymeric precursors

Nanostructural materials are defined as having at least one dimension smaller than 100 nm, and they have been intensively studied over the past two decades for their peculiar and unique properties. Plenty of interesting and novel phenomena are observed on the nano-sized structures, for examples: size dependent excitation or emission[160, 161], quantized conductance[162], Coulomb blockade[163] and metal-insulator transition[164]. The quantum confinement of electrons by the potential wells of nanostructures provides a powerful method to control the electrical, optical, magnetic and thermoelectric properties of functional materials. Miniaturization has been the development tendency in today's science and technology, and a great deal of effort has been spent on the attempt to develop components with critical dimensions. Some nanomaterials already demonstrate superior performances and applications in many fields, such as the development of magnetic and optical

materials with size as small as dozens of nanometers for information storage[165] as well as the successful application in microelectronics (*i.e.*, integrated circuits), where "smaller" has meant greater performance, faster operation, lower cost and less power consumption[166].

The synthesis and investigations of one-dimensional (1D) nanostructures materials (*e.g.*, nanotubes, nanowires, nanobelts) is one of the hot and important research directions in material science and research interest has grown in recent years. 1D nanostructures provide a good experimental subject for the study of the relationship of electrical and thermal transport or mechanical performance on dimensionality and size reduction. In the field of functional material such as the fabrication of electronic, optoelectronic and electrochemical devices at the nanoscale, 1D nanomaterial is considered to be a competitive candidate. At present, 1D nanostructures of metals and ceramics can be produced via many advanced techniques[167, 168], the successful preparation of various types of 1D nanostructures have been reported, such as nanotubes[169, 170], nanocables[171], nanowires and fibers[172, 173]. For the fabrication of 1D nanostructures, a high number of manufacturing strategies have been developed[168, 174]. Among all of these technologies, the usage of polymer precursors is considered as a novel and promising method due to their high tailorability of chemical composition on a molecular scale and ease of processing. Various types of 1D nanostructures with different compositions (*i.e.*, carbon, SiC, Si_3N_4) have been prepared directly from the corresponding precursors. Usually, the 1D nanostructures can be prepared from polymeric precursors by means of basically three approaches: (i) the utilization of gaseous byproducts derived from the decomposition of the precursors at high temperatures, with or without the catalysis of transition metal additives; (ii) template modulated method and (iii) electrohydrodynamic method such as electrospinning.

1D nanostructures prepared by the template-assisted approach show some advantages, for example, the ability to control shape, size and impurity level of the structures; nevertheless, the additional cost caused by using the template, etchant and the time-consuming process hinders the development of this method. Electrospinning is considered as another promising approach that can produce 1D nanostructures with high yield, desired properties and functionalization; however, the precursors with high molecular weight and suitable viscosity are required in the process, which causes the technical difficulties and limits the application of this approach. Recently, most studies that reported fabricating 1D nanostructures were based on approach (i) due to its low cost and simple operability, and different transition metals (Fe, Co, Ni, etc) are usually employed as a catalyst source in the production of nanostructures derived from precursors to improve the yield of nanostructures, which is known as catalyst-assisted pyrolysis (CAP). The CAP of precursors is a relatively simple, cheap and fast method, and it can be designed as a one-pot process and does not require additional materials or equipment. For instance, carbon nanotubes (CNTs) were produced by pyrolysis of a PCS precursor doped with iron nanoparticles[175] or a borazine-based precursor containing nickel as a catalyst[176]. Polysilazane precursors were doped with the catalytic action of $FeCl_2$, and then the *in situ* grown single crystal Si_3N_4 nanowires can be obtained[177]. SiC/SiO_2 nanocables with core-shell structure was synthesized by using poly(dimethylsiloxane) modified with ferrocene[178].

According to all of the research achievements introduced above, it is believed that nanomaterials greatly affect the productivity of science. However, most of the research work in this field still focuses on the preparation and characterization of 1D nanostructures. The discovery and application of these as-obtained 1D nanostructures have been rarely covered, and only a few studies report that the 1D nanostructures exhibit good photoluminescence and interesting semiconducting properties[170, 179]. Further development in this field will lead to development of 1D nanostructural materials in various advanced applications, including catalysis, electrical conductivity/resistivity and magnetic fields.

3. EXPERIMENTAL PROCEDURES

3.1 Chemicals

The chemicals used in this work are perhydropolysilazane (PHPS, 22.5 wt.% solution in di-n-butyl ether, AZ Electronic Materials GmbH, Germany), tetrakis(dimethylamido) hafnium(IV) (TDMAH, Sigma-Aldrich), vanadium(IV)oxy acetylacetonate (or vanadyl acetylacetonate, $VO(acac)_2$, Sigma-Aldrich), polystyrene (PS, average Mw=35000, Sigma-Aldrich), linear low density polyethylene (LLDPE, Sigma-Aldrich), poly(isobutyl methacrylate) (PBMA, average Mw=70000, Sigma-Aldrich), iron(II) acetylacetonate ($Fe(acac)_2$, Sigma-Aldrich) and anhydrous toluene. All chemicals were stored in an inert atmosphere and used as-received without further purification.

3.2 Synthesis of Si-M-N (M=metal) single-source precursors

All single-source precursors were synthesized under inert atmosphere in order to avoid contact with oxygen and moisture. Synthesis was performed using the Schlenk technique with the protection of argon or nitrogen. The as-obtained precursors were handled, stored and prepared for measurement in a glovebox with the protection of an Ar atmosphere.

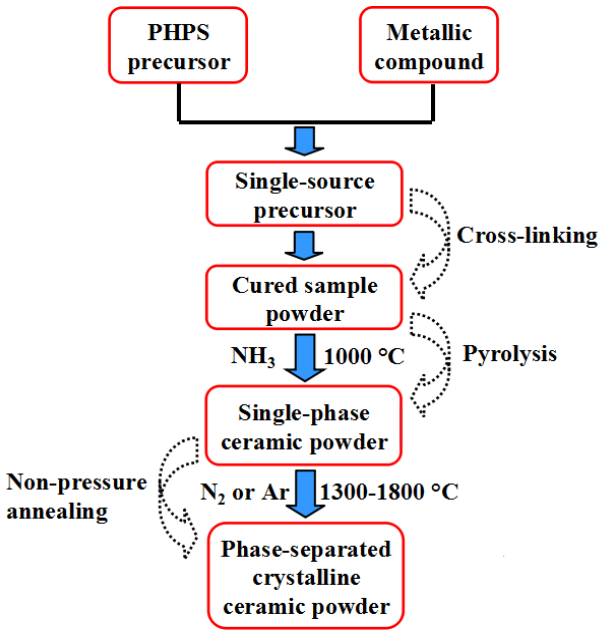

Figure 3-1. Simple flow diagram of preparing the single-source precursors and corresponding ceramics.

3.2.1 Synthesis of SiHfN single-source precursor

The synthesis of SiHfN single-source precursor was performed using a commercially available perhydropolysilazane solution (PHPS) and tetrakis(dimethylamido)hafnium(IV) (TDMAH). SiHfN precursors with different hafnium content were synthesized in order to study the influence of the hafnium content on their ceramization behavior and on the phase composition microstructure of the resulting ceramics. The TDMAH was added into PHPS in different mass ratio, i.e., TDMAH : PHPS = 2:98, 15:85 and 30:70 (referred to as samples SiHfN-1, SiHfN-2 and SiHfN-3), respectively. A typical synthesis of the SiHfN single-source precursor (as for SiHfN-3) was performed using following procedure: 1.0 g of TDMAH was dissolved in 5 mL anhydrous toluene. Then the resulting solution was added dropwise to 10.37 g PHPS solution (2.3 g pure PHPS) in 15-20 min. This reaction mixture was constantly stirred at room temperature for 6 h with flowing argon, reaction can be carried out adequately and a milk white gel-like product was obtained. After removing the solvent and low molecular weight byproduct such as $HNMe_2$ in vacuum at 50 ℃ for 5 h, a white powdery precursor (SiHfN-1 single-source precursor was a viscous liquid because only 2 wt.% TDMAH was introduced and the precursor was not highly cross-linked) was obtained. The yield of SiHfN precursors was about 95 wt.%.

3.2.2 Synthesis of SiVN(O) single-source precursor

The synthesis of SiVN(O) single-source precursors was carried out by using perhydropolysilazane (PHPS) and vanadium(IV) oxide acetylacetonate ($VO(acac)_2$) as the raw materials. Different weight ratios of vanadium were introduced into PHPS in order to study the effect of different vanadium proportions on the modification reaction and the microstructure evolution of obtained ceramics.

$VO(acac)_2$ was added into PHPS with different weight ratio, the weight ratios of PHPS : $VO(acac)_2$ were 98:2, 85:15 and 70:30, and the precursors were denoted as SiVN(O)-1, SiVN(O)-2 and SiVN(O)-3, correspondingly. Because of the poor solubility of $VO(acac)_2$ in toluene, a large amount of toluene was used and the PHPS solution was added dropwise into the $VO(acac)_2$. One typical synthesis of the SiVN(O) precursor is described as the following procedure: 2.143 g $VO(acac)_2$ was dissolved in 80 mL anhydrous toluene in a 250 mL Schlenk flask (but most of the $VO(acac)_2$ still cannot be solved after 24 h stirring), and then 22.2 g PHPS solution (5.0 g pure PHPS) was added dropwise into the flask, the reaction mixture was constantly stirred at room temperature for 12 h. The solution became dark blue, and finally a black gel was obtained, with the consumption of undissolved $VO(acac)_2$. In order to remove the toluene, the mixture was dried under vacuum at 50 ℃ for 5 h and a brown cross-linked powdery SiVN(O)-3 precursor was obtained. The yield of SiVN(O) precursors was about 97 wt.%.

3.2.3 Synthesis of SiVN/Polymer template compounds

As before, all reactions and blend were carried out in purified Ar atmosphere using standard Schlenk techniques. PS, PE and PBMA were used as the self-sacrificial template, respectively, here the synthesis of SiVN(O)3-PS2 was taken for example, one typical synthesis of the compounds is described as follow: In a round bottom Schlenk flask, 2.0 g PS were degassed in vacuum for 3 h to remove residual water. The PS particles with M_w=35000 can be easily solved in 30 mL toluene under stirring, and then 0.7 g the commercial available precursor PHPS was added to obtain a homogeneous mixture of the polymer template and the preceramic polymer by intensive stirring. The modification with transition metal and cross-linking of the PHPS precursor can be achieved simultaneously by adding 0.3 g $VO(acac)_2$ into the mixed solution, after the reaction overnight, a black solution was obtained. In order to improve the crosslinking degree of the SiVN(O) precursor, the black solution was further heated up to 80 ℃ and kept for 12 h in an Ar atmosphere and the PS polymer could be sealed in the SiVN precursor matrix. Finally, a viscous black SiVN(O)3-PS2 compound was obtained after the solvent was stripped off under vacuum. In the present research, the weight ratio of PHPS/VO(acac)2 was fixed in 7/3 and denoted as SiVN(O)3, the weight ratio of SiVN(O)3 to different polymer templates were fixed in 1/1, and the obtained samples were abbreviated as SiVN(O)3-PS1, SiVN(O)3-PE1 and SiVN(O)3-PBMA1, respectively. Additionally, the influence of different percentages of PS template was also checked, the weight ratios of SiVN(O)3 to PS were1/0.5, 1/1, 1/2 and 1/3, and they corresponded to the sample SiVN(O)3-PS0.5, SiVN(O)3-PS1, SiVN(O)3-PS2 and SiVN(O)3-PS3, respectively. A control test was also performed under the same conditions, but no polymer template was added, and the resultant sample was named SiVN(O)3-blank.

3.2.4 Synthesis of SiFeN(O) precursors

The synthesis of SiFeN precursor with PHPS and $Fe(acac)_2$ is similar to the synthesis of SiVN(O) and described as follow. A quantity of 1.00 g $Fe(acac)_2$ was added into a 50 mL Schlenk flask in an inert atmosphere, 10 mL anhydrous toluene was used as solvent. Next, 1.00 g pure PHPS was also introduced into the flask with intensive stirring at room temperature. The mixture was heated up to 100 ℃, after reflux at 100 ℃ for 12 h with intensive stirring, a viscous dark red Fe-modified polysilazane precursor was synthesized. It is important to mention that the reaction was incomplete and some unreacted $Fe(acac)_2$ still suspended in the precursor. The weight ratio of PHPS to $Fe(acac)_2$ were 50/50 and 95/5, and the corresponding samples were named SiFeN(O)-50 and SiFeN(O)-5, respectively. The yield of SiFeN(O) precursors was about 92 wt.%.

3.2.5 Preparation of SiFeN(O)-based ceramic paper

In order to fabricate the ceramic paper, filter paper was chosen due to its simple chemical composition (only cellulose fibers) and macro-porous structure. One typical preparation of the SiFeN(O)-based ceramic paper was

described as follow: the filter paper with the dimension of 1.5 × 1.5 cm^2 was dried at 80 ℃ for 24 h and subsequently dipped into the SiFeN(O)-50 precursor toluene solution for 1 second under argon atmosphere, after removing the solvent and high-temperature treatment, SiFeN(O)-based ceramic paper was successfully prepared. The filter paper was dipped in different SiFeN(O) precursors and the obtained samples were abbreviated as Paper-SiFeN(O)50 and Paper-SiFeN(O)5, respectively. A control test was also performed under the same conditions by dipping the paper into the PHPS toluene solution, and the control sample was named Paper-PHPS.

3.3 Pyrolysis of precursors

The as-obtained single-source precursors were pyrolyzed in a Schlenk furnace (Gero GmbH & Co., Neuhausen, Germany) equipped with a mass flow controller (Model 5850E, Brooks Instrument B.V. Netherlands). Firstly, the precursor polymer was finely ground in an agate mortar, and then it was weighed and put into a quartz boat, which was kept in a quartz Schlenk tube. The precursors were pyrolyzed at a heating rate of 100 ℃/h to the target temperature under constant high-purity ammonia (99.98% Air Production) supplied with the rate of about 1.5 L/h. The ammonia was fed from a gas bottle to the Schlenk tube through the inner part of a coaxial hose, in order to decrease the hydrolysis of ammonia during ammonolysis, increase ammonia concentration around the precursors and facilitate the exhaust of waste gas. At the target temperature, the samples were held for 3 h to complete the polymer-to-ceramic transformation and then cooled down to room temperature.

3.4 Annealing of ceramics

The ceramics derived from 1000 ℃ ammonolysis were further annealed at higher temperature under nitrogen atmosphere. In the range from 1000 to 1300 ℃, the annealing experiments were performed in an alumina tube furnace (Gero GmbH & Co., Neuhausen, Germany). And from 1400 to 1800 ℃, the heat-treatments were performed in an Astro graphite furnace (Thermal Technology Inc., CA, USA). The heating schedules was described as follow: from room temperature to 1000 ℃, heating rate was 10 ℃/h; from 1000 ℃ to target temperature, heating rate was 5 ℃/h, and held for 5 h at target temperature. The thermolysis was completed by cooling the sample to room temperature at a rate of 10 ℃/h.

3.5 Characterization techniques

3.5.1 Fourier transform infrared (FT-IR)

The as-synthesized polymer precursors were air-sensitive and were measured by means of attenuated total reflection FT-IR spectroscopy (ATR FT-IR) on a Bruker Varian FT-IR spectrometer (Brucker, VARIAN 670-

IR, USA). The FT-IR spectra of ceramics powder were investigated by using the same equipment in transmission geometry model with KBr pellets. .

3.5.2 Raman spectroscopy

Raman spectroscopy was measured using a Horiba HR 800 micro-Raman spectrometer (Horiba Jobin Yvon, Bensheim, Germany) equipped with an argon laser. The excitation line has its own interference filter and a Raman notch filter. The measurement were performed from 200 to 4000 cm^{-1} with a green laser (irradiation wavelength of 514.5 nm) and a confocal microscope (magnification 50×) with a 100 μm aperture, giving a resolution of 2-4 μm.

3.5.3 Nuclear magnetic resonance (NMR) spectroscopy

For liquid precursors, NMR measurements were performed on a Bruker AV 300 NMR spectrometer (Bruker, Germany) operating at 300.13 MHz for ^{1}H spectroscopy, 75.46 MHz for ^{13}C (^{1}H decoupling) and 59.63 MHz for ^{29}Si (^{1}H decoupling), the delay time was 30 seconds. C_6D_6 or $CDCl_3$ were used as solvents for different precursors, the chemical shifts of ^{1}H, ^{13}C and ^{29}Si were all referred to tetramethylsilane (TMS) as the external standard.

For solid cross-linked precursors and ceramics powder, the solid state MAS NMR measurements were carried out on a Bruker AV 300 NMR spectrometer (Bruker, Germany) using a 4.00 mm Bruker double resonance MAS probe at the spinning speed of 6.0 kHz. The ^{13}C isotropic chemical shifts were referenced to the carbonyl carbon of glycine (assigned to 173.2 ppm). Both ^{13}C and ^{29}Si MAS NMR spectra were recorded using a 90° pulse of 6 μs and recycle delays of 60 s. ^{13}C and ^{29}Si chemical shifts were determined relative to the external standards adamantane and kaolin, respectively, and are given with respect to the primary standard TMS (δ = 0 ppm).

3.5.4 Elemental analysis (EA)

The ceramics powder was measured with elemental analysis to acquire the chemical composition. For the carbon content of the samples, a carbon analyzer LECO C-200 (LECO Instrument GmbH, Monchengladbach, Germany) was employed. While the oxygen and nitrogen content was tested with an O/N analyzer LECO TC-436 (LECO Instrument GmbH, Monchengladbach, Germany). The measurement of silicon and hafnium content of the ceramics were carried out at Mikroanalytisches Labor Pascher (Remagen, Germany).

3.5.5 X-ray diffraction (XRD)

X-ray powder diffraction measurements were performed on a STOE $STAD_1$ P X-ray diffractometer (STOE & Cie. GmbH, Germany) in transmission mode, with monochromatic Mo *Kα* radiation at a scanning speed of 1 °/min in the range of 5-45° (2θ).

3.5.6 Thermal gravity analysis (TGA)

In order to study the polymer-to-ceramic transformation of these precursors and high temperature stability of the ceramics, thermal gravity analysis (TGA, Netzsch STA 449C Jupiter, Germany) was carried out with 5 °C/min heating and cooling rate, holding at 1400 °C for 2 h, coupled with a quadrupole mass spectrometer (QMS, Netzsch 403C Aëolos, Germany) and *in-situ* FT-IR.

3.5.7 Scanning electron microscopy (SEM)

The morphological features of the ceramic samples were analyzed using a scanning electron microscopy (SEM, Philips XL30 FEG high-resolution scanning electron microscope, FEI Company, USA). Because the conductivity of obtained ceramics is poor, ceramic samples were grinded to fine powder, and then dispersed on the conducting tape and sputtered with a conductive gold nano-particle (5-10 nm thick) before the investigation.

3.5.8 Transmission electron microscopy (TEM)

(Scanning) Transmission electron microscopy [(S)TEM, JEM-2100F, JEOL Ltd.] measurement was used to observe the microstructure of the SiHfN and SiVN(O) samples. Specimens for high-resolution transmission electron microscopy (HRTEM) were prepared by depositing powders on Cu grid. A 200 kV JEM-2100F microscope equipped with a spherical-aberration corrector (CEOS GmbH), which enabled structures to be probed with sub-angstrom resolution, was utilized for STEM imaging and selected area electron diffraction (SAED) observations. A convergence angle of 25 mrad and a dwell time less than 20 μs, together with annular dark-field detector inner/outer angles of 70/240 mrad, were chosen for high-angle annular dark-field (HAADF) STEM imaging. Electron energy loss (EELS) and energy-dispersive X-ray spectroscopy (EDXS) were also performed on the samples to detect the composition.

For the SiFeN(O) ceramic powder, specimens for (scanning) transmission electron microscopy (S)TEM observations were prepared by depositing the samples on amorphous carbon film supported with Cu grids. SAED patterns (selected-area electron diffraction) and BF-TEM (bright-field) images were obtained from a 200 kV JEM-2010HC (JEOL Ltd.) For chemical composition analysis with STEM-EDXS (energy dispersive x-ray spectroscopy), a 300 kV JEM ARM300CF equipped with an aberration corrector (JEOL COSMO corrector) was used.

For the SiFeN(O)-based ceramic paper, samples of the transformed ceramic paper materials, which are inherently brittle, in particular upon pyrolysis at 1000 ℃, were mildly ground and small particles of the samples were deposited on a lacy carbon grind for TEM inspection with a JEOL JEM-2100F instrument, operated at 200 kV. All samples were lightly carbon coated to minimize charging under the incident electron beam.

3.5.9 Nitrogen adsorption isothermal analysis

Nitrogen adsorption analysis was carried out at 77 K using an Autosorb-3B (Quantachrome Instruments, USA). The samples were firstly preheated at 100 ℃ for 24 h under vacuum before testing. The nitrogen isotherm at 77 K was used to calculate the specific surface area (SSA) from the linear Brunauer-Emmett-Teller (BET) plots over the relative pressure range of $0.05 < p/p_0 < 0.3$. The total pore volume (V_t) was obtained from the amount of vapor adsorbed at a relative pressure $p/p_0 \approx 1$ [180]. The micro-pore volume (V_m) was calculated using the de Boer's t-plot analysis [181]. And the pore size distribution for meso-porous samples was estimated using Barrett-Joyner-Halenda (BJH) method from the desorption branch of the isotherm [180].

4. RESULTS AND DISCUSSION

4.1 SiHfN ceramics

Metal-organic compounds are often used as precursors for highly refractory materials and high-temperature composites, among these chemicals, alkylamide organometallic precursors such as tetrakis(dimethylamido) hafnium(IV) (TDMAH) have attracted great attention of researchers due to their high vapor pressures, chlorine-free and oxygen-free ligands, as well as mild reaction conditions. Alkylamide organometallic polymers have been widely studied in the field of fabrication of hafnium dioxide or hafnium nitride films by atomic layer deposition (ALD) method, and some ALD experiments suggested that the metal alkylamide-water system is both kinetically and thermodynamically superior than the metal chloride-water system[182]. Based on above reasons, TDMAH was adopted as hafnium source for the modification of perhydropolysilazane (PHPS).

The procedures for the synthesis of SiHfN single-source precursors and the pyrolysis of Si-Hf-N single-phase ceramics were described in Chapter 3. In this section, characterization results for the single-source precursors and the subsequent as-obtained Si-Hf-N ceramics are presented. The reaction between PHPS and TDMAH were characterized by FT-IR, Raman and solid state NMR spectroscopy and the reaction mechanism is discussed in Section 4.1.1. Then the polymer-to-ceramic transformation process and the crystallization behavior of the SiHfN ceramics are discussed in Section 4.1.2 and 4.1.3, followed by the high-angle annular dark-field (HAADF) STEM images of the nanostructures of the ceramics.

4.1.1 Synthesis of the SiHfN single-source precursors

The SiHfN single-source precursors were synthesized through the reaction between perhydropolysilazane (PHPS) and tetrakis(dimethylamido)hafnium(IV) ($Hf[N(CH_3)_2]_4$, TDMAH) at ambient temperature. In the present study, TDMAH was chose as the source of hafnium for two reasons: (i) TDMAH has a higher theoretical pyrolysis yield for the formation of HfN and less carbon residue in the ceramics, because of the smaller ligands ($-N(CH_3)_2$) relative to those of other alkylamide organometallic compounds such as $Hf[N(CH_3)(C_2H_5)]_4$ (TMEAH) or $Hf[N(C_2H_5)_2]_4$ (TDEAH); (ii) the large ligands of TDEAH may cause a lower reaction rate due to the steric hindrance during the nucleophilic attack of the PHPS and result in heterogeneous distribution of Hf in the precursors, which is not suitable for the fabrication of nanocomposites. Perhydropolysilazane (PHPS) has been considered as one of the most suitable precursors in forming high purity silicon nitride ceramics because it is composed of only silicon, nitrogen and hydrogen without other elements. Various PHPS were synthesized by the ammonolysis of dichlorosilane[183], and the structure of precursors, heat treatment conditions, convention mechanism as well as the structure and properties of PHPS derived ceramics have been widely and deeply studied. Additionally, the application of PHPS was also explored and it shows promising prospect in the fabrication of fibers[184], thin films[185] and coatings[186, 187].

The reaction was investigated by means of FT-IR and the spectra were shown in Fig. 4-1(a). Pure PHPS exhibits absorption bands at 3372 and 1171 cm^{-1} (N-H), 2137 cm^{-1} (Si-H), as well as at 840-1030 cm^{-1} (Si-N-Si). The FT-IR spectrum of TDMAH contains absorption bands corresponding to C-H bonds vibrations at 2948, 2822 and 2766 cm^{-1}; the absorption bands at 932 and 1251 cm^{-1} are characteristic vibrations of TDMAH and were assigned to the Hf-N-C units[188]. The FT-IR spectra of the as-synthesized SiHfN precursors with different hafnium content are also shown in Fig. 4-1(a) and reveal a decreasing tendency in the relative intensity of N-H and Si-H bands with the increase of TDMAH used for the modification of PHPS, indicating that a chemical reaction occurred between the PHPS and TDMAH.

However, the FT-IR spectra were not normalized, as there is not a sharp and characteristic absorption band which is stable in the reaction; Si-N-Si absorption band is stable in the modification reaction, however it is too broad to be used. In order to study the reaction between PHPS and TDMAH, FT-IR absorption peaks integrated area ratios between the Si-H and N-H bands in each SiHfN single-source precursor were calculated and the data are listed in Table 1. The integrated ratio between Si-H (2137 cm^{-1}) and N-H (3372 cm^{-1}) in pure PHPS is 6.77, and this value rises upon the modification of PHPS with TDMAH to reach a value as high as 28.05 in the single-source precursor for SiHfN-3; and then the ratio between Si-H (2137 cm^{-1}) and N-H (1171 cm^{-1}) showed the similar tendency. Consequently, the evolution of A(Si-H)/A(N-H) indicated that the N-H groups react with TDMAH and its reaction activity is higher than the Si-H groups in the modification reaction.

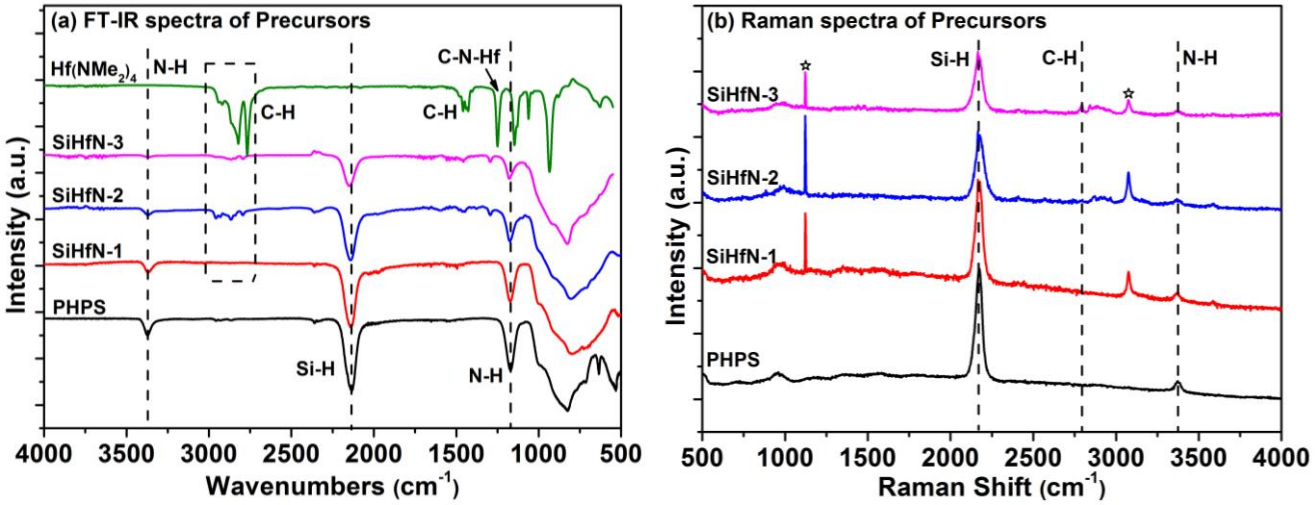

Fig. 4-1. FT-IR (a) and Raman (b) spectra of pure PHPS, TDMAH and SiHfN precursors with different hafnium content. (In (b), ☆ indicates residual toluene solvent in the samples).

Later, the reaction between PHPS and TDMAH was also characterized by means of Raman spectroscopy, and the Raman spectra and the peak area ratios of the bands assigned to Si-H and N-H from Raman spectra are shown in Fig. 4-1(b) and Table 1, respectively. The Raman spectra of SiHfN precursors are relatively simple, only Si-H (2175 cm^{-1}) and N-H (3375 cm^{-1}) showed apparently two peaks (except for the sharp peak at 1100 cm^{-1} which belonged to the residual toluene in the precursors), while the Raman peaks of C-H and Si-N bonds were negligible. And it displayed the same trend as observed by FT-IR spectroscopy, i.e. decrease of the intensity of

the Si-H (2175 cm^{-1}) and N-H (3375 cm^{-1}) bands as well as the faster reaction of N-H with TDMAH as compared to that of Si-H.

Table 1. Peak area ratios of the bands assigned to Si-H and N-H from FTIR and Raman spectra of different SiHfN single-source precursors.

	PHPS	SiHfN-1	SiHfN-2	SiHfN-3
Mass ratio of TDMAH : PHPS in the precursors	____	2 : 98	15 : 85	30 : 70
A(Si-H, 2137 cm^{-1})/A(N-H, 3372 cm^{-1}) in FT-IR spectra	6.77	10.92	18.61	28.05
A(Si-H, 2137 cm^{-1})/A(N-H, 1171 cm^{-1}) in FT-IR spectra	2.04	3.16	3.53	3.93
A(Si-H, 2175 cm^{-1})/A(N-H, 3375 cm^{-1}) in Raman spectra	12.11	16.52	23.97	26.08

To the best of our knowledge, the reaction between TDMAH and PHPS has not been reported yet. However, reactions of tetrakis(dimethylamido) titanium ($Ti[N(CH_3)_2]_4$, TDMAT) and tetrakis(diethylamido) titanium ($Ti[N(C_2H_5)_2]_4$, TDEAT) with N-H groups have been extensively studied. It has been reported that NH_3 can react with TDMAT in a transamination process[189, 190]. Weiller reported that TDMAT reacted rapidly with NH_3 even at room temperature in a transamination reaction to form $HNMe_2$, with the cleavage of a N-H bond being the rate limiting step (Equation. 1)[191].

$$Ti(NMe_2)_4 + NH_3 \leftrightarrow (Me_2N)_3Ti\text{-}NH_2 + HNMe_2 \qquad \text{(Equation 1)}$$

In a separate study[192], TDMAT was shown to react with NH_x-terminated Si(100) surfaces also upon transamination process as well as the elimination of $HNMe_2$ by-product. Moreover, it has been shown that the reaction of TDMAT with N-H groups is thermodynamically more favorable than the reaction between TDMAT and Si-H bonds[192], and this conclusion is in good agreement with our observation.

Based on the spectroscopic evidence and on related observations from literature, two possible (and parallel) pathways for the reaction between TDMAH and PHPS are proposed in Fig. 4-2. Firstly, the N-H bonds of PHPS reacted with TDMAH at room temperature in a transamination process leading to a hafnium modification of PHPS at N centers, and then $HNMe_2$ was released as gas by-product [Fig. 4-2(a)].

Based on the investigation results of spectroscopy, a large amount of $-NMe_2$ groups are found to remain in the single-precursors, some of them are from the $HNMe_2$ by-product, and another part of them belong to the unreacted $-Hf-NMe_2$. It is believed that steric hindrance takes most responsibility for the incomplete reaction of TDMAH. The direct connection between TDMAH and side groups and the PHPS backbone would hinder each other strongly and only every second N-H group with respect to PHPS polymer was supposed to be active in the amine displacement reaction [131].

For the reaction between Si-H groups and TDMAH, Aravind *et al.*[193] reported the reaction of (TDMAT) with self-assembled alkyltrichlorosilane monolayers (SAM) possessing –OH, $–NH_2$ and $–CH_3$ terminal groups, and the reaction probabilities followed the order $–OH > –NH_2 > –CH_3$ on the SAM terminated surfaces. It was also reported that TDMAH showed very high reactivity at the terminal $–NH_2$ group, the reaction could even be

carried out at temperature as low as -50 ℃ with the elimination of -$N(CH_3)_2$ ligands, and the extent of reaction was controlled by temperature and the steric limitation. Moreover, Li *et al.*[188] have also studied the reaction between TDMAH and hydrogen terminated Si(100) surface. The reaction may follow three paths leading to the formation of (i) Hf-Si (byproduct $HNMe_2$), (ii) Hf-N-Si (byproduct CH_4) or (iii) HfNC-Si bonds (byproduct H_2), and the calculated reaction energies were 10.2 kcal/mol, -21.3 kcal/mol and 8.7 kcal/mol, respectively. Moreover, the calculated bond dissociation energies at the CCSD(T)/CBS level was also reported and it roughly followed the order of Hf-O > Hf-N > N-H, C-H, Si-N > Si-H, Si-C > N-C, Hf-H > Hf-Si. According to the reaction energies above mentioned, it is obvious that the formation of Hf-N-Si linkage between TDMAH and Si-H groups is thermodynamically favored. However, on the one hand, it has been reported that for the reactivity of PHPS towards TDMAT, the polysilazane reacted with TDMAT only at the N-H groups, while the Si-H groups were not involved in the reaction. On the other hand, one research concerning the reaction between TDMAH and an allyl hydrido polycarbosilane (SMP10) was published recently[194], SMP10 is a silicon-based precursor containing only Si-H groups but no N-H groups, and this research clearly indicated that TDMAH reacted with the Si-H groups to form Si-N-Hf linkages and released CH_4. As can be seen from the references above, the chemical reaction of alkylamide organometallic compounds with silicon-based precursors is complicated. But it is obvious in the present work that TDMAH, unlike TDMAT, is involved in reaction with the Si-H groups of PHPS, which leads to the formation of Si-N-Hf linkages with the release of gaseous CH_4 by-product [Fig. 4-2(b)], and this reaction is minor.

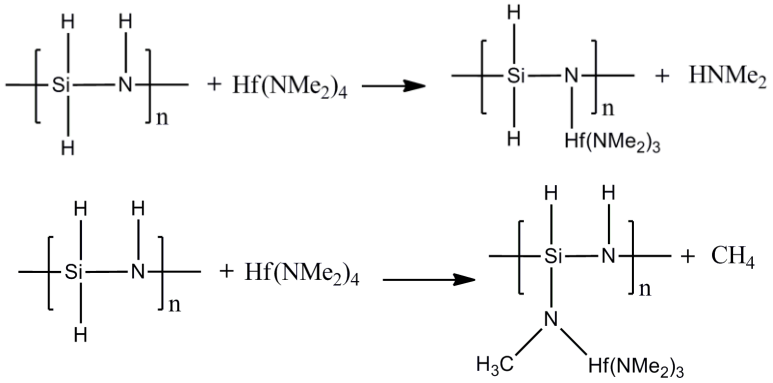

Fig. 4-2. Possible parallel pathways of the reaction between TDMAH and PHPS. The spectroscopic data suggest that the reaction (a) is significantly faster than reaction (b).

In order to further study the synthesis reaction between PHPS and TDMAH, solid state MAS NMR measurement was performed on the as-prepared SiHfN-3 single-source precursor. Both ^{13}C and ^{29}Si NMR spectra were measured by CP/MAS NMR. In Fig. 4-3(a), the ^{13}C NMR spectrum of the SiHfN-3 precursor exhibited a prominent chemical shift at 38.1 ppm which is attributed to the methyl groups bonded to the N atoms. The low-intensity peaks observed at 19.8 ppm (methyl groups bonded to benzene ring) as well as 120.6 and 128.9 ppm (carbon in the benzene ring) were assigned to the residual solvent toluene. As no Si-C bond was observed upon reacting PHPS and TDMAH, the reaction is considered to not occur via dehydrocoupling

mechanism, this result is consistent with the above mentioned calculated reaction energies of the reaction between Si-H and TDMAH [188], the dehydrocoupling reaction energy is positive and not favored in this system.

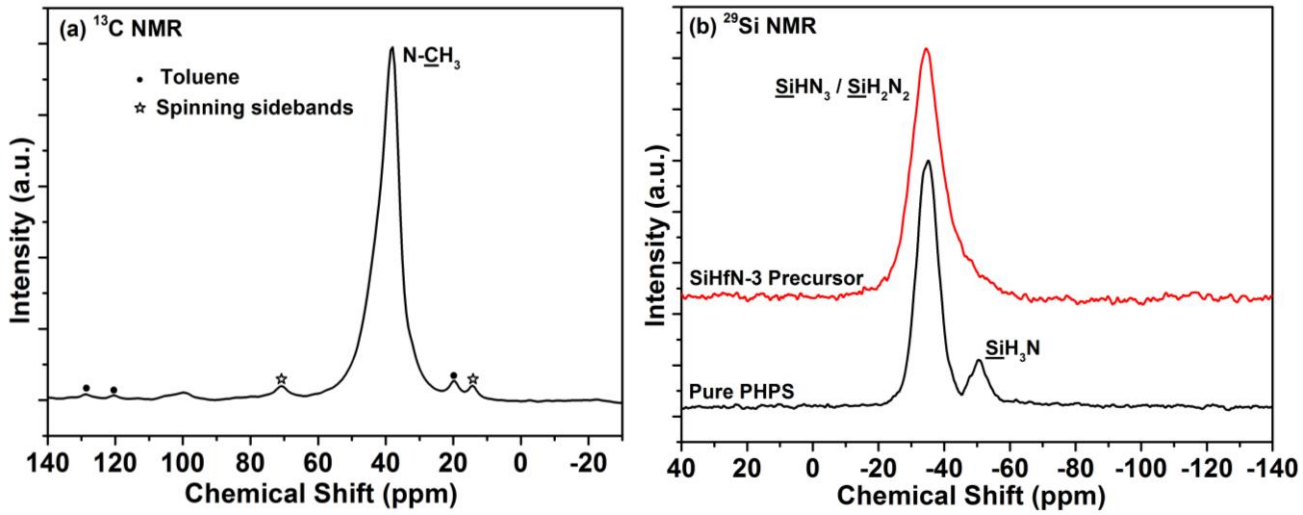

Fig. 4-3. CP/MAS NMR spectra of SiHfN-3 precursor: (a) ^{13}C NMR spectrum; (b) ^{29}Si NMR spectrum.

In Fig. 4-3(b), the ^{29}Si NMR spectrum of the pure PHPS exhibited two peaks, i.e. a signal at *ca.* -35 ppm which was assigned to SiHN_3/ SiH_2N_2 sites and a signal at -50 ppm attributed to SiH_3N end groups of PHPS[195, 196]. It is considered that the SiHfN precursor contained pendant -N$(CH_3)_2$ groups and inter-ring -N$(CH_3)_2$-containing bridge, which may improve the extent of the polymeric network up to a relatively high molecular weight and contribute to further cross-linking. While in the ^{29}Si NMR spectrum of the SiHfN-3 precursor, the SiH_3N peak almost disappeared, thus providing clear evidence that Si-H groups of PHPS were consumed in the reaction with TDMAH. Moreover, the ^{29}Si NMR spectrum did not show any signals related to Si-Hf or Si-CNHf bonds. Consequently, it is clear that the reaction of Si-H bonds with TDMAH occurred via the formation Si-N-Hf linkages. It can also be inferred from this result that only a part of Si-H groups reacted with TDMAH, and it was believed that most of the reactions happened on the SiH_3N end groups of PHPS according to the solid NMR spectrum, this was because that the end groups had more available Si-H groups for the reaction and lower steric hindrance. Therefore, large amounts of Si-H bonds were still present in the precursor after the modification with TDMAH. This is consistent with the spectroscopic results, which indicates that TDMAH reacts faster with the N-H bonds than with the Si-H groups of PHPS.

As the reaction of PHPS with TDMAH induces the strong decrease of N-H groups and SiH_3N end groups in the polymers (i.e., they get cross-linked via ≡Hf-N-Si≡ linkages), it was expected that the Hf-modified single-source precursors exhibited significantly higher degree of cross-linking and would provide higher ceramic yield as compared to that of the pure PHPS. The ^{29}Si MAS NMR peak area ratio between SiHN_3/SiH_2N_2 and SiH_3N in pure PHPS is 6.8 : 1 (i.e., the site fraction of the end groups SiH_3N accounted for 12.8%); whereas the SiH_3N site fraction in the Hf-modified PHPS was less than 5%. Consequently, the ceramic yield of the SiHfN-3 precursor was found to be significantly higher than that of pure PHPS, as discussed below (see Table 2).

In conclusion, the FT-IR, Raman and solid state MAS NMR spectroscopic data related to the reaction of PHPS with TDMAH indicated that both N-H and Si-H bonds were reactive sites, and the possible reaction pathways are shown in Fig. 4-2. The reaction between N-H groups and TDMAH is predominant, and it leads to the formation of ≡Hf-N-Si≡ with the release of $HNMe_2$ by-product; the reaction of Si-H groups with TDMAH is secondary but it also takes place and promotes the cross-linking. The modification of PHPS with TDMAH not only introduced hafnium into the polymer precursor at the molecular level, but also improved the cross-linking degree of the single-source precursor and consequently its ceramic yield.

4.1.2 Polymer-to-ceramic transformation of SiHfN ceramics

Usually, metal nitrides can be obtained by ammonolysis of metal amides[197], with a significant mass loss due to the elimination of amine (HNR_2) and ammonia by-product in the heating temperature range 200 - 400 ℃, and it was reported that the nitrogen content of the nitrides was derived from ammonia and not from the parent amide. Additionally, nitrogen-rich Hf_3N_4 powders can also be simply synthesized via a slow and gentle ammonolysis of hafnium dialkylamides, the obtained Hf_3N_4 powders are crystalline with a rhombohedrally distorted NaCl-type structure[198]. Therefore, in order to increase the nitrogen content of the ceramics, SiHfN precursors were pyrolyzed in flowing ammonia.

In the present work, PHPS and the SiHfN single-source precursors were all pyrolyzed at 1000 ℃ in ammonia atmosphere for 3 h to produce silicon nitride and SiHfN ceramics, respectively. The XRD measurements showed that the as-obtained silicon nitride and SiHfN ceramics were all X-ray amorphous. The ceramic yield of the SiHfN ceramics modified with different content of TDMAH was in the range of 83.5-92.3 wt.% and was found to be improved with increasing the content of TDMAH in feed, while the ceramic yield of pure PHPS was 82.7 wt.% (Table 2). The incorporation of TDMAH within the PHPS precursor has shown a good promotion for the cross-linking and resulted in an increase of the ceramic yield. It is well-known that the ceramic yield of a polymeric precursor can be significantly improved by a previous cross-link treatment before the pyrolysis. In the SiHfN system, the SiHfN precursors were already cross-linked via the chemical modification reaction process, apparently, the SiHfN precursors were solid powders rather than PHPS which was sticky liquid. Accompanying with the cross-linking and the increase of the molecular weight, the low-molecular-weight oligomers were connected with each other and then the decomposition and evaporation of these oligomer efficiently reduced in the ammonolysis process, as a result, the weight loss of the SiHfN precursors was greatly restrained. In Table 2, it can be found that the ceramic yield of SiHfN-1 was higher than PHPS but the increase was insignificant, because only 2 wt.% TDMAH was added into the precursors and the changes was extremely limited. When the addition of TDMAH was raised to 15 wt.%, the improvement of ceramic yield became apparent; while in SiHfN-3, even the addition of TDMAH was as much as 30 wt.%, but the ceramic yield is only 1.7 wt.% higher than that of SiHfN-2, this is because that excess TDMAH cannot react with PHPS completely due to the reactivity and steric hindrance, and lots of $–NMe_2$ ligands would remain in the

precursors and then decompose during the polymer-to-ceramic transformation, finally affected the ceramic yield negatively.

Table 2. Ceramic yield of different precursors pyrolyzed at 1000 ℃ for 3 h in ammonia atmosphere.

Sample	PHPS	SiHfN-1	SiHfN-2	SiHfN-3
Ceramic Yield (wt.%)	82.7	83.5	90.6	92.3

The precursors were heat-treated at different temperatures under NH_3 atmosphere for 3 h, and then the structural evolution during the polymer-to-ceramic transformation of the single-source precursor PHPS and SiHfN-3 was researched by FT-IR and Raman spectroscopy measurements and the spectra were shown in Fig. 4-4. In Fig. 4-4(a) and (c), with the temperature increasing from room temperature (RT) to 300 ℃, the intensity of Si-H peak significantly decreased, due to the cross-linking reaction *via* dehydrocouplings (Si-H/Si-H and Si-H/N-H). As already reported, the dehydrocoupling of Si-H/Si-H bonds started at higher temperatures (*ca.* 300 ℃) (see Equation 2)[199]. The intensity of N-H peak at 3372 cm^{-1} also decreased, due to both the dehydrocoupling (Si-H/N-H, see Equation 3) and the transamination reaction (Equation 4) which was previously reported[200, 201]. Besides, the precursors were pyrolyzed in ammonia atmosphere, then the Si-H bonds could react with NH_3, which was beneficial to promote the cross-linking and enhance the nitrogen content of the resultant ceramics. At 500 ℃, the N-H absorption peaks almost vanished, indicating that the dehydrocoupling and transamination reactions were almost completed. At 700 ℃, Si-N-Si peak and a small peak assigned to Si-H remained in the spectra. With the pyrolysis temperature increasing, the peak of Si-H would eventually disappear at higher temperature, while Si-N peak would become sharper due to the crystallization of the pyrolyzed products.

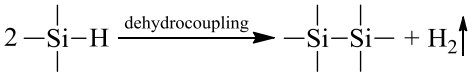

(Equation 2)

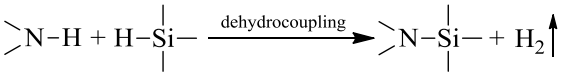

(Equation 3)

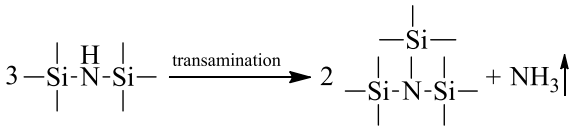

(Equation 4)

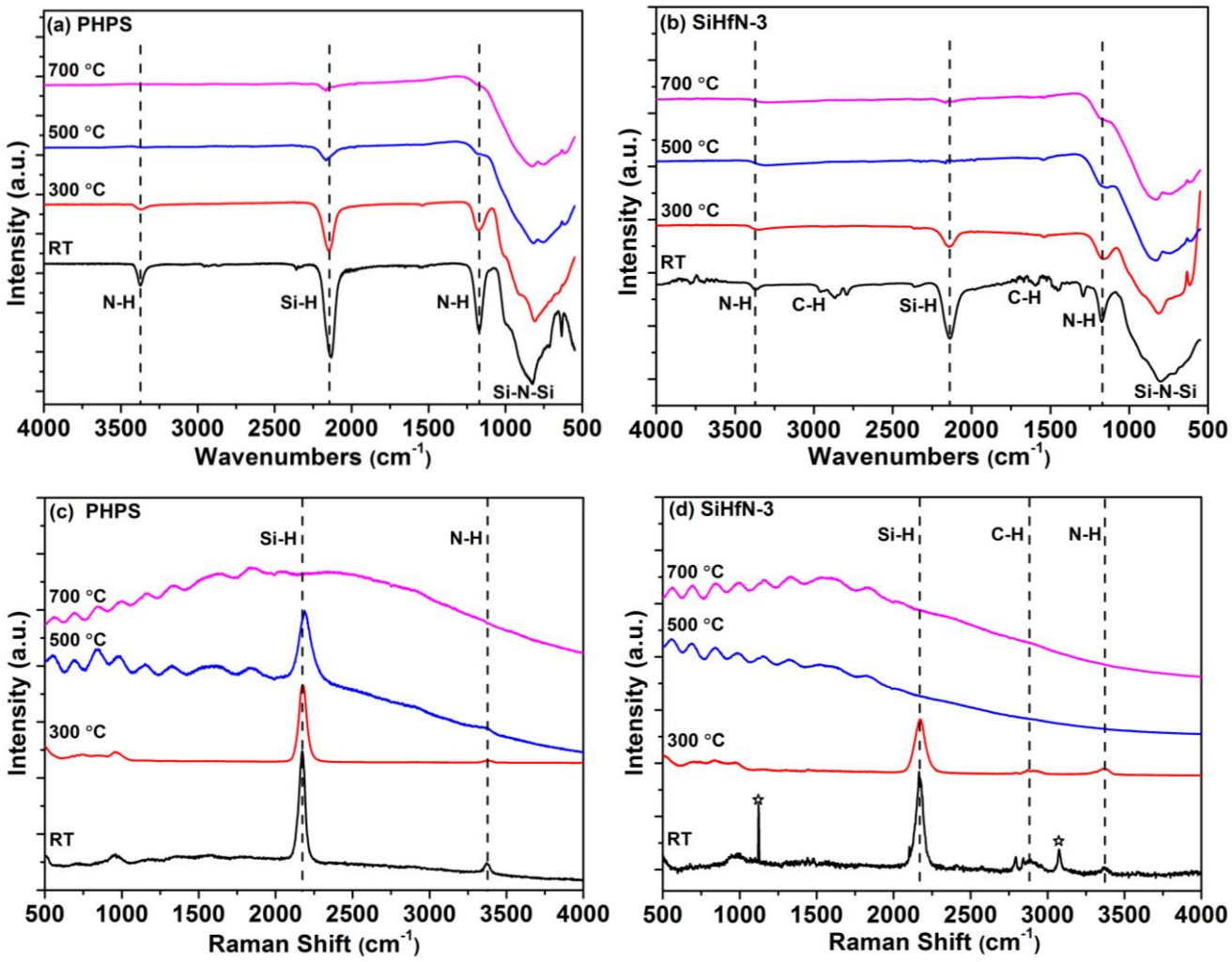

Fig. 4-4. FT-IR and Raman spectra of PHPS and SiHfN-3 heat-treated at different temperatures in ammonia atmosphere: (a,c) FT-IR and Raman spectra of PHPS; (b,d) FT-IR and Raman spectra of SiHfN-3.

However, as shown in Fig. 4-4(b) and (d), in the beginning, the intensities of the N-H, Si-H and N-CH_3 absorptions also decreased significantly with the temperature increasing from R.T. to 300 ℃, these changes were similar with the trend of pure PHPS heat-treated at the same temperature. Except for the dehydrocoupling and transamination reactions mentioned above, the decrease of the intensities of the Si-H and N-H vibrations can also be attributed to the further reaction between the N-CH_3 ligands of TDMAH and the N-H/Si-H groups of PHPS (see Fig. 4-2), and these reactions also consumed the N-CH_3 groups of the precursors, this explained that why the functional groups (Si-H, N-H and N-CH_3) in SiHfN-3 consumed faster than those of PHPS. As a result, in the spectra of 300 ℃-treated SiHfN-3, the absorption peaks of N-H and N-CH_3 nearly disappeared, and only a weak peak of Si-H remained, which is analogous to the results of 500 ℃-treated pure PHPS. Additionally, residual ≡Hf-NMe_2 can take an ammonolysis reaction with NH_3 during heating (see Equation 5) [198], which further improved the cross-linking degree of the sample without nitrogen losses. When temperature reached 500 ℃, the absorption peaks for all the N-H, Si-H as well as N-CH_3 were totally disappeared in both FT-IR and Raman spectra, and only a broad peak remained at around 800 - 1000 cm^{-1}. The characteristic band of Hf-N-C at

about 932 cm^{-1} still existed and it was overlapped with broad Si-N peaks. At 700 ℃, there was not an obvious variation in the spectra.

$$\equiv Hf\text{-}NMe_2 + NH_3 \rightarrow \equiv Hf\text{-}N + HNMe_2 \quad \text{(Equation 5)}$$

By comparing, it was found that the Si-H and N-H functional groups were consumed completely in 500 ℃-treated SiHfN-3, while a little Si-H groups still remained in 700 ℃-treated pure PHPS, which indicated that, in the pyrolysis process, the SiHfN-3 precursors reacted and cross-linked faster and more complete than pure PHPS. Then it can be deduced that the modification with TDMAH promoted the cross-linking reaction between each functional groups, improved the cross-linking and ceramization of precursors, and increased the ceramic yield in the end.

4.1.3 Microstructural evolution and crystallization behavior of SiHfN ceramics

Elemental analysis (EA) data are shown in Table 3 and reveal that the ammonolysis of the SiHfN-3 precursor at 1000 ℃ furnishes a ceramic with the composition $Si_1Hf_{0.056}N_{1.32}$. The carbon and oxygen contents in the as-prepared ceramic were found to be lower than 2 wt.% and 1 wt.%, respectively. It is worthy to note that a strong influence of TDMAH on the chemical composition of the resulting SiHfN ceramics was observed. It can be seen clearly in Table 3 that the N/Si molar ratio of SiHfN ceramics (N/Si = 1.32 in 1000 ℃-obtained SiHfN-3) is significantly higher than that of the PHPS-derived material (N/Si = 0.71 in 1000 ℃-obtained PHPS). In fact, the pure PHPS derived ceramic is rich in silicon. Thus, despite the fact that the thermal treatment was performed in reactive ammonia atmosphere, the PHPS-derived SiN_x ceramic still exhibited ca. 47 mol.% of excess silicon.

Table 3. Elemental analysis of the pyrolyzed SiHfN ceramics.

Specimens	Composition[(a)]					Empirical formula
	Si	Hf	N	C	O	
PHPS(1000 ℃ in NH_3)	72.9	0	25.89	0.11	1.04	$Si_1N_{0.71}(C_{0.003}O_{0.025})$
SiHfN-3(1000 ℃ in NH_3)	47.1	16.7	31.08	1.31	1.03	$Si_1Hf_{0.056}N_{1.32}(C_{0.065}O_{0.038})$
SiHfN-3(1400 ℃ in N_2)	47.0	16.2	33.84	1.82	1.29	$Si_1Hf_{0.054}N_{1.44}(C_{0.09}O_{0.048})$
SiHfN-3(1600 ℃ in N_2)	49.0	17.4	31.49	1.50	0.56	$Si_1Hf_{0.056}N_{1.28}(C_{0.071}O_{0.02})$

[(a)] The hydrogen content of PHPS was neglected

The modification of PHPS with TDMAH leads to a strong enrichment in nitrogen in the resulting SiHfN ceramics. This indicates that firstly TDMAH is not only the hafnium source, but also the nitrogen source, a large amount of nitrogen was introduced into the sample via the ligands of TDMAH; secondly, the Hf-containing single-source precursors reacted with ammonia during the polymer-to-ceramic conversion and thus their nitrogen content is significantly higher than that of the silicon nitride resulting from the ammonolysis of PHPS. Thus, the modification of PHPS with TDMAH does not merely improve the cross-linking degree of the polymeric precursors (and consequently the ceramic yield), but also facilitate the reaction between the precursors and ammonia and therefore significantly increases the nitrogen content in the resultant SiHfN

ceramics. According to bond dissociation energy values (BDE) followed as Hf-N > Si-N > Si-C > Si-Hf[188], introduction of more nitrogen is beneficial to the formation of high temperature resistant HfN and Si_3N_4, and the stability of the SiHfN materials will be improved.

The Raman spectra of PHPS and SiHfN-3 annealed at different temperatures are shown in Fig. 4-5(a, b). The Raman spectra of silicon nitride prepared upon ammonolysis of PHPS and annealed at different temperatures [Fig. 4-5(a)] exhibit an absorption band at 521 cm^{-1}, indicating the presence of segregated elemental silicon. Interestingly, the intensity of the absorption band seems to increase as the annealing temperature increases, which might be a consequence of some decomposition of Si_3N_4 into elements at high temperature (cf., Si_3N_4 = 3 Si + 2 N_2), which furnishes additional segregated silicon within the material. However, the silicon absorption band was not observed in the as-prepared SiHfN-3 [Fig. 4-5(b)]. However, annealing of SiHfN-3 at high temperatures leads to the appearance of two Raman absorption bands located at 1351 cm^{-1} and 1602 cm^{-1}, which were assigned to the presence of small amounts of segregated carbon within the samples. The results of Raman characterization are consistent with the EA data, and the two measurements indicate that the pure silicon nitride ceramic is rich in silicon, while SiHfN-3 ceramic is not; and they also show that there is some residue of carbon in the SiHfN ceramics which is from the TDAMH, and it exists in the form of free carbon.

FT-IR measurements of the annealed ceramics were also performed and the results are shown in Fig. 4-5 (c, d). After ammonolysis at 1000 ℃ for 3 h, although it was generally accepted that the polymer-to-ceramic transformation almost completed at 1000 ℃, but the PHPS-derived ceramic still retained a small amount of Si-H bonds, and this peak vanished gradually in the higher temperature treatment. By further increasing the annealing temperature, the Si-N vibration located at about 800-1100 cm^{-1} had no significant changes. While in the FT-IR spectrum of the 1000 ℃-obtained SiHfN-3 sample, the Si-H absorption peak was not found, indicating that Si-H groups were exhausted in the pyrolysis process and the transformation of SiHfN precursors was more complete than that of PHPS. Only a broad peak was observed at around 800-1200 cm^{-1}, composed by the mixture of Si-N and Hf-N or even Si-N-Hf/C-N-Hf peaks, and this result accorded with the nature of the as-obtained single-phase ceramic. With further increasing the annealing temperature, the absorption peaks got separated and become sharper, along with an increase in the intensities of those peaks, due to the crystallization and phase separation from the amorphous SiHfN composite. After heat-treatment of the samples at 1600 ℃, the SiHfN-3 ceramics displayed three broad absorption bands which were mostly attributed to the vibrations of Si-N (at *ca.* 1047, 934, 854 and 570 cm^{-1}). By further increasing the temperature to 1800 ℃, the intensities of three peaks became stronger and sharper, owing to the further phase separation and grain growth at high temperature.

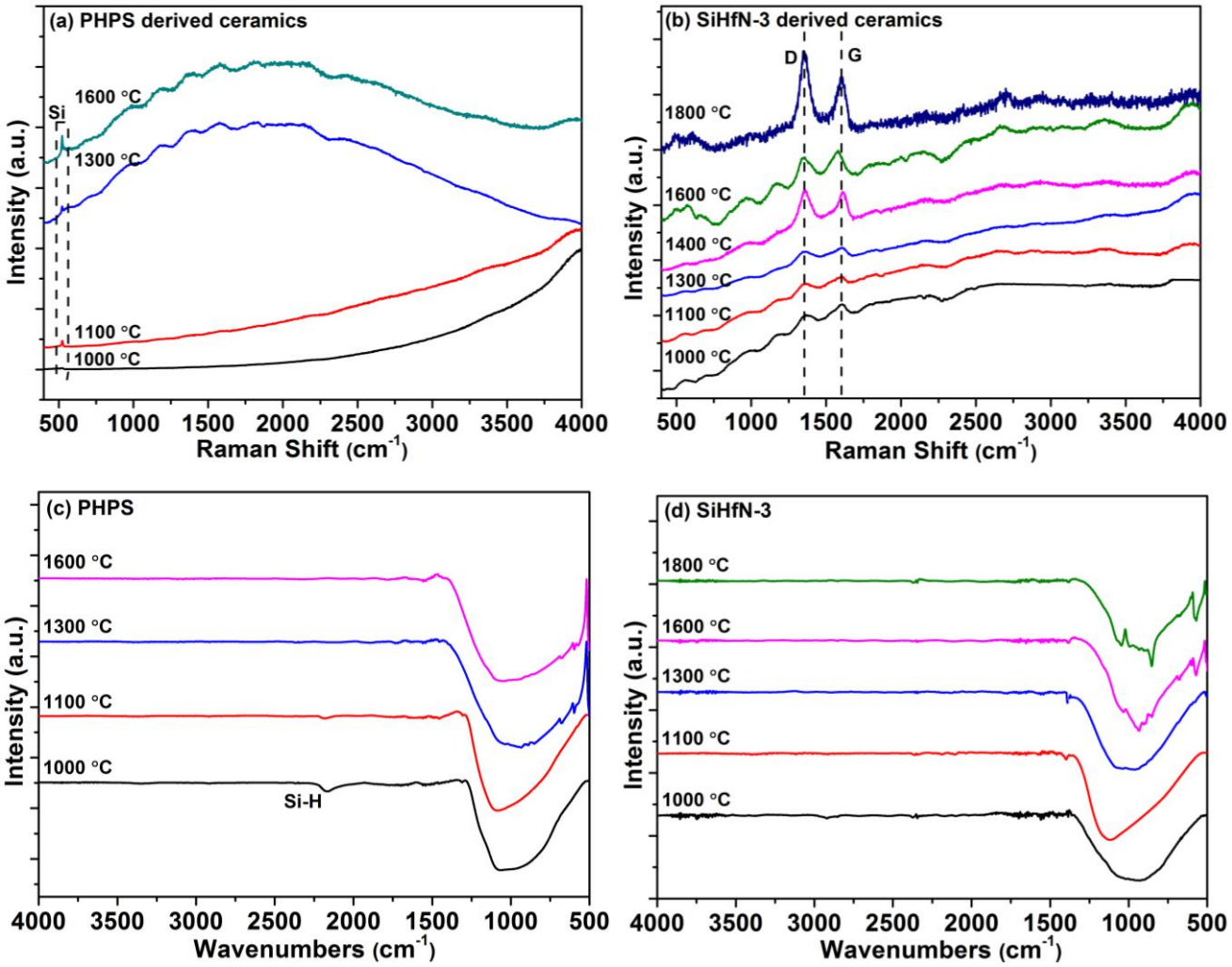

Fig. 4-5. (a, b) Raman spectra and (c, d) FT-IR spectra of PHPS-derived silicon nitride and SiHfN-3 annealed at different temperatures.

In order to assess the crystallization behavior of the SiHfN ceramics, X-ray powder diffraction measurement of the materials sintered at different temperatures were carried out and the XRD patterns are shown in Fig. 4-6. The 1000 ℃ as-prepared PHPS-derived silicon nitride is X-ray amorphous; whereas the sample annealed at 1100 ℃ exhibits broad, low-intensity reflections which were assigned to cubic silicon, this is consistent with the results obtained from EA and Raman spectroscopy mentioned above, pure PHPS-derived ceramic is rich in silicon. Annealing of silicon nitride at higher temperatures in nitrogen atmosphere leads to the crystallization of α-Si_3N_4 and β-Si_3N_4, as shown by the XRD pattern of the samples annealed at 1300 ℃ [Fig. 4-6(a)], and the α-Si_3N_4 phase is predominant in the composite, demonstrating that the pure PHPS-derived ceramic started the crystallization and phase separation at temperature below 1300 ℃. At 1600 ℃, the diffraction peaks of both α- and β-Si_3N_4 became intensive and sharper, suggesting the grain coarsening of the crystallites. Obvious transformation occurred at 1800 ℃, most of the α-Si_3N_4 was phase transformed to β-Si_3N_4; moreover, strong peaks assigned to crystalline cubic silicon were observed in the pattern again, indicating the decomposition of silicon nitride at such high temperature.

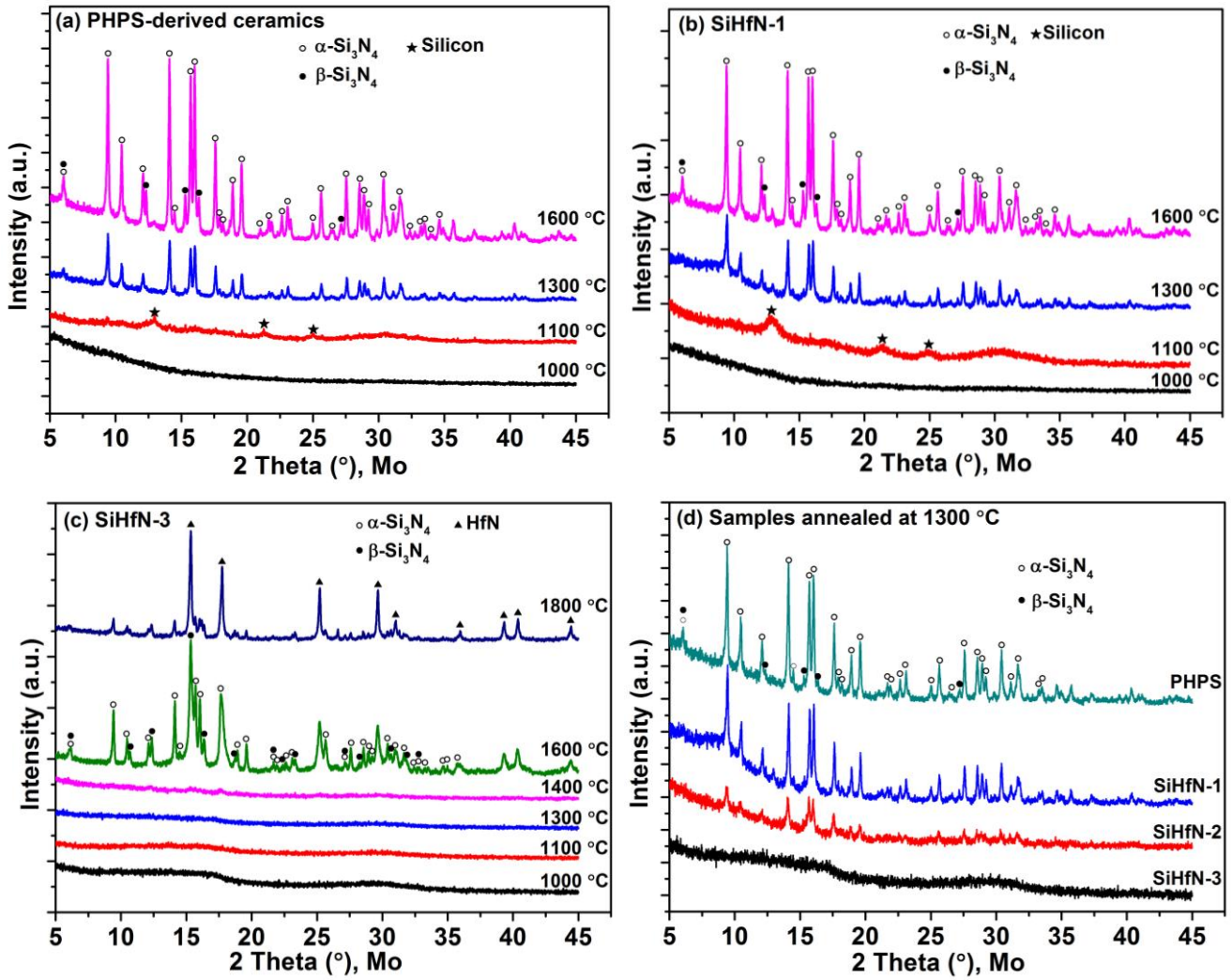

Fig. 4-6. XRD patterns of pure PHPS-derived and SiHfN ceramics annealed at different temperatures.

The XRD patterns of SiHfN-1 ceramic annealed at different temperatures [Fig. 4-6(b)] were found to have no obvious difference with respect to those of PHPS-derived silicon nitride; thus, very small amounts of TDMAH in the single-source precursor (i.e., small amounts of Hf in SiHfN ceramics) did not show a significant impact on the crystallization behavior of silicon nitride ceramics. Nevertheless, as the Hf content in SiHfN ceramics increased [as for SiHfN-3, see Fig. 4-6(c)], significant effect of Hf on the crystallization behavior was observed. In particular, the SiHfN-3 samples annealed at temperatures up to 1400 ℃ were found to maintain X-ray amorphous, unlike the Hf-free silicon nitride samples. This result clearly indicates that the incorporation of appropriate amount of Hf within silicon nitride can effectively suppress the crystallization of Si_3N_4. Annealing of SiHfN-3 at 1600 and 1800 ℃ induced the further crystallization of α-Si_3N_4 and β-Si_3N_4 as well as of cubic HfN. As a result, the single-phase SiHfN-3 sample seemed to undergo upon annealing at high temperature phase separation and crystallization processes and converts into HfN/Si_3N_4 nanocomposites. It was reported that cubic HfN and HfC were able to form complete quasi-binary solid solutions , since that both of them were interstitial compounds with the face center cubic (fcc) structure and the difference of the covalent radii of the N and C atoms was only 2.6%[202, 203]. However, the reflections of the HfN phase of SiHfN-3 did not show any shifts

along *2θ* values with increasing the sintering temperature, this result demonstrate that free carbon did not react with HfN in our case.

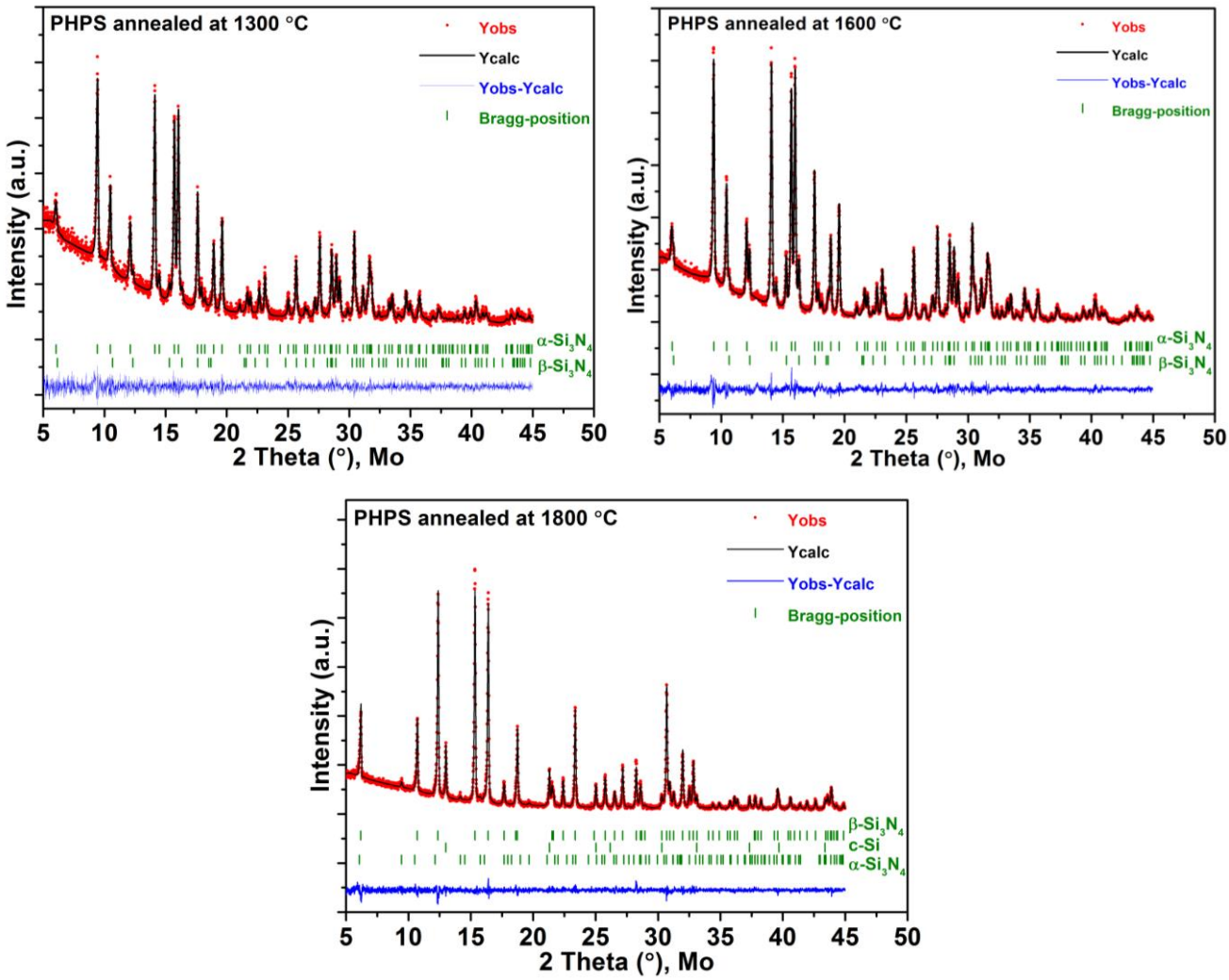

Fig. 4-7. Rietveld refinement of the XRD patterns of PHPS-derived silicon nitride annealed at different temperatures.

(Green tick marks are Bragg peak positions of c-Si, α-Si_3N_4 and β-Si_3N_4. The blue line at the bottom of each XRD pattern denotes the difference intensities between the observed and calculated profiles)

The XRD patterns of selected samples were refined by Rietveld refinement (PHPS and SiHfN-3 ceramics annealed at different temperatures are shown in Fig. 4-7 and Fig. 4-8, respectively), and the volume fractions, grain sizes and lattice constants of Si_3N_4 and HfN obtained from Full-Profile Rietveld refinement are listed in Table 4 and Table 5, correspondingly. The refined XRD pattern of the PHPS-derived silicon nitride indicated that the predominant phase in the ceramic was α-Si_3N_4 before 1800 ℃, which was supported by the reports that α-Si_3N_4 was the stable phase of silicon nitride at low temperature and it usually transformed into the β-phase at temperature higher than 1600 ℃ without additives[204, 205]. In the 1300 ℃ heat-treated sample, the volume fraction of α-Si_3N_4 was 95.3%, the rest being β-Si_3N_4 and small amount of cubic silicon, and in the 1600 ℃ heat-treated sample, the volume fraction of α-Si_3N_4 dropped to 90.97%, with the increase of the β-Si_3N_4 portion.

At 1800 ℃, the content of β-Si_3N_4 crystallites raised to 89.76%, accompany with 3.37% cubic-Si, with very small amount of α-Si_3N_4. The grain size grew significantly with the increasing temperature, and the grain size of both c-Si and β-Si_3N_4 reached *ca.* 100 nm at 1800 ℃. The α- to β-Si_3N_4 phase transformation was thought to be critical to the densification of Si_3N_4, and the presence of liquid silicon promoted the α- to β-Si_3N_4 phase transformation at relative low temperature[206].

The assessment of the XRD pattern of SiHfN-3 annealed at 1600 ℃ revealed a crystalline phase composition consisting of HfN (21.04 wt.%), α-Si_3N_4 (67.27 wt.%) and β-Si_3N_4 (11.69 wt.%). The fractions of the three crystalline phases determined by Rietveld refinement were in excellent agreement with the elemental analysis data (e.g., from EA data, a HfN content of 19.27 wt.% is calculated). The grain size of HfN in SiHfN-3 sample annealed at 1600 °C was determined to be 9.4 nm and the grain size of α-Si_3N_4 / β-Si_3N_4 was 35.5 / 28.3 nm, respectively. Interestingly, the grain size of the two crystal forms of Si_3N_4 phases in SiHfN-3 was found to be both lower than that of the Si_3N_4 phases found in the PHPS-derived sample annealed at the same temperature (α-Si_3N_4: 40.3 nm; β-Si_3N_4: 56.9 nm), indicating that the presence of HfN in SiHfN-3 significantly affects the grain growth of silicon nitride. In fact, even in the 1600 ℃-annealed SiHfN-2 ceramic, the grain size of 1600 ℃-obtained SiHfN was at the same level with 1300 ℃-obtained PHPS, proved that the grain coarsening was greatly suppressed. Furthermore, the content of crystalline HfN in both SiHfN-2 and 3 was largely in line with the weight ratio of TDMAH/PHPS in the precursors.

Table 4. Phase composition of the samples shown in Fig. 4-7, as from Rietveld refinement of the XRD patterns.

Specimens	c-Si (*Fd-3m*, Nr. 227)	α-Si_3N_4 (P31c, Nr. 159)	β-Si_3N_4 ($P6_3/m$, Nr. 176)	R-factors
1300 ℃ annealed PHPS	——	95.30 v.% a=7.76061 Å, c=5.62209 Å Grain size: 35.6 nm	4.70 v.% a=7.62369 Å, c=2.90937 Å Grain size: 30.7 nm	Rp: 5.80 Rwp: 7.56 Rexp: 7.63
1600 ℃ annealed PHPS	——	90.97 v.% a=7.78138 Å, c=5.62899 Å Grain size: 40.3 nm	9.03 v.% a=7.63205 Å, c=2.91382 Å Grain size: 56.9 nm	Rp: 4.65 Rwp: 6.03 Rexp: 5.18
1800 ℃ annealed PHPS	3.37 v.% a=5.42736 Å Grain size: 100.0 nm	6.88 v.% a=7.74413 Å, c=5.60963 Å Grain size: 32.7 nm	89.76 v.% a=7.60052 Å, c=2.90625 Å Grain size: 82.8 nm	Rp: 5.27 Rwp: 6.84 Rexp: 6.24

The SiHfN-3 sample annealed at 1800 ℃ was found to consist of HfN (27.65 wt.%), α-Si_3N_4 (54.16 wt.%) and β-Si_3N_4 (18.19 wt.%). This suggested that the mass fraction of HfN and β-Si_3N_4 increased upon increasing the annealing temperature. Cubic-Si crystal was not detected in the XRD patterns of SiHfN-3 ceramics, and it is in agreement with the previous EA and Raman characterizations. It was noteworthy that α-Si_3N_4 was still the main crystal phase in the composite, which was quite different with the observation of PHPS, meaning that the α- to β-Si_3N_4 phase transformation was successfully depressed by the modification with TDMAH. On the basis of the above results, it clearly supports the assumption that the extraordinary high temperature stability of the resulting

SiHfN ceramics was related to the formation of HfN in the matrix, the Si_3N_4 phase transformation and the decomposition of Si_3N_4 at high temperature were both effectively inhibited.

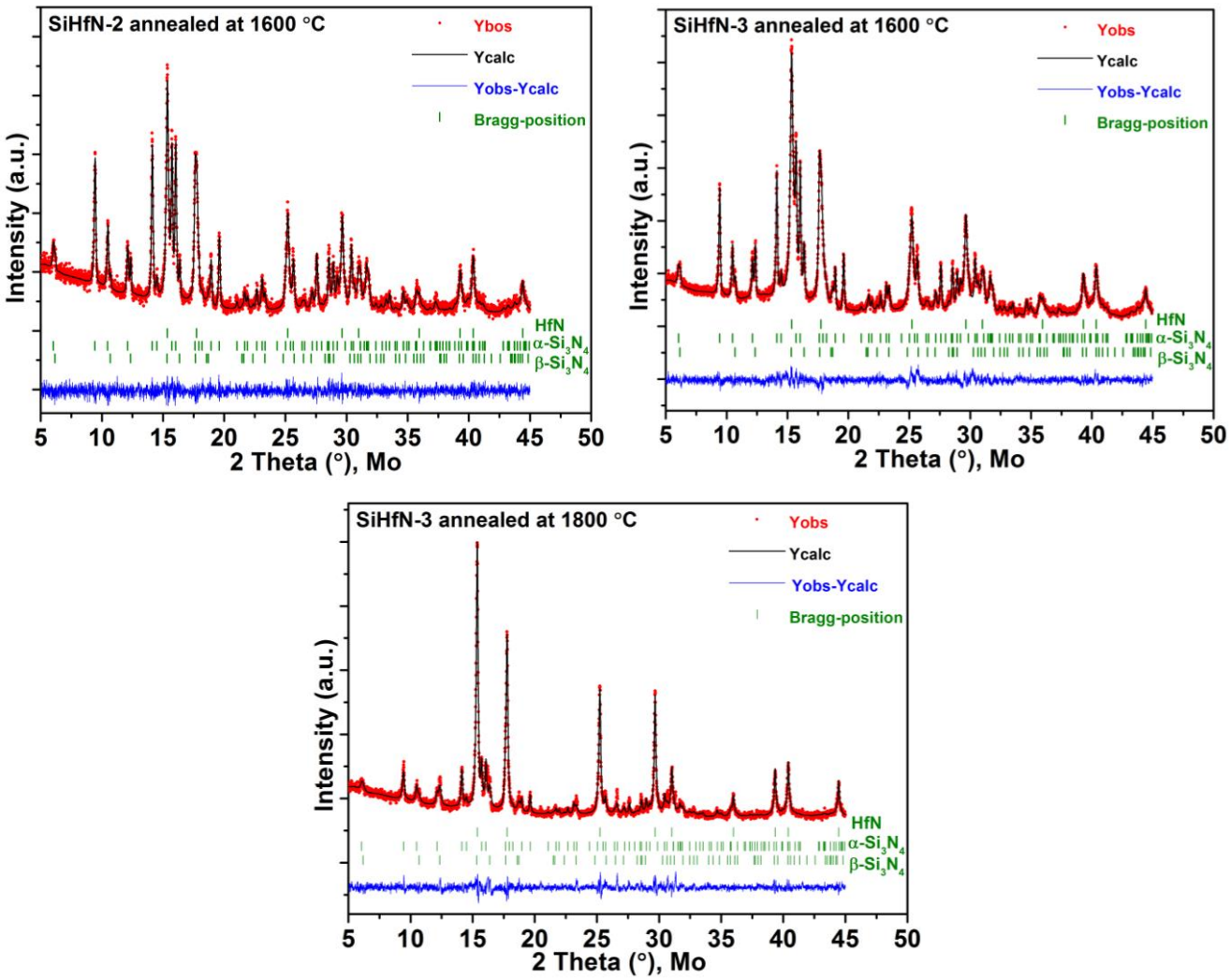

Fig. 4-8. Rietveld refinement of the XRD patterns of SiHfN-3 ceramics annealed at different temperatures (Green tick marks are Bragg peak positions of HfN, α-Si_3N_4 and β-Si_3N_4. The blue line at the bottom of each XRD pattern denotes the difference intensities between the observed and calculated profiles).

The ^{29}Si MAS NMR spectrum of the as-prepared SiHfN-3 is shown in Fig. 4-9(a) and reveals the presence of three signals -39.8, -47.8 and -51.9 ppm. The signals with chemical shifts at -39.8 and -47.8 ppm were assigned to SiN_4 sites. The difference in the chemical shift of the two signals comes from the environment at the SiN_4 sites. Thus, the signal at -47.8 ppm exhibits a typical chemical shift for SiN_4 sites in silicon nitride ceramics[207]; whereas the signal at -39.8 ppm is strongly low-field shifted, which is considered to be a consequence of the presence of hafnium attached to SiN_4 via nitrogen [see Fig. 4-9(a)]. This effect was also reported in SiHfCNO and SiHfOC materials prepared from hafnium-alkoxide-modified polysilazanes and polysiloxanes, respectively[208]. The third signal in the NMR spectrum of the PHPS derived silicon nitride (chemical shift at -51.9 ppm) was assigned to SiN_3H and it indicates that some hydrogen is retained in the as-prepared sample.

Table 5. Phase composition of the samples shown in Fig. 4-8, as from Rietveld refinement of the XRD patterns.

Specimens	HfN (*Fm-3m*, Nr. 225)	α-Si_3N_4 (P31c, Nr. 159)	β-Si_3N_4 ($P6_3$/m, Nr. 176)	R-factors
1600 ℃ annealed SiHfN-2	11.36 v.% a=4.59803 Å	77.37 v.% a=7.76869 Å, c=5.61992 Å	11.27 v.% a=7.61775 Å, c=2.90614 Å	Rp: 5.51 Rwp: 7.05 Rexp: 7.19
	Grain size: 15.1 nm	Grain size: 30.3 nm	Grain size: 39.4 nm	
1600 ℃ annealed SiHfN-3	21.04 v.% a=4.59868 Å	67.27 v.% a=7.76662 Å, c=5.62837 Å	11.69 v.% a=7.61756 Å, c=2.90811 Å	Rp: 4.58 Rwp: 5.94 Rexp: 4.08
	Grain size: 9.4 nm	Grain size: 35.5 nm	Grain size: 28.3 nm	
1800 ℃ annealed SiHfN-3	27.65 v.% a=4.59424 Å	54.16 v.% a=7.75837 Å, c=5.62148 Å	18.19 v.% a=7.60688 Å, c=2.91110 Å	Rp: 5.27 Rwp: 6.84 Rexp: 6.24
	Grain size: 31.4 nm	Grain size: 50.6 nm	Grain size: 52.9 nm	

The ^{29}Si spectrum of SiHfN-3 annealed at 1300 ℃ is shown in Fig. 4-9(b) and exhibits the presence of a narrow and symmetric peak at -49.3 ppm, revealing the presence of SiN_4 sites typical for crystalline silicon nitride. Interestingly the signal was not low-field shifted as observed in the as-prepared SiHfN-3 sample. This strongly indicates that at 1300 ℃ the phase separation of hafnium nitride occurs (note that the sample was X-ray amorphous, thus the sample can be described as an amorphous HfN_x/SiN_x nanocomposite). Furthermore, no SiN_xH_{4-x} sites were detected in the NMR spectrum, indicating that the hydrogen was released from the sample upon annealing at 1300 ℃. By further raising the temperature, the SiN_4 peak at -49.3 ppm splitted into two separated peaks sited at -45.5 and -48.5 ppm [in Fig. 4-9(c)]. The two main peaks belong to the α-Si_3N_4 or the mixed peaks of α- and β-phases, because the α-phase contains two unique silicon positions, while β-Si_3N_4 contains an additional center of inversion and has only one unique site, then it reveals only one peak in its MAS NMR spectrum[207]. This result agreed well with the measurements of standard α- and β-Si_3N_4 published[209, 210], and demonstrated very good agreement with the XRD patterns, meaning that the 1600 ℃ annealed SiHfN-3 was highly crystallized and the predominant phase was α-Si_3N_4.

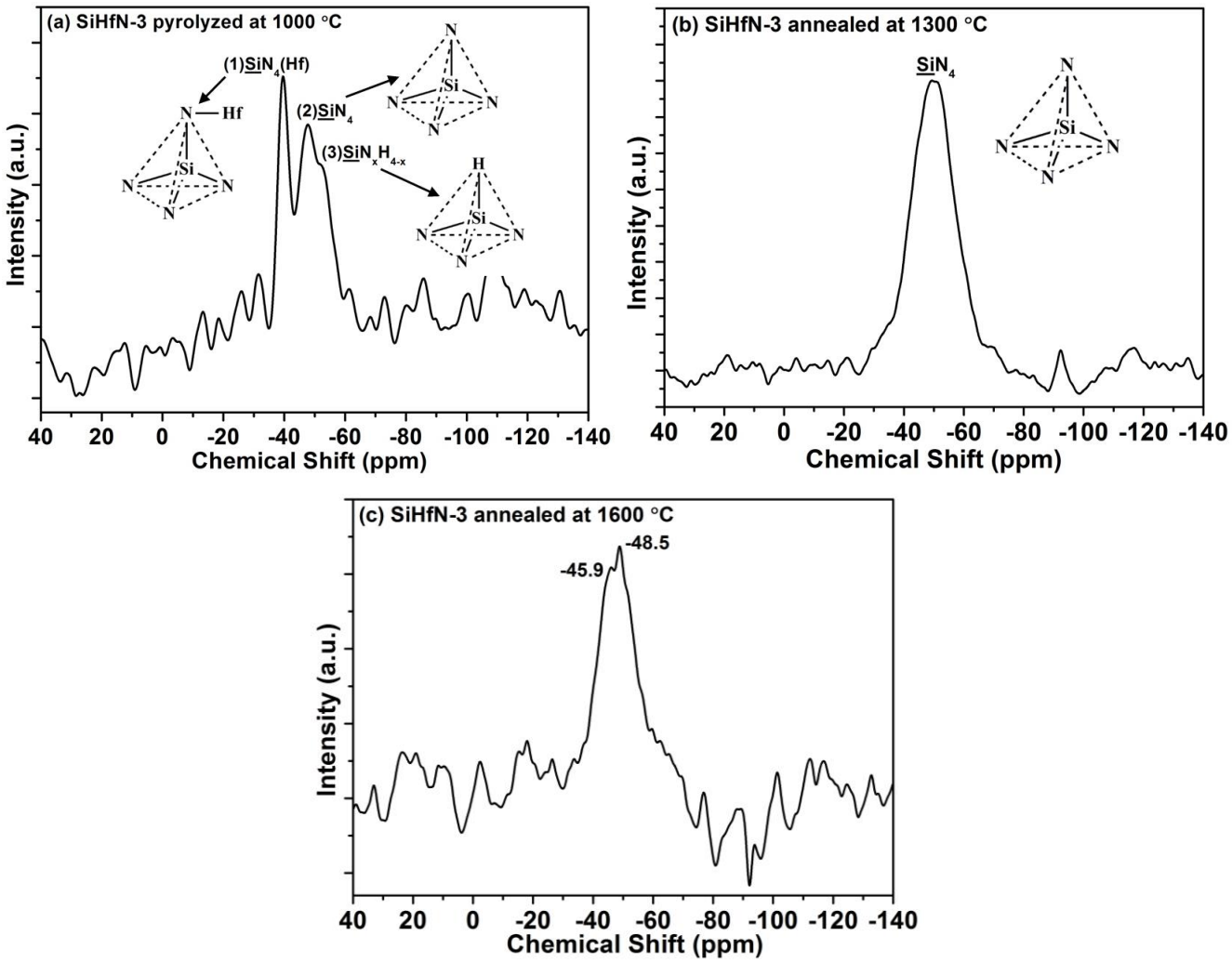

Fig. 4-9. MAS NMR ^{29}Si spectra of (a) SiHfN-3 pyrolyzed at 1000 ℃; (b) SiHfN-3 annealed at 1300 ℃ and (c) SiHfN-3 annealed at 1600 ℃.

Samples with different content of hafnium pyrolyzed at 1000 ℃ were further heat-treated at 1100, 1300, 1600 and 1800 ℃ with a holding time for 5 h in nitrogen atmosphere at the target temperatures, and the obtained mass residue of the samples were listed in Table 6 to study the high temperature stability of the materials. Accordingly, the SiHfN ceramics show almost no mass loss up to 1600 ℃ in flowing nitrogen, demonstrating their excellent thermostability. At 1600 ℃, the mass loss of SiHfN-3 ceramic is less than 10 wt.%, even at 1800 ℃, the ceramic yield of SiHfN-3 is still as high as 83.6 wt.%. The residual mass combines the EA data listed in Table 3, it can be drawn that the mass loss of the SiHfN-3 ceramics annealed at temperatures below 1400 ℃ is negligible and the contents of all the elements change slightly. The obvious weight loss occurred at 1600 ℃ and 1800 ℃ was due to the loss of N and O[211], the ceramic began to decompose and released N_2, NO, CO, and SiO at such high temperature. However, the PHPS-derived ceramic displayed mass addition at 1600 ℃, this abnormal phenomenon was due to the reaction of silicon with N_2 atmosphere. It was reported that Si powders were used as active fillers in the preparing ceramic composite materials, and Si may react with solid or gaseous decomposition products or even with the heating gas atmosphere[204, 212]. In the present study, the PHPS-

derived ceramic was rich in silicon which was confirmed by the EA, Raman and XRD, and the silicon might react with N_2 and result in the mass increase. Besides, the weight loss of SiHfN-3 sintered at 1800 ℃ was less than 20 wt.%, suggesting an improved high-temperature stability compared with that of pure PHPS-derived ceramic, which exhibited a ceramic yield of *ca.* 70 wt.%[213].

Table 6. Residual Mass of the SiHfN ceramics annealed at different high temperatures for 5 h in nitrogen atmosphere.

Samples	1100 ℃ (wt.%)	1300 ℃ (wt.%)	1400 ℃ (wt.%)	1600 ℃ (wt.%)	1800 ℃ (wt.%)
PHPS	99.7	99.5	n.d.	106.5	72
SiHfN-1	99.1	94.6	n.d.	102.7	n.d.
SiHfN-2	97.3	95.0	n.d.	96.3	n.d.
SiHfN-3	99.1	97.5	97.0	90.2	83.6

n.d.: not determined

4.1.4 Nanostructure of SiHfN ceramics

The 1000 ℃ as-prepared SiHfN-3 sample and 1600 ℃ annealed SiHfN-3 ceramic were investigated by SAED and HAADF-STEM in order to study the nano-structural composition. Fig. 4-10(a) shows a low-mag HAADF image together with a featureless selected area electron diffraction (SAED) pattern as inset, revealing a fully amorphous nature of the as-prepared sample, which is consistent with the XRD pattern. Further, in the high magnified HAADF micrograph [Fig. 4-10(b)], a homogeneous microstructure with randomly dispersed bright hafnium (Z=72) atoms (shown as arrowed) was obviously observed. This clearly demonstrated in addition to the spectroscopic results that the 1000 ℃ as-prepared SiHfN-3 sample is a homogeneous and amorphous single-phase ceramic. It is intriguing that nano-sized HfN was also observed in the as-obtained ceramic, but the crystallites did not fully developed and the grain size was only 1-2 nm; additionally, large numbers of hafnium atoms were found due to the heavy atomic mass of hafnium. This result means that, after the pyrolysis procedure in ammonia, a part of TDMAH was transformed to crystalline HfN_x, while another part of TDMAH was reduced to Hf atoms, and this special structure may play an important role in the following crystallization behavior at higher temperatures.

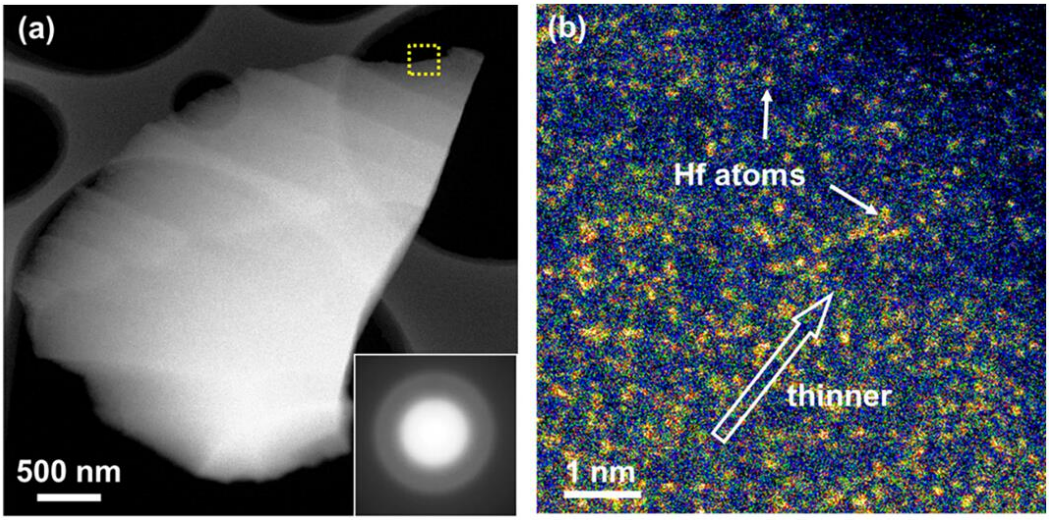

Fig. 4-10. (a) Low-magnified HAADF micrograph and SAED pattern (inset) taken from the 1000 ℃ as-obtained SiHfN-3. (b) High-magnified HAADF micrograph taken from the thin specimen region marked in (a).

In comparison, Fig. 4-11(a) shows the SiHfN-3 sample annealed at 1600 ℃, which is composed of crystalline phases with bright particles (sized around 30-50 nm) distributed randomly on the less bright particles which are larger in size (around 200 nm). The two different kinds of particles were found to have structures that can be well-indexed by cubic-HfN and β-Si_3N_4 in the high-magnified HAADF micrographs, as shown in Fig. 4-11(e) and (f), respectively. It is worthy to note that the light nitrogen atoms (Z=7) are invisible in the HAADF images. The clear and ordered polycrystalline diffraction pattern indicated the high crystallinity of the ceramic, but the SAED was difficult to index the diffraction rings due to the mixed reflections of the Hf-N and Si-N phases, which was original from the multiple crystalline phase within the SiHfN-3 ceramic. Besides, the grain sized from the microstructural observations are consistent with the calculated results from XRD measurements discussed above.

Except for the large-sized crystalline HfN, plenty of single Hf atoms and clustered single Hf atoms, as well as small-sized HfN with the size of 1-5 nm were also found in abundance within the 1600 ℃-annealed ceramic [Fig. 4-11(b)]. These small-sized HfN were found to be homogeneously dispersed in the silicon nitride matrix, and some of them sited around the large-sized HfN as shown in Fig. 4-11(c). Intriguingly, one small-sized HfN was being merged into the adjacent large crystal, it was reasonable to assume that the grain growth of HfN was based on the coalescence of small crystallites during the sintering stage, while the single Hf atoms and small-sized HfN dispersed in the surrounding area acted as raw materials for the grain coarsening. It was worth mentioning that furthermore substitutional and interstitial doping of hafnium in Si_3N_4 unit cell was observed by extensive STEM, which was marked by the red arrows in the inset of Fig. 4-11(b). To the best of our knowledge, this observation has not been reported so far, and this novel structure may exhibit some new properties.

Moreover, the HfN crystallites no matter in large or small sizes seemed to be aligned along the same direction, and it may be caused by lattice match with the Si_3N_4 matrix. Grain boundaries were observed between the Si_3N_4

crystals in the 1600 ℃-annealed SiHfN-3 [Fig. 4-11(d)], and they were consisted of clusters of Hf atoms and HfN, and it was believed that the grain boundaries played an important role in the inhibition of the grain growth, because the clustered Hf atoms and HfN blocked the coalescence of neighboring Si_3N_4 crystals.

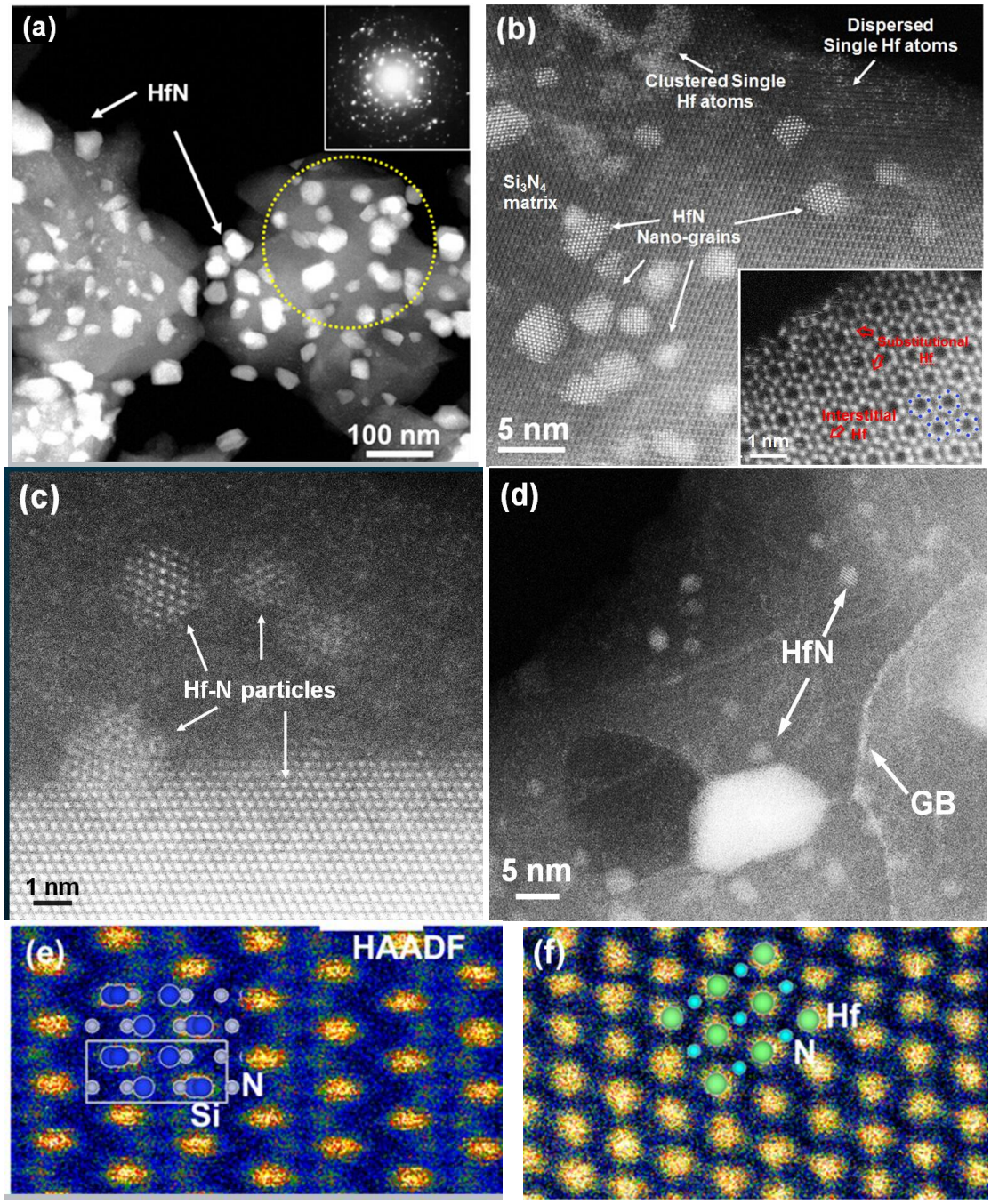

Fig. 4-11. (a) Low-magnified HAADF micrograph and SAED pattern (inset) taken from the SiHfN-3 sample annealed at 1600 ℃. The SAED pattern was taken using a selected aera aperture covering the region labeled by a circle; (b) (c) and (d) High-magnified HAADF micrograph taken from the thin specimen region of (a); (e) and (f) High-magnified HAADF micrographs taken from the bright HfN and less bright α-Si_3N4 grains along their [110] and [10-10] direction, respectively. Insets of (e) and (f) are atomic structure schemes indicating the atom column positions of Hf (green), Si (dark blue) and N (light blue).

4.1.5 Summary

In this study, a single-phase SiHfN ceramic was prepared from a hafnium-containing polysilazane-based single-source precursor and its high-temperature behavior concerning phase separation and crystallization was investigated, and the results of the research are listed as follows.

(1) TDMAH was used to chemically modify PHPS precursor, and then a single-source SiHfN precursor was successfully synthesized with the formation of Si-N-Hf linkage. TDMAH can react with both N-H and Si-H functional groups of PHPS, and N-H bonds showed higher reactivity than Si-H bonds.

(2) The modification of PHPS with TDMAH improved the cross-linking degree of the single-source precursors and consequently their ceramic yield, the ceramic yield of the precursors pyrolyzed at 1000 ℃ in ammonia was improved from 82.7 wt.% of PHPS to 92.3 wt.% of SiHfN-3 with increasing the weight ratio of TDMAH in feed. An investigation of the inorganic conversion of SiHfN precursors was performed, hydrocoupling and transamination were the major reactions in the pyrolysis process, leading to an amorphous single-phase SiHfN ceramic. Interestingly, nano-sized HfN and Hf atoms were found to be dispersed in the 1000 ℃-obtained ceramic matrix by STEM.

(3) The as-obtained single-phase SiHfN ceramic was found to exhibit outstanding resistance against crystallization at high temperature, which could be explained by the formation of HfN between the grain boundary of Si_3N_4 domains. Annealing at 1300 ℃ induced a phase separation process of hafnium nitride and thus the single-phase SiHfN ceramic converted into amorphous HfN_x/SiN_x nanocomposite. Further heat-treatment of the sample at higher temperatures induced the crystallization of HfN as well as α- and β-Si_3N_4. It is notable that the decomposition of ceramics and α- to β-Si_3N_4 phase transformation were both restrained in the SiHfN ceramics.

In conclusion, the modification of PHPS with TDMAH has a strong influence on its high-temperature crystallization behavior and furnishes a convenient preparative access to metal nitride/silicon nitride nanocomposites.

4.2 SiVN(O) ceramics

A commercially available perhydropolysilazane (PHPS, 22.5 wt.% solution in di-n-butyl ether, AZ Electronic Materials GmbH, Germany) was chosen as a suitable precursor for the preparation of silicon nitride. Vanadyl acetylacetonate (99% purity, Sigma-Aldrich) was used as a vanadium source to chemically modify the PHPS. The chemical modification reaction between $VO(acac)_2$ and PHPS as well as the heat-treatment of the as-obtained SiVN(O) ceramics were presented in Chapter 3 in detail. The chemical reaction between $VO(acac)_2$ and PHPS are analyzed and discussed in Section 4.2.1. Then, the phase separation, crystallization behavior and microstructures of the obtained SiVN(O) ceramics are analyzed and discussed in Section 4.2.2 and 4.2.3, respectively. Finally, Section 4.2.4 presents the preparation of mesoporous SiVN(O) ceramics using polystyrene as a self-sacrificial template.

4.2.1 Synthesis of the SiVN(O) single-source precursors

SiVN(O) single-source precursors were synthesized by the reaction of PHPS with $VO(acac)_2$ in different weight ratios at room temperature for 24 h. The FT-IR spectra of the precursors are shown and compared in Fig. 4-12. As previously mentioned in Section 4.1.1, infrared absorption peaks at 3372 and 1171 cm^{-1} (N-H), 2137 cm^{-1} (Si-H) and at 840-1030 cm^{-1} (Si-N-Si) were observed, and they were assigned to PHPS. In the FT-IR spectrum of $VO(acac)_2$, most of the absorption peaks were located in the ranges between 1600 to 500 cm^{-1}, and they were listed as follow: 1554 and 1587 cm^{-1} (C-O stretching), 1526 and 1287 cm^{-1} (C-C-C stretching), 1420, 1344, 1357 and 1188 cm^{-1} (C-H bending), 1020 cm^{-1} (C-CH3 rocking) and 991 cm^{-1} (V=O stretching)[214, 215]. The sharp absorption bands at 1521 cm^{-1} (C=C stretching vibration) and 1570 cm^{-1} (C=O stretching vibration) were the characteristic peaks derived from the acetylacetonate groups of $VO(acac)_2$. In the FT-IR spectra of SiVN(O) precursors, the relative intensities of the Si-H and N-H peaks were observed to be decreased in comparison to pure PHPS, suggesting that there was a chemical reaction between PHPS and $VO(acac)_2$. However, it was difficult for all the ligands of $VO(acac)_2$ involved in the reaction because of the reaction activity and steric hindrance. Therefore, a part of the acetylacetonate ligands still remained in the precursors and it was confirmed by the observation of C=C and C=O absorption peaks in the FT-IR spectra of SiVN(O) precursors. Moreover, a new absorption band seated on the shoulder of Si-N-Si peak was found, and it can be assigned to the Si-O-V unit (922 cm^{-1}), which was generated upon the reaction of $VO(acac)_2$ with Si-H of PHPS . Another new peak sited at 440 cm^{-1} can be attributed to the generation of new V-N bands[216]. Additionally, the C=O peak shifted from 1587 cm^{-1} to 1570 cm^{-1} due to the formation of C=N bands[216] or the mixed peaks of C=N and C=O groups. In order to understand the reaction between PHPS and $VO(acac)_2$, the calculation of integrated area ratios of the Si-H/N-H peaks was carried out here. The calculated results are listed in Table 7; however, there was no obvious change observed in the integrated area ratios of the Si-H/N-H peaks of different SiVN(O) precursors.

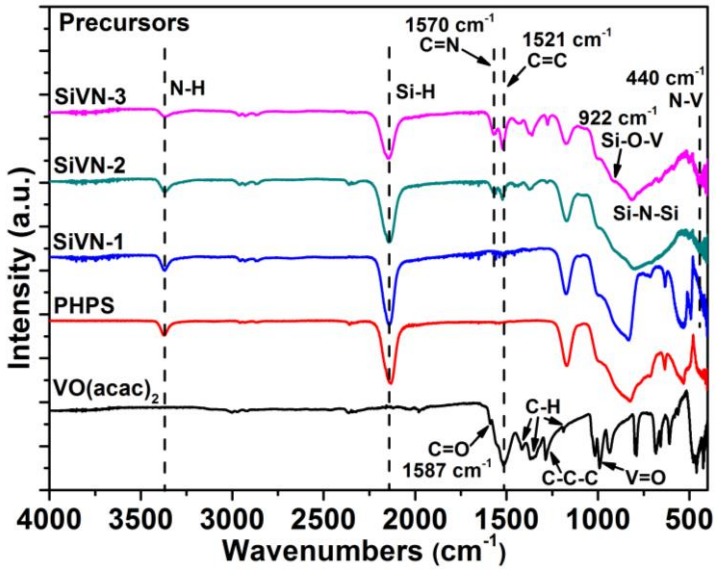

Fig. 4-12. FT-IR spectra of pure PHPS, $VO(acac)_2$ and SiVN(O) precursors with different vanadium content.

It is reported that $VO(acac)_2$ can react with polycarbosilane, which is a kind of Si-based polymer precursor containing Si-H and C=C functional groups[217]. In this report, it was proposed that $VO(acac)_2$ reacted with Si-H upon formation of a Si-O-V linkage located at 948 cm^{-1}; consequently, vanadium was incorporated into the polymer chain.

For the reaction of N-H bond with $VO(acac)_2$, $VO(acac)_2$ was reported to be anchored onto the amine-functionalized substrate as a catalyst, and the complex anchoring was achieved by Schiff condensation between the carbonyl groups of the acetylacetonate ligand and the free amine groups from the substrate, with the formation of C=N-V. Additionally, the $VO(acac)_2$ was further studied by anchoring with two different amine groups: (a) an air-oxidized carbon functionalized with (3-aminopropyl)triethoxysilane (APTES), which contained only $-NH_2$ groups in the end and (b) an acid-oxidized carbon functionalized with trien, which contained both -NH- in the middle of polymer chain and $-NH_2$ end groups. The results clearly demonstrated that $VO(acac)_2$ only reacts with $-NH_2$ rather than -NH- [218]. Combining previous literature with our experimental results, PHPS also contained ample $-NH_2$ terminal groups in the polymer chains, and then it was conjectured that $VO(acac)_2$ could also react with $-NH_2$ groups of PHPS in a similar way.

Table 7. Peak area ratios of the bands assigned to Si-H and N-H from FTIR and Raman spectra of different SiVN(O) single-source precursors.

	PHPS	SiVN(O)-1	SiVN(O)-2	SiVN(O)-3
Mass ratio of $VO(acac)_2$: PHPS in the precursors	____	2 : 98	15 : 85	30 : 70
A(Si-H, 2135 cm^{-1})/A(N-H, 3372 cm^{-1}) in FT-IR spectra	6.77	5.83	6.18	7.29
A(Si-H, 2135 cm^{-1})/A(N-H, 1171 cm^{-1}) in FT-IR spectra	2.04	2.12	2.67	2.61

As a result, according to the spectroscopic measurements and the related information obtained from past studies, two proposed routes for the chemical reaction between and the Si-H or N-H are displayed in Fig. 4-13(a) and (b),

respectively. The Si-H groups reacted with VO(acac)2 to form Si-O-V bonds, and the -NH_2 groups of PHPS reacted with $VO(acac)_2$ at ambient temperature via Schiff condensation. Then, $VO(acac)_2$ was anchored to the polymer chain. Consequently, the modification of PHPS with $VO(acac)_2$ resulted in the preparation of a novel polymeric SiVN(O) single-source-precursor.

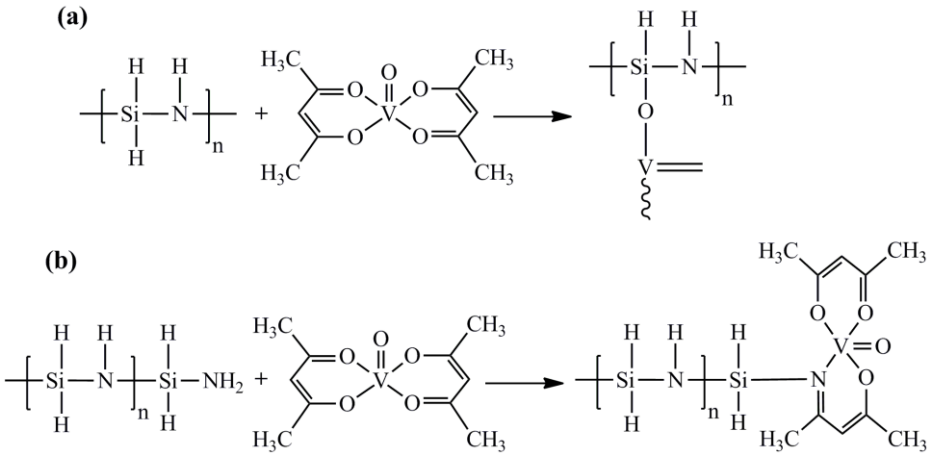

Fig. 4-13. Proposed reaction routes between $VO(acac)_2$ and PHPS: (a) Si-H bonds reacts with $VO(acac)_2$ and (b) –NH_2 bonds reacts with $VO(acac)_2$.

4.2.2 Ceramization and crystallization behavior of Si-V-N ceramics

The pyrolysis of the SiVN(O) precursors with different vanadium content under an ammonia atmosphere at 1000 ℃ yielded a series of SiVN(O) ceramics and the ceramic yield are listed in Table 8. It can be found that there is not a distinct difference between the ceramic yields. One reasonable explanation is proposed as follow: on the one hand, although the crosslinking degree of precursors was improved by the chemical modification of PHPS with $VO(acac)_2$, there were a large amount of unreacted acetylacetone ligands in the precursors, and they reacted with PHPS and evaporated during the pyrolysis progress, finally causing a great mass loss; one the other hand, a large amount of oxygen were incorporated into the precursors due to the modification with $VO(acac)_2$, and oxygen could be greatly removed in the reducing ammonia atmosphere. As a result, the ceramic yield of the V-modified samples was not improved.

Table 8. Ceramic yield of SiVN(O) precursors and pure PHPS pyrolyzed in ammonia for 3 h and residual mass of the as-prepared ceramics annealed at different high temperatures for 5 h in nitrogen atmosphere.

Samples	1000 ℃ in NH_3	1100 ℃ in N_2	1300 ℃ in N_2	1400 ℃ in N_2	1600 ℃ in N_2
PHPS	82.7	99.7	99.5	n.d.	106.5
SiVN(O)-1	80.1	99.6	99.7	n.d.	91.4
SiVN(O)-2	80.5	98.5	98.0	n.d.	83.1
SiVN(O)-3	83.3	97.2	97.0	93.1	73.4

(a) Ceramic yield and residual mass of samples are calculated in terms of weight percentage;

(b) Weight loss at high temperature are calculated with respect to the 1000 ℃-prepared ceramics;

(c) n.d. = not determined.

The chemical reactions and structural evolution of the SiVN(O)-3 precursor in the ammonolysis process was investigated by FT-IR measurements. As shown in Fig. 4-14(a), the N-H, C=O and C=C bonds disappeared completely with the temperature increasing from room temperature to 140 ℃. Besides, the intensity of the Si-H absorption decreased significantly. However, the V-N, V-O and Si-O absorptions were overlapped by the broad Si-N-Si bond and were difficult to be distinguished. The Si-H bond decreased continuously with raising temperature and finally disappeared at 700 ℃. It was reported that pure $VO(acac)_2$ melted incongruently at 260 ℃ under an inert atmosphere, while the C-C-C and C-O bonds in the chelate rings disappeared above 430 ℃ and caused subsequent formation of gaseous CO, H_2, H_2O and solid $VO(OH)_2$. Then, the hydroxide decomposed into solid VO_2 above 250 ℃[215, 219]. By comparison, it can be deduced that $VO(acac)_2$ not only decomposed at high temperature but also further reacted with PHPS and ammonia during the pyrolysis. The V-O bond was reduced by NH_3, and VN was formed.

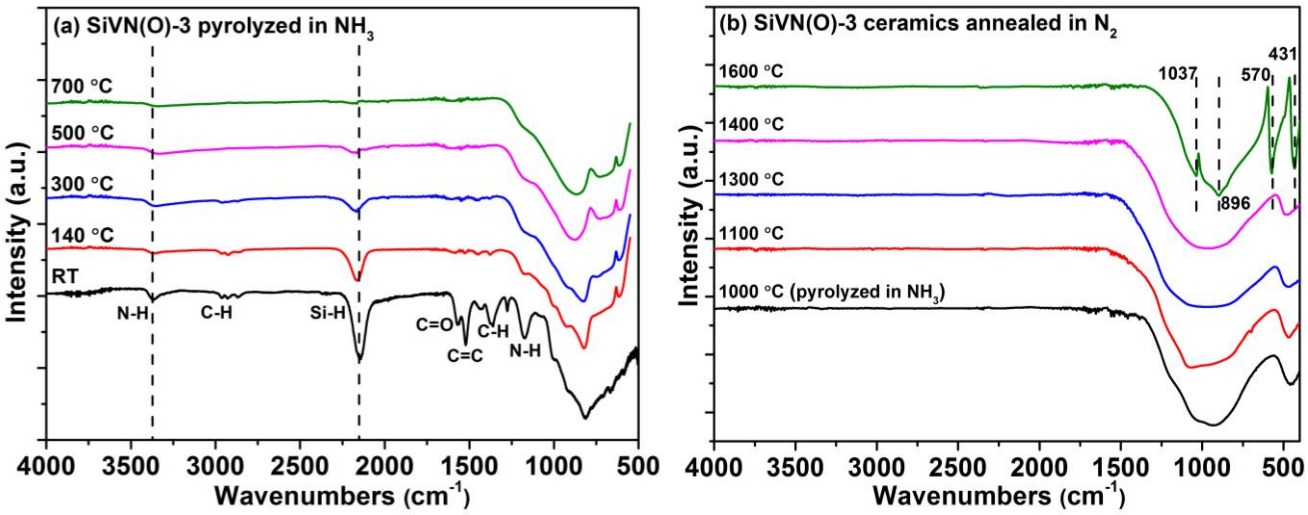

Fig. 4-14. FT-IR spectra of (a) SiVN(O)-3 precursor heat-treated at different temperatures in NH_3 and (b) SiVN(O)-3 ceramics annealed at different high-temperature in N_2.

In order to investigate the crystallization behavior of the SiVN(O), FT-IR measurements were also performed on the ceramics that were heat-treated at different temperatures to assess the structure of the SiVN(O) ceramics, and the spectra are shown in Fig. 4-14(b). In the temperature range from 1000 to 1400 ℃, only a broad peak at around 800-1200 cm^{-1}, which was the region of the vibrations attributed to Si-N, Si-O and V-N bonds, along with a small broad peak at 455 cm^{-1} assigned to Si-O-Si bond. The Si-O-Si bond diminished gradually with increasing sintering temperature and finally vanished at 1600 ℃, meaning that the Si-O bond was not stable and was reduced at high temperature. At 1600 ℃, the broad peak split into several sharp vibrations and demonstrated the intense phase separation and grain coarsening within the ceramic composite. The absorption bonds at 1037, 896, 570 and 431 cm^{-1} can be attributed to Si-N bonds[220]. The peak at 896 cm^{-1} was still very broad; meanwhile, the vibrations of V≡N (ca. 960 cm^{-1}), V=O (970 cm^{-1}) and V-O (790 cm^{-1}; in crystalline V_2O_5,

V=O at 1020 cm^{-1} and V-O at 840 cm^{-1}) were all located in this region[221, 222]. Therefore it was difficult to distinguish them.

Additional structure information of SiVN(O) ceramics was obtained by Raman spectroscopy, and the influence of the modification with different content of $VO(acac)_2$ on the structure of the ceramics was evident from the Raman spectra. In the Raman spectra of SiVN(O)-3 [Fig. 4-15(a)], only two broad absorption bands assigned to D (1348 cm^{-1}) and G (1602 cm^{-1}) bands were observed in the samples annealed from 1000 to 1400 ℃, indicating the existence of a small amount of free carbon within the ceramics, and the results were in agreement with the EA data. However, a series of strong and sharp peaks were observed in the 1600 ℃-annealed SiVN(O)-3 ceramic, which were not found in any other samples annealed at relatively lower temperatures. The Raman spectra of 1600 ℃-annealed SiVN(O) ceramics with different contents of vanadium are shown in Fig. 4-15(b), and the effect of different amounts of $VO(acac)_2$ on the structure of the ceramics is clearly displayed. The PHPS annealed at 1600 ℃ showed only one peak at 521 cm^{-1} (assigned to Si), and the spectrum of SiVN(O)-1, which was modified by only 2 wt.% $VO(acac)_2$, was similar with that of PHPS. SiVN(O)-2 ceramic annealed at 1600 ℃ showed several peaks at 224, 256, 359 and 511 cm^{-1}, and they were belong to α-Si_3N_4. In the Raman spectrum of 1600 ℃-annealed SiVN(O)-3, which is shown in Fig. 4-15(b), the peaks located at 204, 223, 446, 615, 858, 920, 929 and 1041 cm^{-1} can be attributed to β-Si_3N_4[220]. The peaks sited at 281, 302, 405, 478, 523, 691 and 992 cm^{-1} are strong and can be assigned to VN(O). The literature concerning the VN vibration modes is scarce, and the Raman peaks of VN are difficult to be found in the spectra because of the weak intensity of the Raman active scattering mode of VN[223, 224]. But the presence of surface oxides on VN, which may be formed on the VN particles during the annealing, can display a well resolved signature in the spectrum, even if the oxides are present in quite low amounts and not detectable by XRD [225, 226].

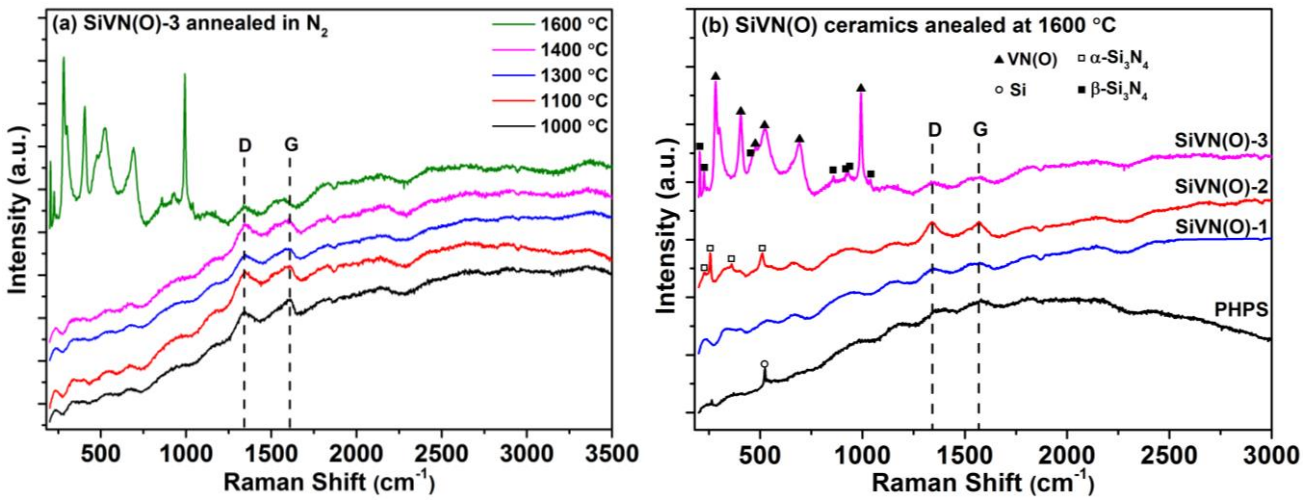

Fig. 4-15. Raman spectra of SiVN(O) ceramics: (a) SiVN(O)-3 ceramic annealed at different temperatures and (b) SiVN(O) ceramics with different vanadium contents annealed at 1600 ℃.

The Raman spectra indicated that no obvious changes occurred in the SiVN(O) ceramics when annealing temperature was below 1400 ℃, suggesting the structural stability of the SiVN(O) ceramics at high

temperatures. But strong phase separation and crystallization occurred in the ceramic annealed at 1600 ℃ and led to the formation of Si_3N_4 and VN crystallite. The introduction of different amounts of $VO(acac)_2$ exhibited significant influence on the structure of the SiVN(O) ceramics. Additionally, it is also confirmed the existence of oxygen on the VN particles[225, 226]. The variational tendency of the Raman spectra is in good agreement with that of FT-IR result, the SiVN(O)-3 ceramic is relatively stable with respect to crystallization before 1400 ℃, and shows high crystallinity at 1600 ℃.

X-ray powder diffraction is also a powerful method to investigate the crystallization behavior and structural evolution of the ceramics annealed at different temperatures. Therefore, SiVN(O) polymer-derived ceramics annealed at different temperatures were measured by XRD, and the spectra are shown in Fig. 4-16. The analysis and discussion for pure PHPS-derived ceramics are already presented in Section 4.1.3 (Fig. 4-6) and not repeated here. At 1000 ℃, all the as-obtained SiVN(O) ceramics were X-ray amorphous, and they can be regarded as single-phase ceramics. The XRD patterns of SiVN(O)-1 ceramics heat-treated at different temperatures seemed to be about the same as the of PHPS, and they were not described separately here. By increasing the $VO(acac)_2$ content in SiVN(O) precursors, the influence of the introduction of vanadium (as well as oxygen) on the crystallization behavior of ceramic composites became remarkable. In the XRD patterns of SiVN(O)-2, which was modified by 15 wt.% $VO(acac)_2$, the 1300 ℃-annealed sample kept its amorphous feature, and the peaks assigned to crystalline silicon were not observed, suggesting that the stability of the ceramic was improved. For the SiVN(O)-3 ceramic with the highest content of vanadium and oxygen, it can be found that SiVN(O)-3 ceramic annealed at temperatures range from 1000 to 1400 ℃ remained X-ray amorphous. Fig. 4-16(c) showed the comparison of XRD patterns of 1300 ℃-annealed SiVN(O) ceramics modified with different amounts of $VO(acac)_2$. Unlike the highly crystallized 1300 ℃-PHPS specimen, it was very distinct that SiVN(O)-2 and SiVN(O)-3 ceramic annealed at 1300 ℃ were X-ray amorphous; even in the case of SiVN(O)-1 ceramic, which was modified with only 2 wt.% $VO(acac)_2$, its XRD pattern exhibited weaker and broader peaks than those of 1300 ℃-PHPS, suggesting a relatively lower crystallinity of SiVN(O) ceramics. As a result, this comparison obviously reveals that the crystallization of the SiVN(O) ceramics can be restrained by addition of $VO(acac)_2$ when temperatures are ≤1300 ℃, and the effect is in direct proportion to the amounts of $VO(acac)_2$ in feed. By further increasing the heating temperature to 1600 ℃, the XRD patterns show three high intense Bragg peaks at 2θ = 16.9 °, 19.6 ° and 27.9 °, corresponding to reflections in the (111), (200) and (220) planes, respectively. Therefore, the aforementioned peaks correspond to a structure face-centered cubic (fcc) Fm-3m related to the cubic-VN phase. At 1600 ℃, the strong diffraction peaks of Si_3N_4 and VN both appeared in the SiVN(O)-2 and SiVN(O)-3 ceramics; thus, the single-phase SiVN(O) ceramics underwent annealing at high temperature crystallization and phase separation, and finally VN/Si_3N_4 nanocomposite material was fabricated that was consistent with preceding FT-IR and Raman results. It is reasonable that the VN phase was not observed in the 1600 ℃-sintered SiVN(O)-1 specimen because of the fairly low vanadium content.

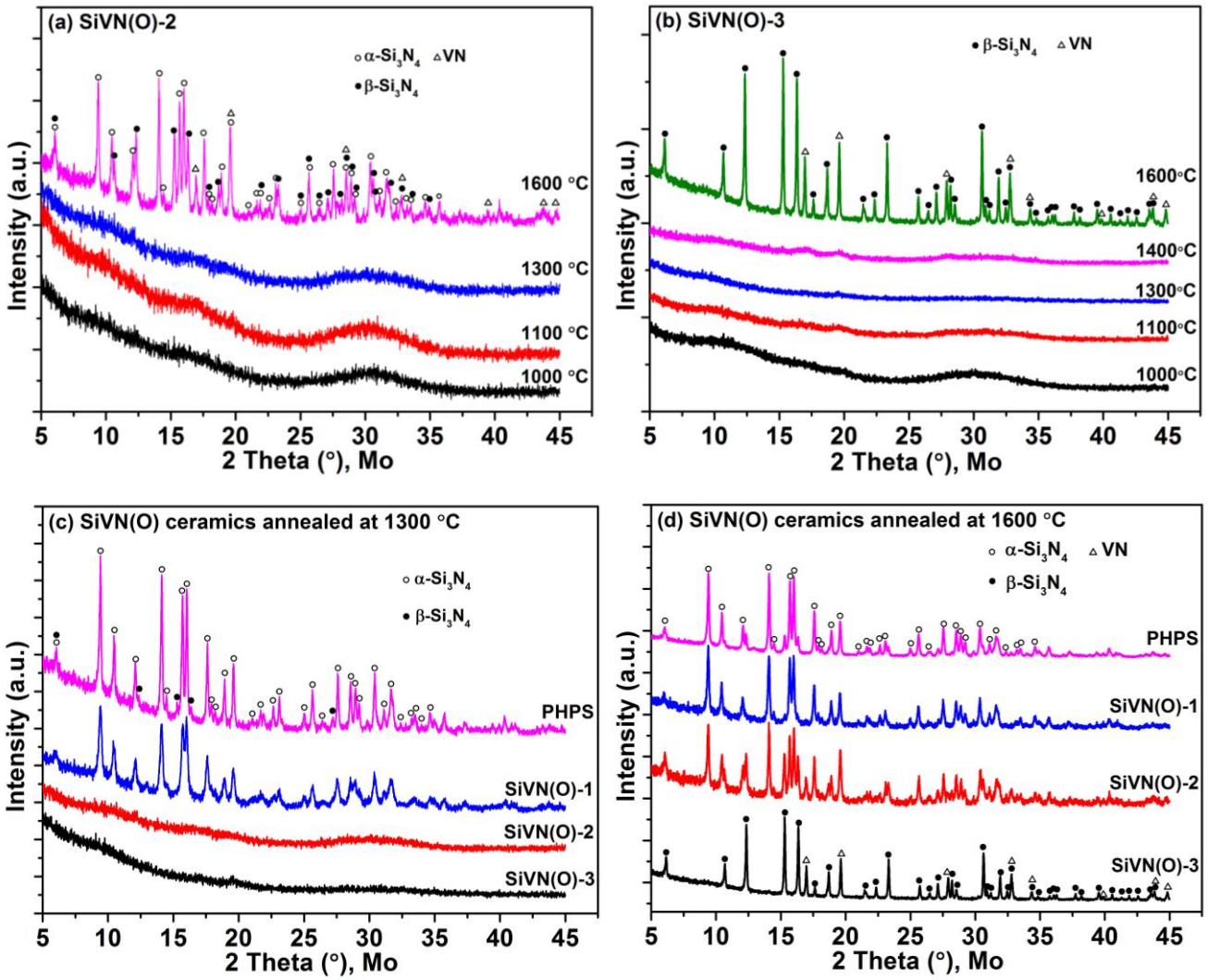

Fig. 4-16. XRD patterns of SiVN(O) ceramics annealed at different temperatures.

Herein, an interesting variation is worthy to be underlined that the predominant crystal phase in the 1600 ℃-annealed PHPS ceramic was α-Si_3N_4, attached with small amount of β-Si_3N_4, while the peak intensities of α- and β-Si_3N_4 in the XRD pattern of SiVN(O)-2 were at the same level; in contrast, only the diffraction peaks of VN and β-Si_3N_4 were observed in the 1600 ℃-annealed SiVN(O)-3 ceramic, and no indication of α-Si_3N_4 was found. The series of gradual changes in the ratio of α/β-Si_3N_4 phase indicated that the modification with $VO(acac)_2$ made a tremendous impact on the crystallization behavior of the resultant ceramics. In other words, it facilitated the phase transformation from α- to β-Si_3N_4, and the effect of promotion was in positive correlation with the amounts of $VO(acac)_2$.

The XRD patterns of several SiVN(O) ceramics were refined by Full-Profile Rietveld refinement, and the refined XRD patterns as well as the calculated volume fraction, grain sizes and lattice constants of VN, α- and β-Si_3N_4 crystallites are shown in Fig. 4-17 and Table 9, respectively. According to the calculated grain size, it can be found that, especially in 1600 ℃-annealed SiVN(O)-3, the grain size of both VN and β-Si_3N_4 was around

100 nm. By comparison with pure PHPS-derived ceramic, the grain coarsening and α/β phase transformation were promoted at relatively low temperatures.

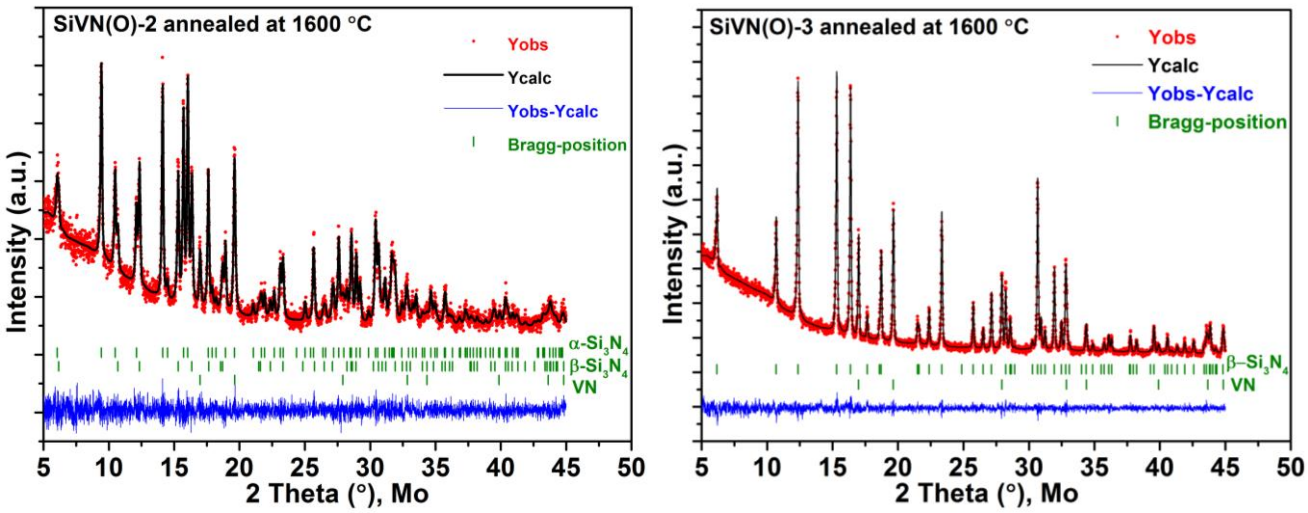

Fig. 4-17. Rietveld refinement of the XRD patterns of selected SiVN(O) ceramics.

(Green tick marks are Bragg peak positions of VN, α-Si_3N_4 and β-Si_3N_4. The blue line at the bottom of each XRD pattern denotes the difference intensities between the observed and calculated profiles)

Table 9. Volume fraction, grain sizes and lattice constants of the samples displayed in Fig. 4-17, as from Rietveld refinement of the XRD patterns.

Specimens	VN (*Fm-3m*, Nr. 225)	α-Si_3N_4 (P31c, Nr. 159)	β-Si_3N_4 ($P6_3/m$, Nr. 176)	R-factors
1600 ℃ annealed SiVN(O)-2	3.65 v.% a=4.16065 Å	66.36 v.% a=7.76236 Å, c=5.62299 Å	30.0 v.% a=7.61375 Å, c=2.90961 Å	Rp: 6.88 Rwp: 8.93 Rexp: 9.24
	Grain size: 21.8 nm	Grain size: 34.9 nm	Grain size: 28.0 nm	
1600 ℃ annealed SiVN(O)-3	6.23 v.% a=4.15666 Å	—	93.77 v.% a=7.60767 Å, c=2.90881 Å	Rp: 4.96 Rwp: 6.52 Rexp: 6.56
	Grain size: 101.0 nm		Grain size: 97.2 nm	

4.2.3 Nano-structure of the SiVN(O) ceramics

The 1000 ℃-ammonolyzed SiVN(O)-3 and the 1600 ℃-annealed SiVN(O)-3 ceramic were investigated by HAADF-STEM, and the images were compared. Fig. 4-18(a) and (b) showed the high-magnified HAADF micrograph of the as-prepared SiVN(O)-3 sample, revealing a fully amorphous nature of the silicon nitride matrix. However, it is intriguing to find that nano-sized VN in the size of 1-2 nm dispersed in the amorphous matrix randomly and homogeneously as well as some bright spots (*i.e.*, vanadium (z = 23) atoms), which was similar to the observation in the HRTEM of SiHfN-3. The crystalline VN at such a tiny size exceeds the testing limit of X-ray diffraction and leads to an X-ray amorphous pattern at 1000 ℃. This result also clearly

demonstrates that the crystalline VN nucleated prior to Si_3N_4. Moreover, the generation of crystalline VN means that vanadium preferred to combine with nitrogen rather than silicon or oxygen with these pyrolysis conditions.

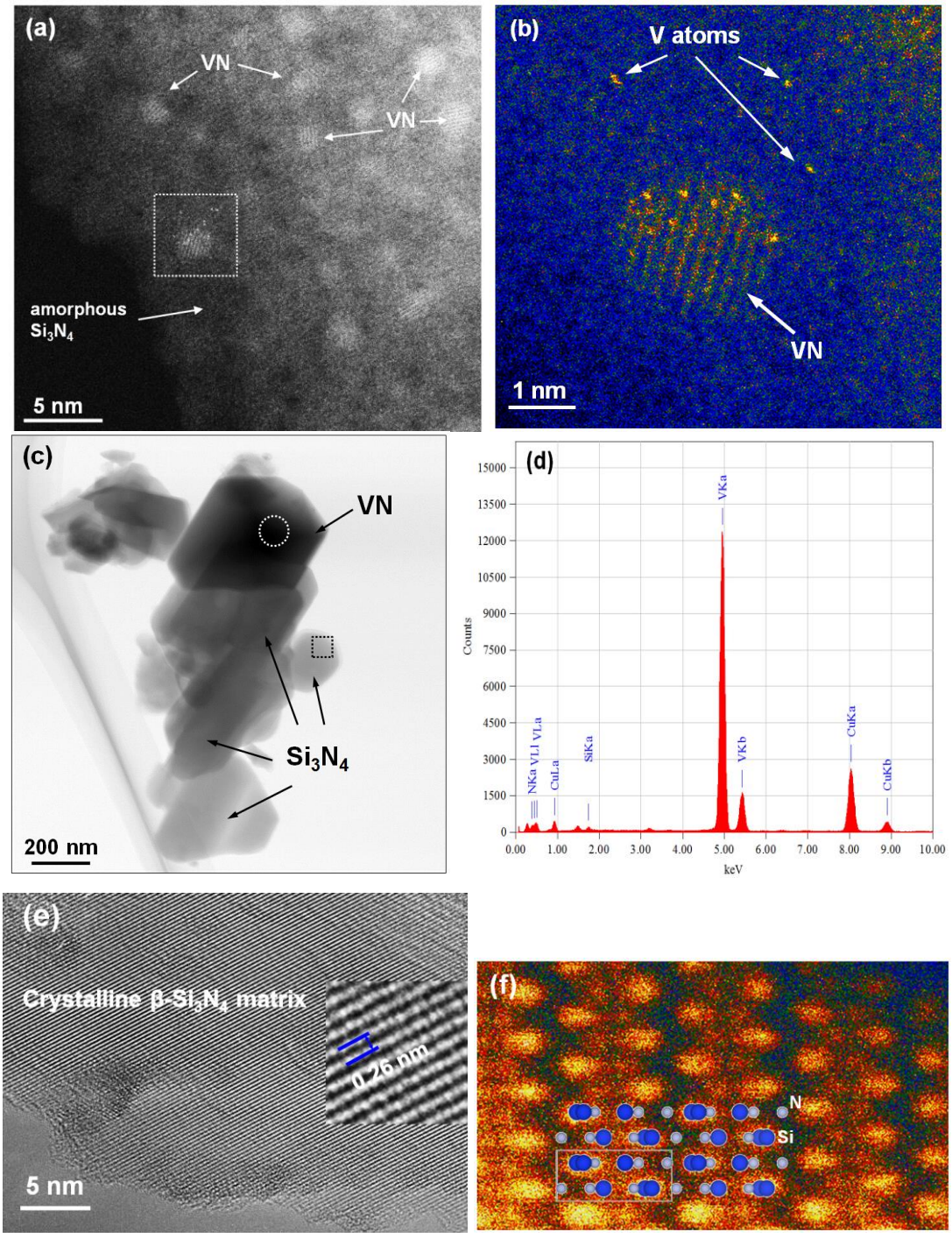

Fig. 4-18. (a) and (b) High-magnified HAADF micrographs taken from the 1000 ℃ as-obtained SiVN(O)-3 ceramic; (c) Low-magnified HAADF micrograph of the SiVN(O)-3 sample annealed at 1600 ℃; (d) Energy Dispersive Spectrometer (EDS) spectrum taken from the region circled in (c); (e) High-magnified HAADF micrograph taken from the thin specimen region of (c); (f) High-magnified HAADF micrographs taken from the β-Si_3N_4 grains Insets of (f) are atomic structure schemes indicating the atom column positions of Si (dark blue) and N (light gray).

Fig. 4-18(c) displays that the SiVN(O)-3 ceramic annealed at 1600 ℃ was composed of two main crystalline phases with the size around 100 nm, and they were confirmed as VN and β-Si_3N_4, which was in good agreement with the Rietveld refinement results. Energy Dispersive Spectrometer (EDS) spectrum taken from the dark region indicated that the V peak was evident, suggesting the presence of VN crystallites, while the weak N peak might be caused by poor electron scattering of N atoms and heavy X-ray absorption by vanadium. Fig. 4-18(e) shows the magnified HREM image of the crystallized silicon nitride matrix. The high resolution image of inset illustrates that the silicon nitride phase had an interplanar spacing of 0.26 nm, which was attributed to β-Si_3N_4, and this β-phase structure was well-confirmed by EDS (not shown) and the atomic structure scheme in the HAADF micrograph, as shown in Fig. 4-18(f).

4.2.4 Mesoporous SiVN(O) ceramics

Polymer derived ceramics (PDCs) are intensively used due to their simple processability, chemical resistance and high thermal stability. Among these applications, the use of PDCs as catalyst support material is promising and has been reported elsewhere. Porous PDCs materials with different pore size can be prepared. The metallic nanoparticles can be generated from metal-modified preceramic polymers, and the metallic nano-particles can be uniformly dispersed in the PDCs matrix. For instance, a catalytic performance as efficient as for homogeneous catalysts has been reported for Ir@SiCN[227]. However, it was unfortunate that the as-prepared catalyst usually showed a low specific surface area (SSA), indicating that most of the metal nanoparticles were not accessible; as a result, the catalytic efficiency was reduced significantly. In the case of SiVN(O) ceramics, the low SSA is also an obstacle for its application in the catalyst field.

In this section, the preparation of mesoporous SiVN(O) nanocomposite ceramics with high surface area is reported. Polyolefin templates such as polystyrene (PS, Mw=35000), linear low density polyethylene (LLDPE) and poly(isobutyl methacrylate) (PBMA, Mw=70000) were used as self-sacrificial templates. The polymer template, PHPS and $VO(acac)_2$ were simply mixed in toluene. After the chemical reaction and removal of the solvent, a polymer blend was obtained. In this study, the SiVN(O) precursor with high vanadium content (weight ratio of PHPS/$VO(acac)_2$ = 7/3) was chosen as the representative, nominated as SiVN(O)3. The subsequent pyrolysis leads to the formation of mesoporous SiVN(O) ceramics, and a series of measurements were performed on the resulting mesoporous samples. The detailed experimental procedure can be found in section 3.2.3.

The mesoporous structured SiVN ceramics were successfully prepared after the pyrolysis of the compound under an NH_3 atmosphere at different temperatures with a tailored program. It was reported that the major mass loss of most polyolefin occurred between 400 and 500 ℃[156, 159, 228, 229]. Besides, the pyrolysis profile with slow heating rates and long dwell time was beneficial to prepare porous ceramics with high SSA[122]. As a result, a

special pyrolysis program is described as follows. The precursor was heated from RT with a rate of 100 ℃/h to 120 ℃ and held for 5 h at 120 ℃ in order to promote the cross-link of the precursor. It was then further heated to 300 ℃ with a rate of 50 ℃/h and held for 3 h at 300 ℃, further heated to 400 ℃ with a rate of 50 ℃/h and held for 3 h at 400 ℃, further heated to 500 ℃ with a rate of 30 ℃/h and held for 5 h at 500 ℃, further heated to 600 ℃ with a rate of 50 ℃/h and held for 3 h at 600 ℃, and then heated to 1000 ℃ with a rate of 50 ℃/h and held for 2 h at 1000 ℃. Finally, it was cooled to room temperature with a rate of 100 ℃/h. Thus, the PS template was ensured to be removed completely, and maximum pore density was obtained.

In order to measure the SSA, pore volume and pore size distribution, a nitrogen absorption measurement was performed on the porous ceramics prepared with different polymer templates at 1000 ℃. As shown in Table 10, a SiVN(O)3 ceramic with large SSA was achieved in the 1000 ℃-obtained sample. By comparison, it can be found that the polymer templates could increase the SSA of the ceramic in different degrees, and the presence of mesopores has been confirmed. It seemed that the polystyrene template performed the best in this system. When PS was used as a template, the SSA of 1000 ℃-obtained SiVN(O)3-PS1 was as high as 332 m^2/g. This may be due to the good solubility of PS in toluene, leading to the uniform mixing of PS template and SiVN(O)3 precursor. It is worth mentioning that the SiVN(O)3-blank ceramic prepared at the same temperature was almost nonporous by N_2 absorption isotherm analysis, which could be attributed to the collapse of the transient pores during the polymer-to-ceramic transformation. It also highlights the prominent role of suitable polymer template in the making of pores.

Table 10. Specific surface area (SSA), total pore volume (V_t) and micropore volume (V_m) of the SiVN(O)3 ceramics prepared at 1000 ℃, obtained from nitrogen adsorption measurement.

Samples name	SSA (m^2/g)	Mesopore SSA (m^2/g)	Vt (cm^3/g)	Vm (cm^3/g)
SiVN(O)3-PE1	40	37	0.086	0.007
SiVN(O)3-PBMA1	285	83	0.222	0.103
SiVN(O)3-PS1	456	292	0.528	0.106
SiVN(O)3-blank	5.6	5.6	0.026	0

Because of the outstanding performance in creating mesopores, polystyrene has become the focal point of this research and it was mixed with SiVN(O)3 precursor in different weight ratios, and the mixtures were transformed into ceramics by subsequent pyrolysis. The 1000 ℃-prepared ceramics were investigated by nitrogen adsorption measurement and the pore parameters are listed in Table 11 (The corresponding figures are shown in Fig. 4-19). It can be deduced from the data that the SSA was improved by increasing the weight ratio of the PS template in the mixture, and the maximum SSA (506 m^2/g) was obtained when the weight ratio of SiVN(O)3/ PS was 1/2. Further increases of the content of the PS template made no contribution to the SSA. In addition, micropores have been found to be present in the SiVN(O)3-PS0.5 and SiVN(O)3-PS1 samples, but the proportion of micropores decreased while raising the percentage of PS template in the mixture. Finally, only mesopores could be observed in the samples SiVN(O)3-PS2 and SiVN(O)3-PS3.

Table 11. Pore parameters of the porous SiVN(O)3-PS ceramics prepared at 1000 ℃.

Samples name	SSA (m^2/g)	Mesopore SSA (m^2/g)	Vt (cm^3/g)	Vm (cm^3/g)
SiVN(O)3-PS0.5	147	65	0.150	0.048
SiVN(O)3-PS1	456	292	0.528	0.106
SiVN(O)3-PS2	506	506	1.009	0
SiVN(O)3-PS3	502	502	1.576	0

Fig. 4-19 shows the nitrogen physisorption isotherms and the pore size distributions (PSD) calculated based on the desorption branches of the isotherms of these 1000 ℃-obtained samples. According to Sing et al.[180], the isotherms of the four samples showed an intermediate feature between type-I and type-IV isotherms, and they revealed a trend from type-I to type-IV isotherms by increasing the ratio of the PS template. The presence of mesopores was also indicated by the hysteresis. The calculated PSD showed a major pore size between 4 and 10 nm in diameter, and the pore size increased gradually by altering the weight ratio of SiVN(O)3/PS from 1/0.5 to 1/3. Finally, large mesopores up to 25~35 nm were present in the SiVN(O)3-PS3 ceramic. This finding demonstrated that the pores of the as-obtained SiVN(O)3 ceramic were predominantly composed of mesopores (2-50 nm in pore diameter), while micropores (< 2 nm in pore diameter) were rare, suggesting that the high cross-linking degree of the SiVN(O)3 precursor stabilized the porous network and avoided the collapse of transient pores during the pyrolysis. Moreover, by using this approach, the SSA and PSD of the final ceramic could be controlled via simply adjusting the weight ratio of the PS template in the feed.

It needs to be emphasized that the SSA obtained in our case was much higher than the result reported by Ewert et al.[159], which showed only 110 m^2/g at 900 ℃. Moreover, their SSA dropped quickly to 50 and 35 m^2/g when the samples pyrolyzed at 1000 and 1100 ℃, respectively, even though the weight ratio of polysilazane/PS was also 1/2. By comparison, the present research demonstrated a huge promotion in producing a mesoporous ceramic. There are several possible reasons for the different results. The first reason is the difference between the two kinds of PS templates, such as the molecular weight and morphology. Another important reason is that the SiVN(O)3 precursor exhibited much higher cross-linking degree than that of the polysilazane employed in Ewert's case, then, the PS template can be better sealed in the cross-linked SiVN(O)3 precursor, and the highly cross-linked sample can further stabilize the mesopores inside the ceramic matrix during the heat-treatment. Usually, the collapse of transient pores in porous PDCs can be attributed to two reasons: (i) the significant volume shrinkage resulting in an unstable matrix and (ii) viscous flow blocking the formation of pores. In the present case, the chemical modification of PHPS with $VO(acac)_2$ can greatly increase the cross-linking degree of precursors, which subsequently stabilized the ceramic framework, and finally reduced the shrinkage and collapse of pores. Moreover, vanadium was uniformly dispersed in the precursor by chemical modification. During the pyrolysis, it *in situ* formed nanoparticles such as V atoms and VN [confirmed by previous TEM images (Fig. 4-18)], which reinforced the porous structure and prevented collapse of the pores. Consequently, mesoporous SiVN(O)3 ceramic with high SSA can be successfully fabricated using polystyrene as a self-sacrificial template with the pyrolysis temperature at 1000 ℃.

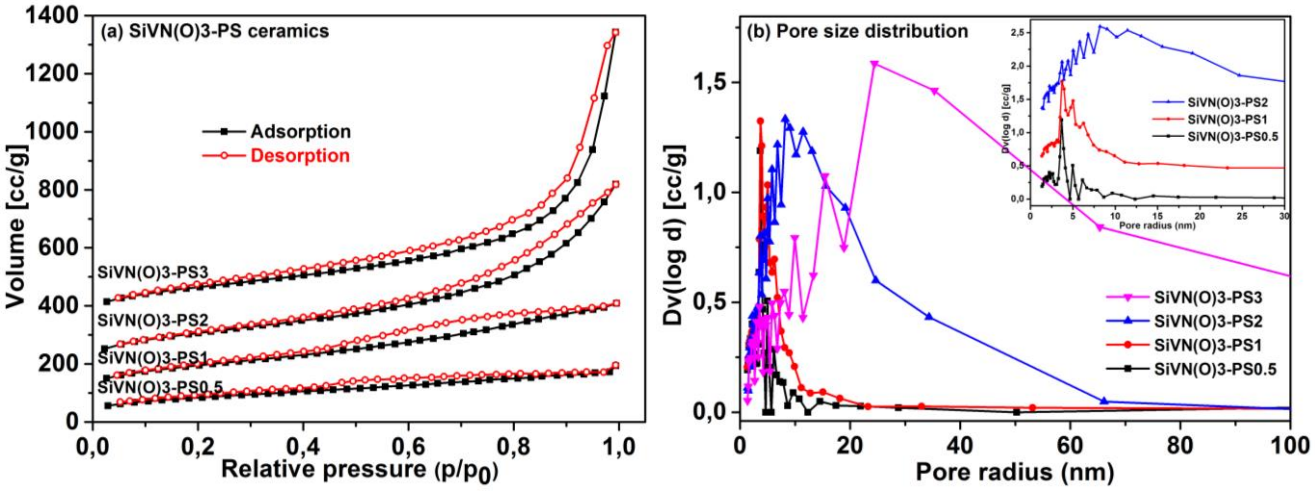

Fig. 4-19. Nitrogen adsorption-desorption isotherms and calculated pore size distribution of the mesoporous SiVN(O)3 ceramics prepared at 1000 ℃ under NH_3: (a) nitrogen adsorption-desorption isotherms, (b) pore size distribution.

Fig. 4-20 shows the schematic diagrams of the mixing, crosslinking and pyrolysis process of fabricating mesoporous SiVN(O)3-PS ceramics. Firstly, both the PHPS precursor and PS template can be completely dissolved in toluene, and a homogeneous solution was obtained. With the introduction of $VO(acac)_2$, PHPS reacted with $VO(acac)_2$, leading to the cross-linking of the SiVN(O)3 precursor. Accompanied with the onset of phase separation, the PS phase was sealed by the SiVN(O)3 precursor matrix. Subsequent pyrolysis resulted in the formation of mesoporous SiVN(O)3-PS ceramics in which mesopores arose from the thermal decomposition and evaporation of the PS template.

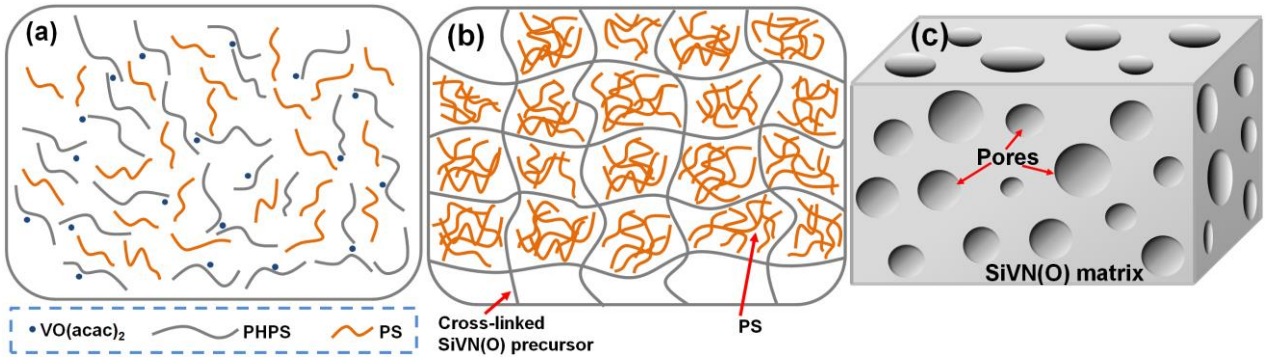

Fig. 4-20. Schematic diagram of (a) mixture of $VO(acac)_2$, PHPS and PS; (b) cross-linking of the SiVN(O)3-PS and (c) final mesoporous SiVN(O)3-PS ceramics obtained via pyrolysis.

In order to study the crystallization behavior of the mesoporous SiVN(O)3-PS ceramics annealed at different temperatures, especially to explore whether there was some influence caused by the addition of PS template, the as-obtained mesoporous SiVN(O)3-PS ceramics were further annealed at 1300, 1400 and 1600 ℃ under a nitrogen atmosphere for 2 h, respectively, and then X-ray diffraction measurement was performed on the ceramic powders. The XRD patterns shown in Fig. 4-21(a) revealed that the SiVN(O)3-PS ceramics prepared at

1000 ℃ were mainly X-ray amorphous, regardless of how much PS template was introduced. By increasing the annealing temperature, the ceramics retained amorphous up to 1300 ℃ [SiVN(O)3-PS2 was taken as representative here]. When the sample was annealed at 1400 ℃, some small humps assigned to silicon nitride and vanadium nitride emerged, indicating the phase separation and grain coarsening occurred at this temperature, leading to the formation of mesoporous Si_3N_4/VN ceramic nanocomposites. At 1600 ℃, only highly crystallized β-Si_3N_4 and VN remained in the residue, which was basically the same with the XRD pattern of 1600 ℃-obtained SiVN(O)3-blank, demonstrating no obvious influence caused by the introduction of PS template.

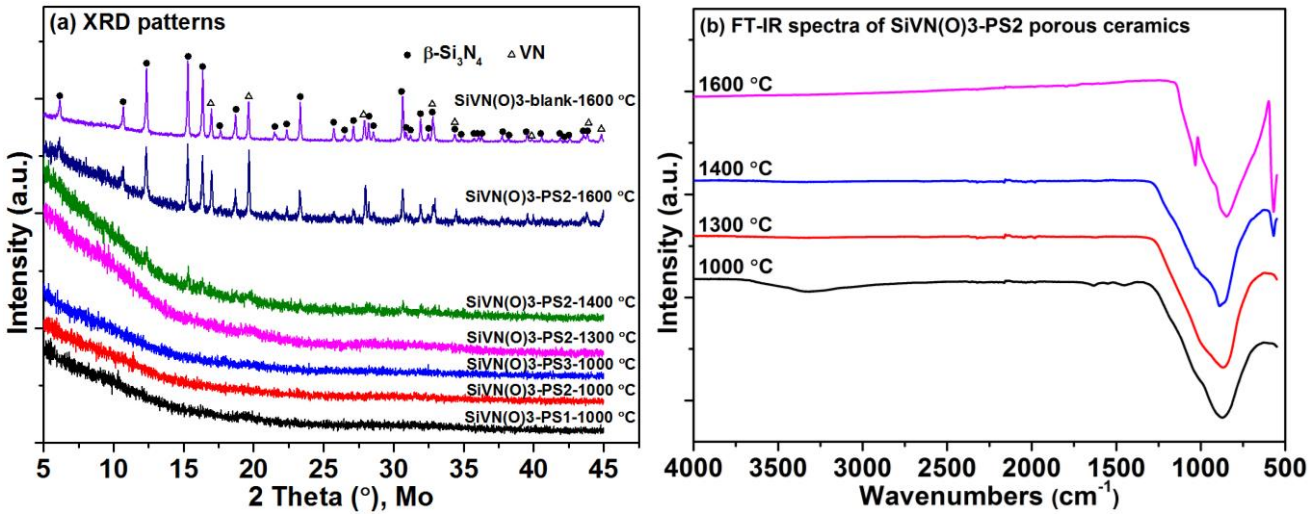

Fig. 4-21. XRD patterns (a) and FT-IR spectra (b) of the SiVN(O)3-PS mesoporous ceramics annealed at different temperatures.

FT-IR measurements were also performed to study the mesoporous SiVN(O)3 ceramics. In the FT-IR spectra [Fig. 4-21(b)], the broad peak from 1250 to 700 cm^{-1} was typical for Si_3N_4 ceramics and can be attributed to the overlapping of Si-N and Si-N-Si bands, which was basically in accordance with the FT-IR spectrum of SiVN(O)3-blank ceramic, confirming the presence of silicon nitride ceramic. When temperatures were increased to 1600 ℃, the broad peak divided into several sharp vibrations, demonstrating intense phase separation and grain coarsening, which is consistent with the XRD results.

Table 12. Pore parameters of the porous SiVN(O)3-PS ceramics annealed at different temperatures.

Samples name	SSA (m^2/g)	Mesopore SSA (m^2/g)	Vt (cm^3/g)	Vm (cm^3/g)
SiVN(O)3-PS1-1300	251	251	0.473	0
SiVN(O)3-PS1-1400	77	77	0.332	0
SiVN(O)3-PS2-800	642	617	1.042	0.039
SiVN(O)3-PS2-1300	317	317	0.879	0
SiVN(O)3-PS2-1400	181	181	0.811	0
SiVN(O)3-PS2-1600	12	12	0.045	0
SiVN(O)3-PS3-1300	329	329	1.346	0
SiVN(O)3-PS3-1400	219	219	1.289	0

The temperature-dependent stability of the mesoporous SiVN(O)3 ceramics was also investigated, and the results of the nitrogen absorption measurement are shown in Fig. 4-22 and Table 12. Compared with the samples obtained at 1000 ℃, heat-treatment caused a certain degree of decrease in the SSA and pore volume. For the sample SiVN(O)3-PS1, after the heat-treatment at 1300 ℃, the micropores cannot be detected, but almost all the mesopores were preserved. In the case of SiVN(O)3-PS2 and SiVN(O)3-PS3, the SSA was about 300 m^2/g in the 1300 ℃ annealed ceramics and further dropped to *ca.* 200 m^2/g at 1400 ℃. This remarkable result revealed the excellent structural stability of the as-obtained porous SiVN(O)3 ceramics. Moreover, it was also found that the pore sizes gradually became larger with increasing temperature. The high-temperature stability of the mesoporous network could be attributed to (i) the intrinsic high-temperature creep resistance property of silicon nitride ceramic matrix and (ii) the modification with $VO(acac)_2$ leading to the crystallization inhibition at 1300 and 1400 ℃, which has been discussed in section 4.2.2. The total collapse of these mesoporous SiVN(O)3 ceramics was observed when the annealing temperature reached 1600 ℃, and the SSA decreased to *ca.*12 m^2/g. The collapse of the mesoporous ceramics could be ascribed to several reasons, and the grain coarsening of the SiVN(O)3 matrix was regarded as the major cause: with increasing heating temperature, especially when the temperature was over 1400 ℃, phase separation took place together with the crystallization of Si_3N_4 and VN, the grain growth destroyed the microstructures of the mesoporous ceramics, resulting in the decrease of SSA.

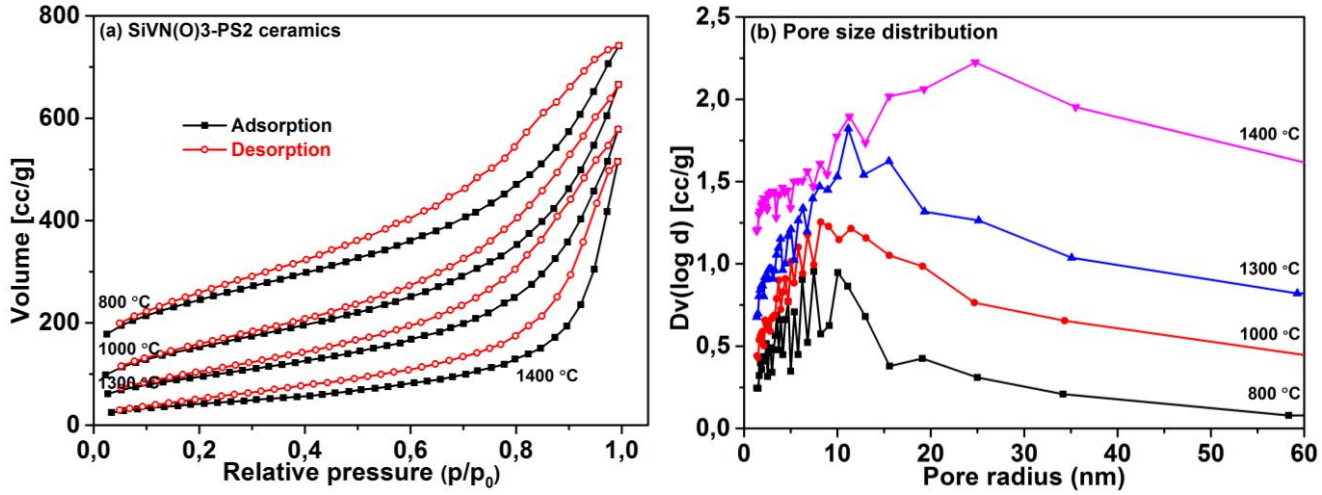

Fig. 4-22. Nitrogen adsorption-desorption isotherms and calculated pore size distribution of the mesoporous SiVN(O)3-PS2 ceramic annealed at different temperatures: (a) nitrogen adsorption-desorption isotherms, (b) pore size distribution.

At 1600 ℃, the high-temperature was favorable to the grain coarsening of ceramics, the crystallinity of Si_3N_4 and VN increased intensively and the their grain size grew up to several dozens or even hundreds of nanometers that was much larger than the pore sizes. Finally, it caused the complete collapse of the mesopores. On the other hand, the Si_3N_4 was not stable and easy to decompose into silicon and nitrogen at such high temperature, which was another negative factor for the mesoporous structure. Additionally, a certain amount of carbon and oxygen

were introduced by PS and $VO(acac)_2$ and remained in the ceramics. The carbon residue caused the carbothermal reduction between C and Si_3N_4, while the oxygen residue caused the decomposition of the ceramic by releasing gaseous CO and SiO. These reasons may also contribute to the disruption of the mesopores. In summary, all these disadvantages worked together at high temperature and caused the collapse of pores in the ceramics, and the mesoporous structure may survive at even higher temperatures if the crystallization and decomposition of the ceramic framework can be suppressed.

4.2.5 Summary

In the present work, a SiVN(O) single-source precursor was synthesized and the corresponding SiVN(O) ceramic was prepared by subsequent heat-treatment under ammonia. The high-temperature properties of the SiVN(O) ceramics were investigated and the results were summarized here.

(1) $VO(acac)_2$ was used as the vanadium source to react with PHPS, and then a single-source SiVN(O) precursor was successfully synthesized. The spectroscopic measurements proved that $VO(acac)_2$ can react with N-H via a condensation reaction, and Si-O-V linkages were formed by the reaction between $VO(acac)_2$ and the Si-H groups.

(2) Although the modification of PHPS with $VO(acac)_2$ improved the cross-linking degree of the single-source precursors, the ceramic yield was not improved due to the loss of carbon and oxygen that were introduced by the addition of $VO(acac)_2$. After ammonolysis, a single-phase SiVN(O) ceramic was obtained, with the nano-sized VN and V atoms in the amorphous matrix.

(3) The as-obtained SiVN(O) ceramic exhibited high-temperature resistance with respect to crystallization up to 1400 ℃. Annealing at 1600 ℃ caused phase separation of the samples, and the nanocomposite composed of VN, α- and β-Si_3N_4 was obtained. It needs to be stressed that the introduction of $VO(acac)_2$ could change the ratio of α/β-Si_3N_4 crystallites in the 1600 ℃-prepared samples, and only the β-Si_3N_4 phase was found in 1600 ℃-annealed SiVN(O)-3 ceramic. Therefore, the proportion of β-Si_3N_4 can be controlled by tuning the $VO(acac)_2$ in the feed.

(4) Mesoporous structured SiVN(O) ceramics with high specific surface areas were successfully prepared by using polyolefin as a self-sacrificial template. The preparation of the green body was simply achieved in a one-pot synthesis by mixing polyolefin, PHPS and $VO(acac)_2$. Among these three kind of polymers (PS, LLDPE, PBMA), the PS template displayed the best result in the SiVN(O) system, and the SSA was as high as 506 m^2/g after pyrolysis at 1000 ℃ when the weight ratio of PS/SiVN(O)-3 was 2/1. Further increases of the proportion of the PS template had less contribution to the surface area, but the pore size was enlarged. The influence of heating temperatures was intensively studied regarding the stability of the pores, and the mesopores can survive up to 1400 ℃, suggesting that the mesoporous SiVN(O) ceramic composites are well-suited materials for catalyst applications.

4.3 SiFeN(O) ceramics

The preparation of material with micro/nano-structures has been increasingly attracted researcher's interest due to their unique morphology and superior properties different with their bulk counterpart, and the use of polymeric precursors is one of the promising manufacturing techniques. In the present work, Si-Fe-N(O) based ceramic paper with in-situ generated hierarchical micro/nano-morphology was simply prepared by pyrolyzing filter paper template impregnated with a Si-Fe-N(O) precursor, which was synthesized by the reaction of perhydropolysilazane (PHPS) with iron(II) acetylacetonate ($Fe(acac)_2$) and the experiment details were presented in Chapter 3. The chemical reaction between $Fe(acac)_2$ and PHPS are analyzed and discussed in Section 4.3.1, and then Section 4.3.2 presents the phase separation, crystallization behavior and microstructures of the SiFeN(O) ceramics obtained after high temperature annealing. After pyrolysis in nitrogen at temperature from 1200 to 1400 ℃, the paper matrix carbonized and consisted of amorphous Si-O-N/C and crystallized Fe_3Si, with the generation of ultra-long silicon nitride nanowires with high aspect ratios (~200 nm in diameter and several millimeter in length) both on the surface and in the pores of paper, decorated with a round Fe_3Si tip at the end of the nanowires, the detailed results are discussed in Section 4.3.3, and Section 4.3.4 analyzes some parameters affecting the formation of 1D nanostructures. The growth mechanism of nanowires is supposed to be vapor-liquid-solid reaction and will be elaborated in Section 4.3.5.

4.3.1 Synthesis of the SiFeN(O) precursors

The FT-IR spectra of SiFeN(O) precursor with different iron content are shown in Fig. 4-23. From a comparison of the FT-IR spectra, it can be found that the SiFeN(O) precursors exhibited characteristic absorption peaks of the PHPS and the $Fe(acac)_2$, such as Si-H (2145 cm^{-1}), N-H (3375 cm^{-1}) (assigned to PHPS) and C=C (1512 cm^{-1}), C=O (1571 cm^{-1}) [assigned to $Fe(acac)_2$] and C-H (2967, 2931, 2871 cm^{-1}) [assigned to CH_3 and C=C-H]. The spectrum of SiFeN(O)-5 showed no obvious changes after the modification reaction. While in the spectrum of SiFeN(O)-30 and SiFeN(O)-50, the Si-H stretch absorption peak decreased significantly, indicating that a chemical reaction occurred between PHPS and $Fe(acac)_2$. By comparison, it was clear that the peak intensity of the Si-H bond of the SiFeN(O) precursors decreased with increasing the weight ratio of $Fe(acac)_2$ in feed, further proved that the reaction of PHPS/$Fe(acac)_2$ proceeded on account of the consuming of the Si-H groups.

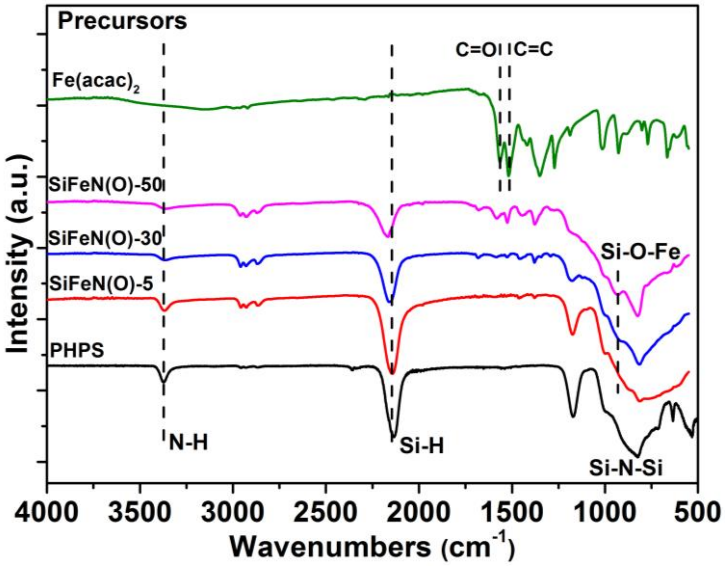

Fig. 4-23. FT-IR spectra of PHPS, $Fe(acac)_2$ and of SiFeN(O) precursors with different iron content.

Few reports can be found about $Fe(acac)_2$, but $Fe(acac)_3$ can be used as a reference due to the similar physical and chemical properties. There is less information in the literature concerning the reaction of Si-H bonds with metal acetylacetonates. Some literatures have reported that polycarbosilane can react with metal acetylacetonates with the formation of Si-M bonds. However, most of the evidence is indirect, such as a strong decrease in the Si-H bonds or the release of acetylacetonate[230, 231], due to the high sensitivity of the Si-M bond against hydrolysis. In this case, a new absorption peak at ca. 930 cm^{-1} was observed and attributed to the formation of Si-O-Fe linkages, as also reported in the literature[22, 232]; moreover, the intensity of the Si-O-Fe absorption band increased obviously with increasing the amount of $Fe(acac)_2$ introduced. However, it is difficult for all the ligands of $Fe(acac)_2$ to participate in the reaction due to the steric hindrance, as a result, the characteristic absorption peaks derived from the ligands of $Fe(acac)_2$ (C=C and C=O) still remained in the spectra of SiFeN(O) precursors. Based on the observed consumption of Si-H groups and formation of Si-O-Fe bonds, it can be concluded that SiFeN(O) single-source precursor was successfully synthesized upon chemical modification of PHPS with $Fe(acac)_2$, and one possible path for the reaction between PHPS and $Fe(acac)_2$ was proposed and shown in Fig. 4-24.

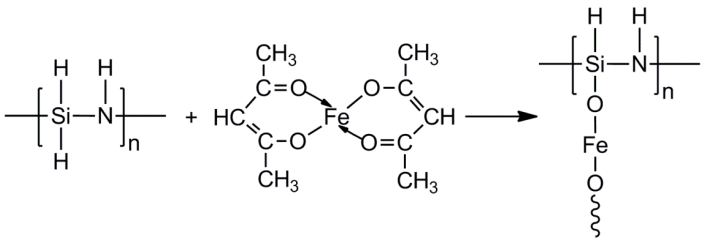

Fig. 4-24. Possible reaction pathway during the synthesis of the SiFeN(O) precursor from PHPS and $Fe(acac)_2$.

4.3.2 Microstructural evolution of SiFeN(O) ceramics powder at high-temperature

In order to investigate the polymer-to-ceramic conversion of the $Fe(acac)_2$-modified PHPS samples as well as the high-temperature evolution of the resulting SiFeN(O) ceramics, the single-source precursors were annealed at different temperatures and the crystalline phase composition was assessed by means of XRD. The XRD patterns of SiFeN(O)-5 annealed at different temperatures are shown in Fig. 4-25(a). Due to the low iron content, α-Fe diffraction peaks were not found in the pattern and the 1000 ℃-obtained SiFeN(O)-5 ceramic was found to be X-ray amorphous. At 1200 and 1300 ℃, some broad humps appeared and they were usually attributed to Si_3N_4, while the Si_2ON_2 peaks were also seated in the same area and difficult to be verified. After annealing at 1400 ℃, the sharp diffraction peaks assigned to α-Si_3N_4 appeared, but no iron-containing crystalline phases were obtained. Moreover, no formation excess silicon was observed, as it was reported for PHPS-derived amorphous SiN_x samples exposed to high temperatures in either ammonia or nitrogen atmosphere[233]. This might be related to the relatively large amount of oxygen contained in the samples, due to the modification of PHPS with iron acetylacetonate.

As shown in Fig. 4-25(b), SiFeN(O)-50 obtained upon ammonolysis of the single-source precursor at 600 ℃ showed a broad, low-intensity reflection at 2θ=19.3 °, which was tentatively assigned to Fe_2N [234]. The intensity of the Fe_2N reflection was shown to increase as the single-source precursor was thermally treated in ammonia at 700 ℃ [235, 236]. This is in agreement to other reports discussing the formation of iron nitrides (e.g. Fe_2N or Fe_3N_{1+x}) as the results of the heat-treatment in ammonia atmosphere of Fe-based compounds such as oxides or halides, elemental iron is generated intermediary as a result of the reduction of the iron compounds and subsequently nitrided by ammonia [235-238]. But if the heating temperature was increased to 1000 ℃, it can be found in the XRD pattern that Fe_2N began to decompose and form α-Fe, which was in agreement with the literature[234, 239, 240]. In the present case, we assume that the conversion of iron nitride into α-Fe occurs due to the large amount of hydrogen present in the ammonolysis atmosphere at those high temperatures (i.e., 700 to 1000 ℃). As reported recently, iron nitrides can exhibit significantly decomposition in the presence of H_2 (even at moderate temperatures, i.e. exceeding 400 ℃) [241]. Hence, it is assumed that the increase of the temperature of the ammonolysis induces the generation of specific partial pressures of hydrogen in the furnace atmosphere, which are high enough to fulfill the denitridation of the iron nitrides and generate α-Fe. When the SiFeN(O)-50 ceramic was further annealed at 1200 ℃ under N_2 atmosphere, except for the intensive peak of α-Fe, a small amount of Si_2ON_2 phase was also found in the XRD pattern. Si_2ON_2 phase was an intermediate product and it was usually reported to be formed after the pyrolysis of polysiloxane precursors in N_2 or ammonia atmosphere at low-processing temperatures. In our case, the modification with $Fe(acac)_2$ also introduced oxygen into the precursor, as a result, the decomposition behavior of SiFeN(O)-50 was similar to that of polysiloxane, this explained that why Si_2ON_2 was observed in the annealed SiFeN(O)-50 specimen. According to the research of Siddiqi and Hendry[242], the equilibrium stable phases formed on nitriding SiO_2:C mixtures in the temperature range from 1300 to 1500 °C were either β-Si_3N_4+C or Si_2ON_2+C, and the stability of the formed phases depended strongly on the O_2 partial pressure, in other words: increase in the O_2 partial pressure can promote the

formation of Si_2ON_2, while Si_3N_4 was more stable than Si_2ON_2 in low O_2 partial pressure[242, 243]. Subsequently, with increasing the heating temperatures or with the extension of the heating time in N_2 atmosphere, the phase transformation from Si_2ON_2 to Si_3N_4 can be accelerated and only Si_3N_4 can be found in the final sample.

With increasing the sintering temperature to 1300 ℃, the intensity of the Si_2N_2O reflections increases; moreover, Fe_3Si was detected as crystalline phase. Whereas the XRD pattern of the sample annealed at 1400 ℃ show the presence of Fe_3Si as a main crystalline phase beside only small amounts of Si_2ON_2 and α-Fe. As the intensity of the reflections assigned to Fe_3Si increased and in the same time those related to α-Fe decreased in intensity, one can assume that the formation of Fe_3Si probably relies on the reaction of α-Fe with the SiFeNO-based amorphous matrix. The reaction of α-Fe with Si_2ON_2 which may also lead to the formation of Fe_3Si *cf.* $Si_2N_2O + 3Fe = Fe_3Si + SiO(g) + N_2(g)$ can be ruled out, as its ΔG values are unfavorable in the temperature range used for the annealing experiments.

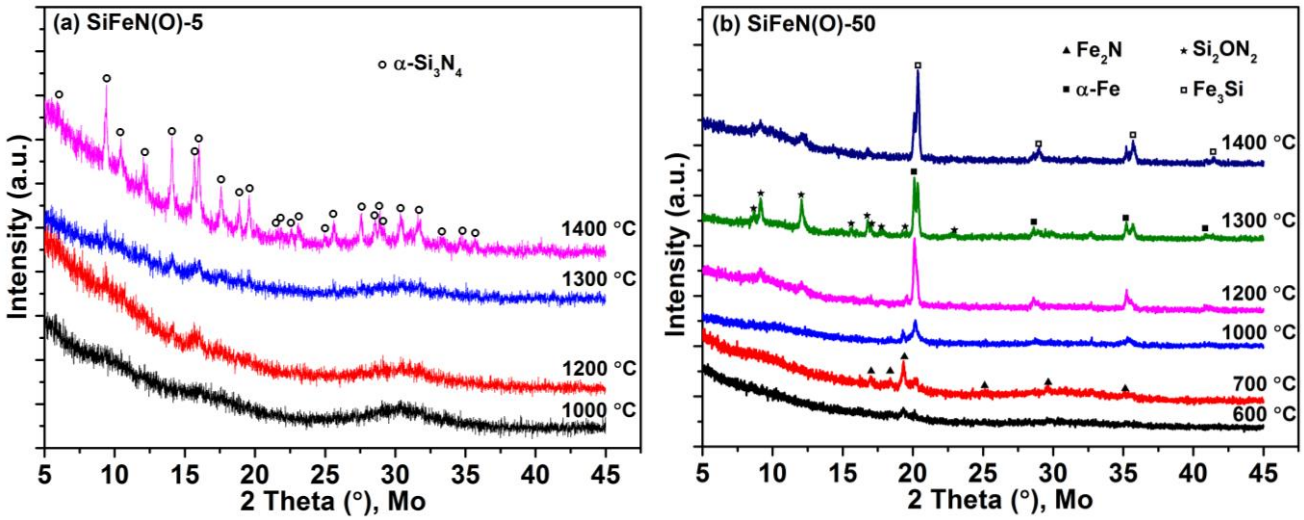

Fig. 4-25. XRD patterns of ceramics powder annealed at different temperatures: (a) SiFeN(O)-5 and (b) SiFeN(O)-50.

Interestingly, only very weak reflections related to Si_3N_4 were observed in the SiFeN(O)-50-based recovered powder samples annealed at different temperatures, indicating a poor crystallization thereof. However, some colorless α-Si_3N_4 nanowires were found on the surface of crucible after sintering at 1400 ℃ in nitrogen atmosphere (Fig. 4-26). The formation of the nanowires is considered to be a consequence of an iron-catalyzed VLS (vapor-liquid-solid) process [244], as they exhibit Fe_3Si tips. However, as the growth of the nanowires was not observed on the powder surface (as it may be expected) but on the surface of the crucible, we assume that during the high-temperature annealing in nitrogen atmosphere iron, being the main crystalline phase in the ceramic powder, evaporated and condensed on the surface of the crucible, thus allowing for the VLS growth of the α-Si_3N_4 nanowires onto it [245]. As the nanowires were decorated with Fe_3Si, we can rule out the VS growth mechanism of Si_3N_4 on the surface of SiC crucible, as recently reported [246].

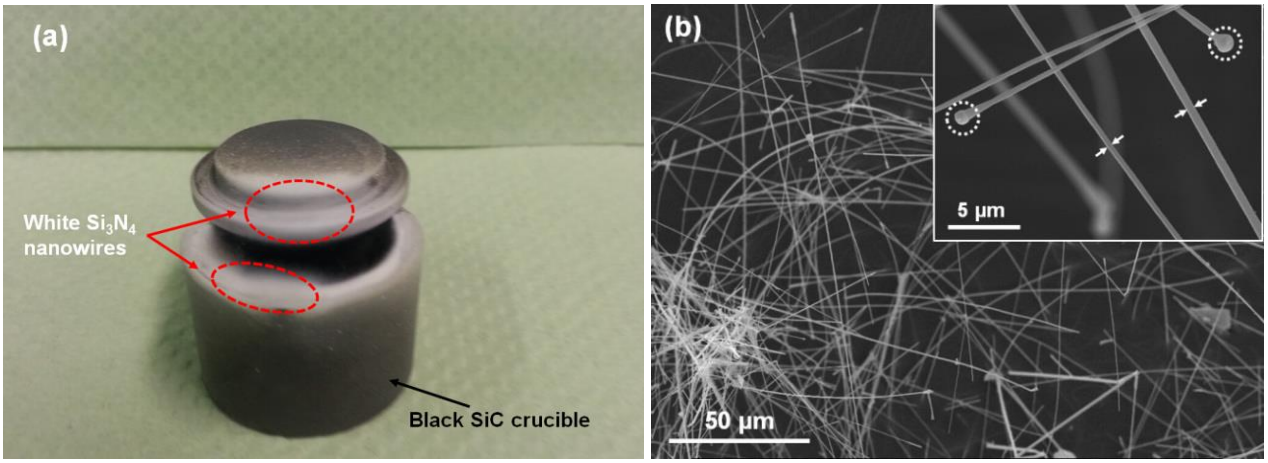

Fig. 4-26. (a) Photograph of the nanowires that formed on the surface of crucible and (b) SEM micrographs of the Si_3N_4 nanowires obtained from the SiFeN-50 ceramic powder annealed at 1400 ℃ under N_2.

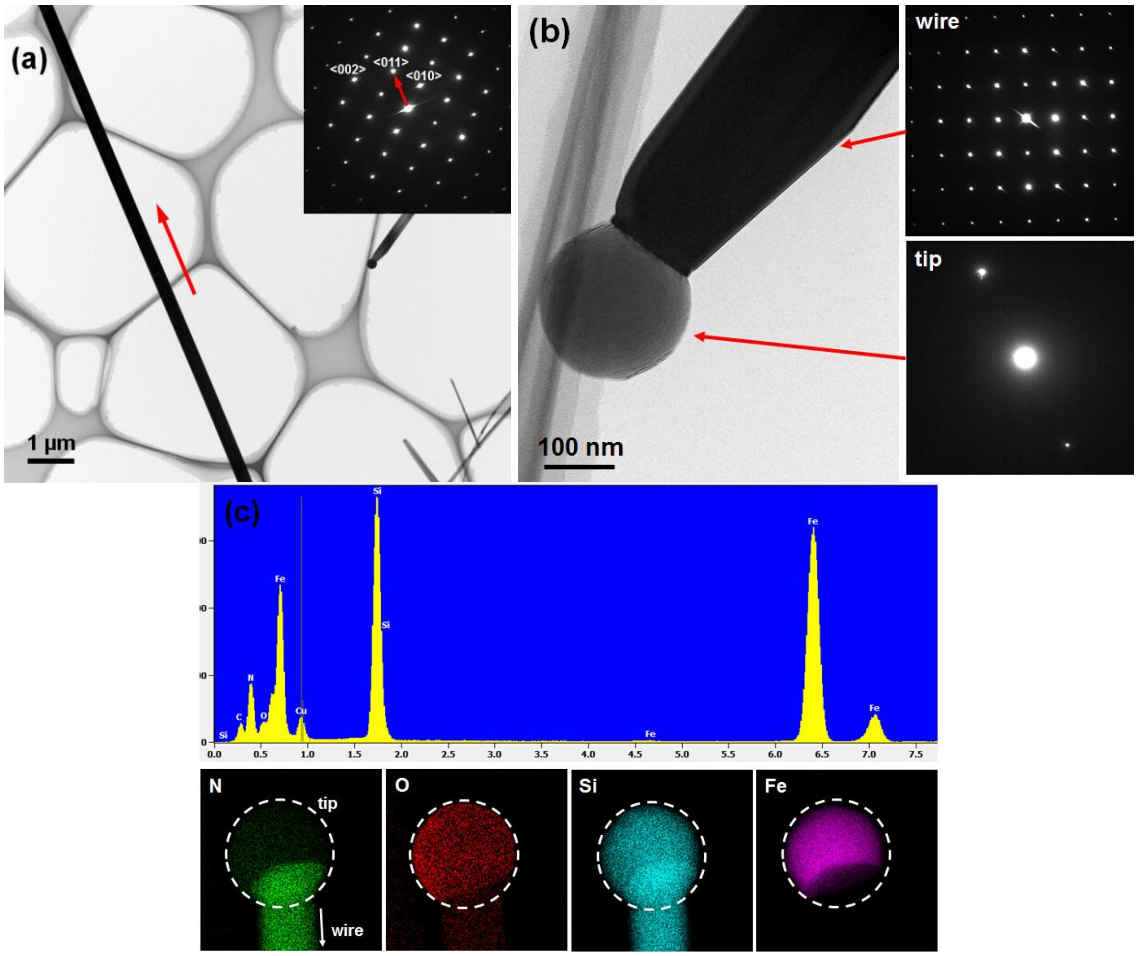

Fig. 4-27. HRTEM analysis of the Paper-SiFeN(O)50 pyrolyzed at 1300 ℃ under N_2 atmosphere: (a) low-magnification TEM overview and SAED pattern (inset) of the α-Si_3N_4 nanowires; (b) TEM image and SAED patterns of the nanowire and the round tip; (c) nano-chemical measurements of the round tip: EDX (top) and element mapping (bottom).

HRTEM micrographs of the silicon nitride-based nanowires obtained upon annealing at 1400 ℃ in N_2 are shown Fig. 4-27. In Fig. 4-27(a), it is shown that the nanowires consist of single-crystalline α-Si_3N_4, have a uniform diameter of *ca.* 300 nm and were growing along the <011> direction. Additionally, the nanowire has uniform surface morphology with few defects, which is in accordance with the SEM observations. Fig. 4-27(b) shows the round tip at the end of a silicon nitride nanowire, which was brighter than the nanowire in the TEM image; the tip was shown also to be single-crystalline, though with no obvious orientation relationship between the tip and nanowire. In Fig. 4-27(c), the EDX profile (top) indicated that the round tip predominantly contained iron and silicon, with a little nitrogen, carbon and oxygen contamination; element mapping indicates that the nanowires consist mainly of Si and N, thus being in agreement with the XRD data, and the tip was composed of Fe_3Si; moreover, Si_3N_4 nanowire was found to grow out from the center of the Fe_3Si tip which was considered to play a catalytic role towards accelerating the growth of 1D nanostructures, clearly supporting the VLS mechanism of the growth of the α-Si_3N_4 nanowires.

4.3.3 SiFeN(O)-based ceramic paper

The cotton linters filter paper consists mainly of cellulose fibers containing O-H groups, which were used to modify the paper surface with the SiFeN(O) single-source precursor. According to the FT-IR spectra shown in Fig. 4-28(a), it was clear that the filter paper was successfully modified by SiFeN(O)-50 precursor. However, it is not clear how the SiFeN(O)-50 precursor was grafted to the cellulose fibers, i.e., whether physical or chemical bonding occurred. The SiFeN(O)-50-modified hybrid paper was pyrolyzed at 700 and 1000 ℃ under NH_3 atmosphere and converted into a black, X-ray amorphous ceramic paper containing small amounts of α-Fe [Fig. 4-28(b)].

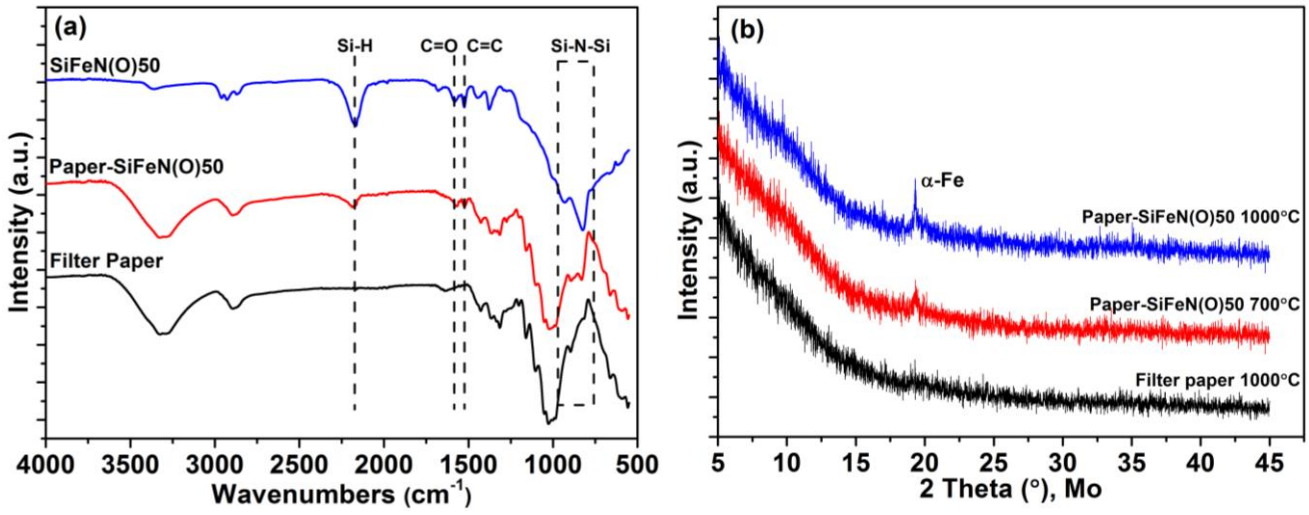

Fig. 4-28. FT-IR spectra (a) and XRD patterns (b) of cotton linters filter paper as well as of the single-source-precursor-modified hybrid paper as prepared (as for the FTIR spectra) and heat-treated at different temperatures in NH_3 atmosphere (as for the XRD patterns).

SEM measurement was also performed on the samples, and the images are shown in Fig. 4-29. Fig. 4-29(a) shows the SEM image of the original filter paper, it was made up of cellulose paper fibers, and lots of pores existed between the fibers. The EDX profile exhibited that the paper was predominantly composed of C and O (as well as H which was difficult to be detected). Fig. 4-29(b) shows the micrograph of the SiFeN(O)50 precursor impregnated paper, and it can be confirmed from the EDX profile that the modification was successful, because both Si and Fe signals were collected from the sample. Additionally, the modification did not change the feature of the original paper, the paper fiber and pores can still be clearly observed. SEM micrographs of the SiFeN(O) ceramic paper obtained upon ammonolysis at 1000 ℃ are shown in Fig. 4-29(c), after the pyrolysis under ammonia, the oxygen signal disappeared in the EDX, but Si and Fe was retained in the ceramic paper, which was in agreement with the XRD result. Although some shrinkage can be observed (compare the thickness of the cellulose fibers in the paper template with that of the resulting carbon(ized) fibers in the ceramic paper) due to the pyrolysis procedure, but its intrinsic morphology of the cellulose-based paper was preserved. The ceramic paper consists mainly of carbon fibers and embedded in a SiFeN(O) matrix.

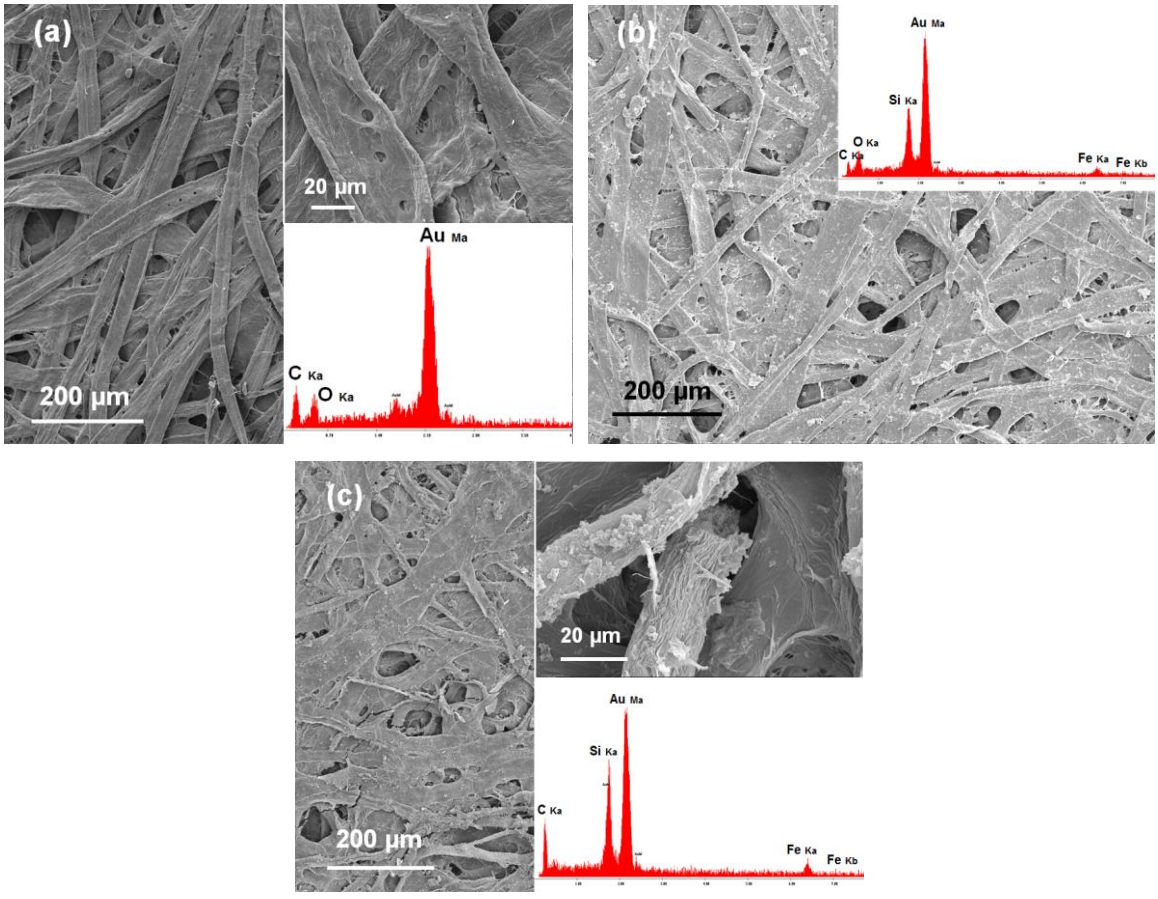

Fig. 4-29. SEM micrographs taken from the surfaces of (a) original filter paper, (b) SiFeN(O)50 precursor impregnated paper and (c) Paper-SiFeN(O)50 prepared at 1000 ℃ under NH_3. Insets show high-magnification images of the samples and EDX profiles.

The TEM micrographs of the SiFeN(O) ceramic paper shown in Fig. 4-30(a) indicate that the ceramic paper is multiphasic, consisting of carbon fibers and ceramic SiFeN(O) matrix. The ceramic is composed of nano-scaled

Fe_3Si particles homogeneously dispersed within an amorphous Si(C)NO matrix. In Fig. 4-30(b), it is shown that the carbonized cellulose fibers consist of disordered, turbostratic carbon. It is worth to mention that the ammonolysis of the non-modified cotton linters paper typically leads to a mass loss more than 85 wt.%; whereas the modification of the paper with the single-source precursor prevent that the cellulose fibers are "burnt out" in ammonia atmosphere. Thus, we assume that the single-source polymeric precursor covers the cellulose fibers and protect them from ammonia attack during their conversion into carbon fibers. However, more detail studies are necessary to understand how the modified cellulose fibers convert in the presence of the SiFeN(O) single-source precursor into turbostratic carbon upon ammonolysis at high temperatures.

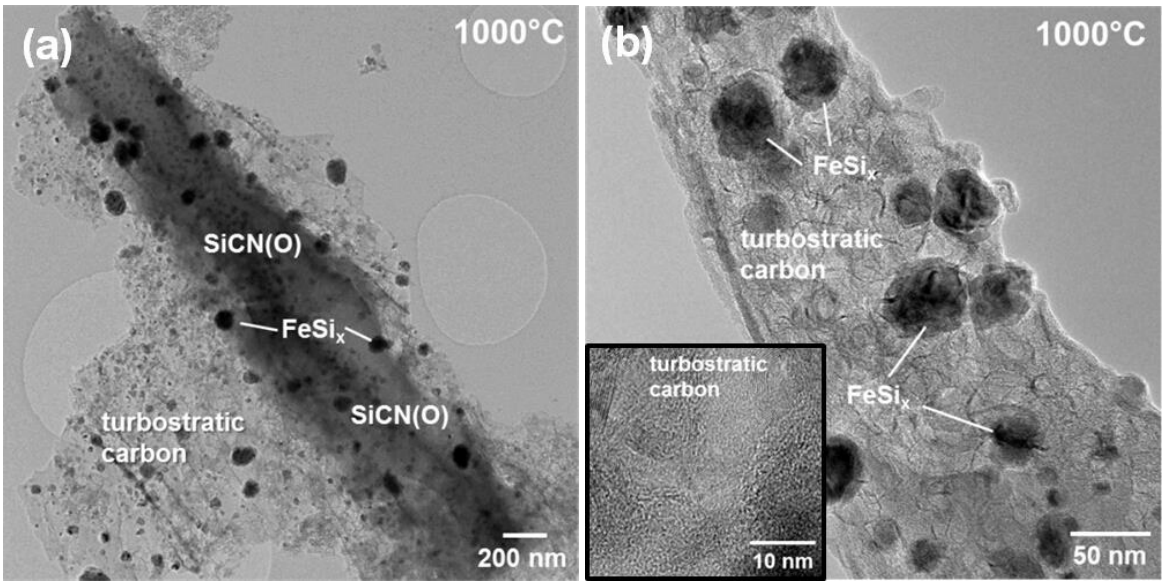

Fig. 4-30. TEM micrographs of SiFeN(O)-50-based ceramic paper obtained upon ammonolysis at 1000 ℃: (a) low-magnification TEM overview of the ceramic paper, (b) high-resolution TEM image of the $FeSi_x$ nanoparticles (inset shows the turbostratic carbon).

The ceramic paper prepared upon ammonolysis at 1000 ℃ was further annealed at temperatures from 1200 to 1400 ℃ in a N_2 atmosphere. The obtained ceramic paper samples exhibited the presence of millimeter-long α-Si_3N_4 nanowires on their surface as well as within their pores. The Paper-SiFeN(O)50 ceramic paper fabricated at 1300 ℃ was chosen as a representative and investigated by X-ray diffraction, SEM and TEM characterizations. In the XRD pattern shown in Fig. 4-31, the diffraction peaks could be indexed to the α- and β-Si_3N_4 as well as crystalline Fe_3Si, respectively.

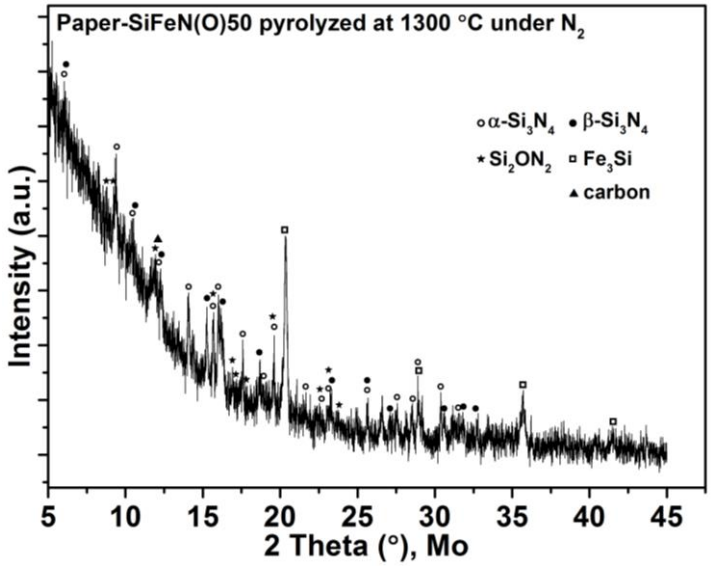

Fig. 4-31. XRD pattern of the Paper-SiFeN(O)50 sample prepared at 1300 ℃ under N_2.

Microstructures of the 1300 ℃-obtained Paper-SiFeN(O)50 ceramic paper were observed by SEM. The low-magnification SEM image Fig. 4-32(a) confirmed that the ceramic paper surface was covered with wire-like structures, and they were referred to as one-dimensional (1D) nanowires. The nanowires were straight with no branches and were grown in random directions; therefore, they arranged in a crisscross pattern and twisted with each other. Interestingly, the morphology of the paper was not significantly changed; thus, the carbon fibers obtained from the carbonization of the cellulose fibers from the paper template can be observed in Fig. 4-32(a) and are *in-situ* decorated with α-Si_3N_4 nanowires upon annealing at high temperatures in a nitrogen atmosphere. The cross-section of the Paper-SiFeN(O)50 was also observed by the SEM and shown in Fig. 4-32(b). Most of the nanowires are concentrated on the both faces of the paper, but some nanowires were still found in the interlayers and pores of the paper template (marked by the dotted box). Both the 1D nanowires and the paper fiber matrix together constituted a hierarchical micro/nano-morphology. The as-obtained nanowires exhibited great aspect ratios. Based on the SEM images, it is found that most of the nanowires were typically several hundred micrometers or even several millimeters in length, and they had widths ranging from 200 to 300 nm [as shown in Fig. 4-32(c)]. High-magnification SEM images [Fig. 4-32(d)] revealed that round tips (or particles) were present at the end of the nanowires. The nanowires were further examined by energy dispersive X-ray spectroscopy (EDS), and the result indicated that almost no signal of iron was detected on the nanowires, while a strong signal of iron was collected at the round tips. This result implied that the growth of the nanowires could be explained by the VLS mechanism. Combined with the above mentioned XRD data, it can be speculated that the nanowires were composited of Si_3N_4 crystallite and the major component of the round tips was Fe_3Si. Besides, each of the nanowires exhibited a needle-like tip, marked by a dotted box in Fig. 4-32(d), suggesting a strongly anisotropic growth in the initial stage of the formation of 1D nanowires.

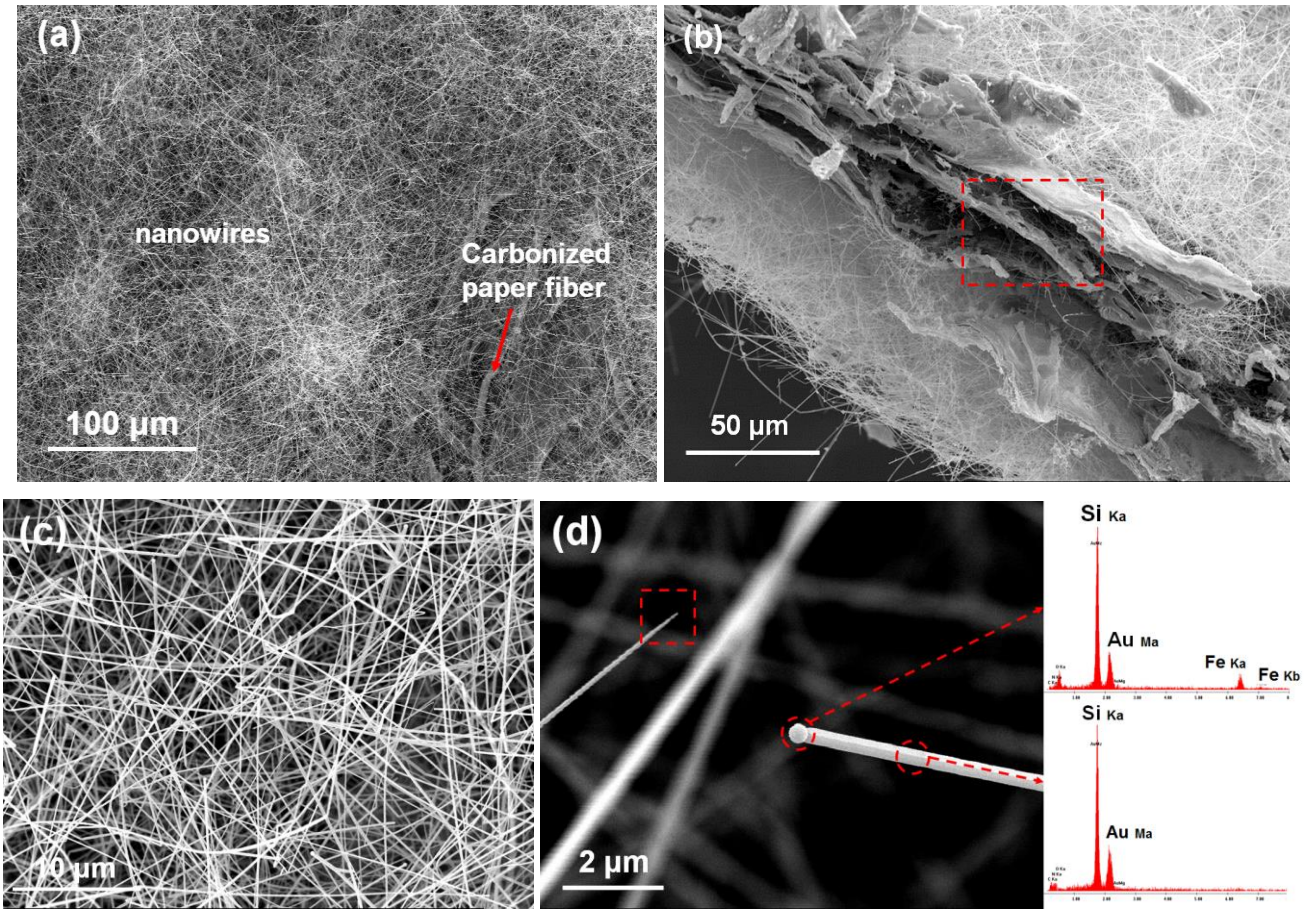

Fig. 4-32. SEM micrographs taken from the Paper-SiFeN(O)50 pyrolyzed at 1300 ℃ under N_2: (a) low-magnification SEM overview of the surface of the Paper-SiFeN(O)50 ceramic paper; (b) SEM image of the cross-section of the sample; (c) SEM image of the nanowires; (d) high-resolution SEM image of the nanowire with the corresponding EDX profile.

TEM micrographs shown in Fig. 4-33 indicate the formation of α-Si_3N_4 nanowires upon annealing of the SiFeN(O)-50 ceramic paper at 1300 ℃ in N_2 atmosphere. The ceramic matrix consists of SiFeN(O) and turbostratic carbon [Fig. 4-33(a, b)]. The *in situ* generated 1D nanostructures also exhibited Fe_3Si tips, indicating that their growth occurred *via* VLS mechanism. Interestingly, the Fe_3Si tips were embedded within a "skin" of turbostratic carbon [Fig. 4-33(c, d)]; whereas the Fe_3Si tips of the nanowires generated from the SiFeN(O)-50 powder (*i.e.*, without using the paper template) did not show any carbon deposition onto their surface. This difference is intriguing and has been assumed to correlate to the amount of gaseous hydrocarbon released during the high-temperature annealing of the samples: thus, the template-free annealing of the SiFeN(O)-50 powder leads to less or no release of hydrocarbons; whereas the annealing of the SiFeN(O)-50-based ceramic paper occurs upon release of hydrocarbons which consequently are responsible for the deposition of turbostratic carbon on the surface of the Fe_3Si tips, as discussed in detail in the next section below.

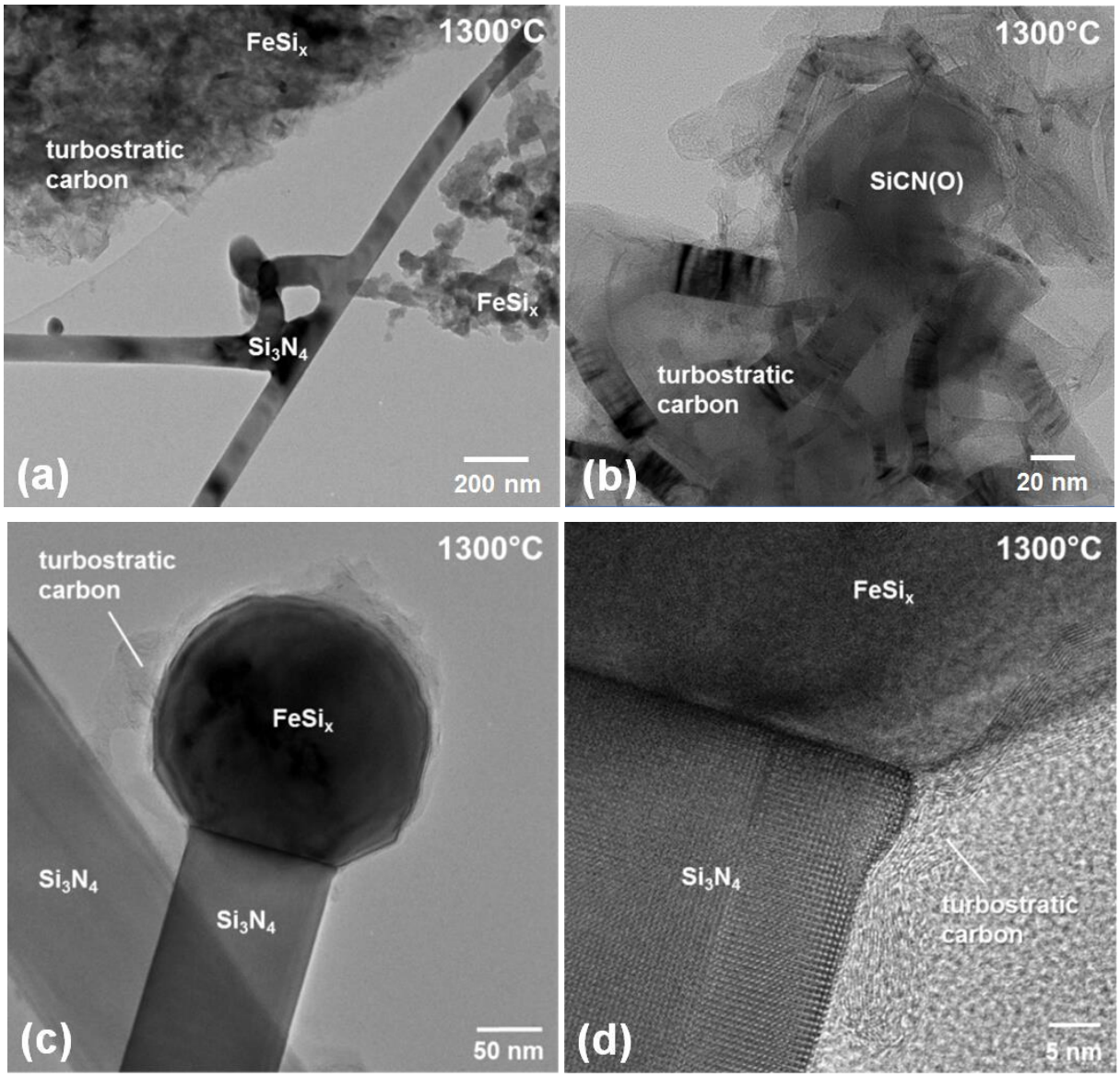

Fig. 4-33. HRTEM analysis of the Paper-SiFeN(O)50 pyrolyzed at 1300 ℃ under N_2 atmosphere: (a) SiFeN(O) ceramic matrix and turbostratic carbon; (b) high-resolution TEM image of the matrix; (c) low-magnification TEM overview of the α-Si_3N_4 nanowires and $FeSi_x$ tip; (d) high-resolution TEM image of the nanowire and the turbostratic carbon.

4.3.4 Parameters affected the formation of 1D-nanostructures on ceramic paper

In order to gain a better understanding of the growth mechanism of the 1D nanostructures, the influence of some preparation conditions such as heating temperature, dipping times and iron content were investigated and discussed in the following section.

(a) Influence of heat-treatment temperature

Temperature is a crucial factor for the fabrication of 1D nanostructures; therefore, the Paper-SiFeN(O)50 was pyrolyzed at different temperatures, and the resultant samples were analyzed by SEM, XRD and Raman measurements. As shown in the SEM images in Fig. 4-34(a), at lower pyrolysis temperature such as 1200 ℃, long nanowires with round tips could also be prepared. However, by comparing with the sample obtained at 1300 ℃ [Fig. 4-34(b)], fewer nanowires were formed at 1200 ℃, and many carbonized paper fibers and macro-pores can be easily observed, implying that the yield of nanowires at 1200 ℃ was lower than that at 1300 ℃. By further increasing the temperature up to 1400 ℃, fewer and shorter nanowires with uneven thickness were obtained [Fig. 4-34(c)]. These short nanowires were only 10 to 100 micrometers long and believed to have just grown out from the ceramic paper substrate in the beginning stage, because the root of the nanowire was found to be connected with the matrix, and the needle-like top was another sign for the initial stage (as shown in the dotted box), seemingly in a "weed growth" mode.

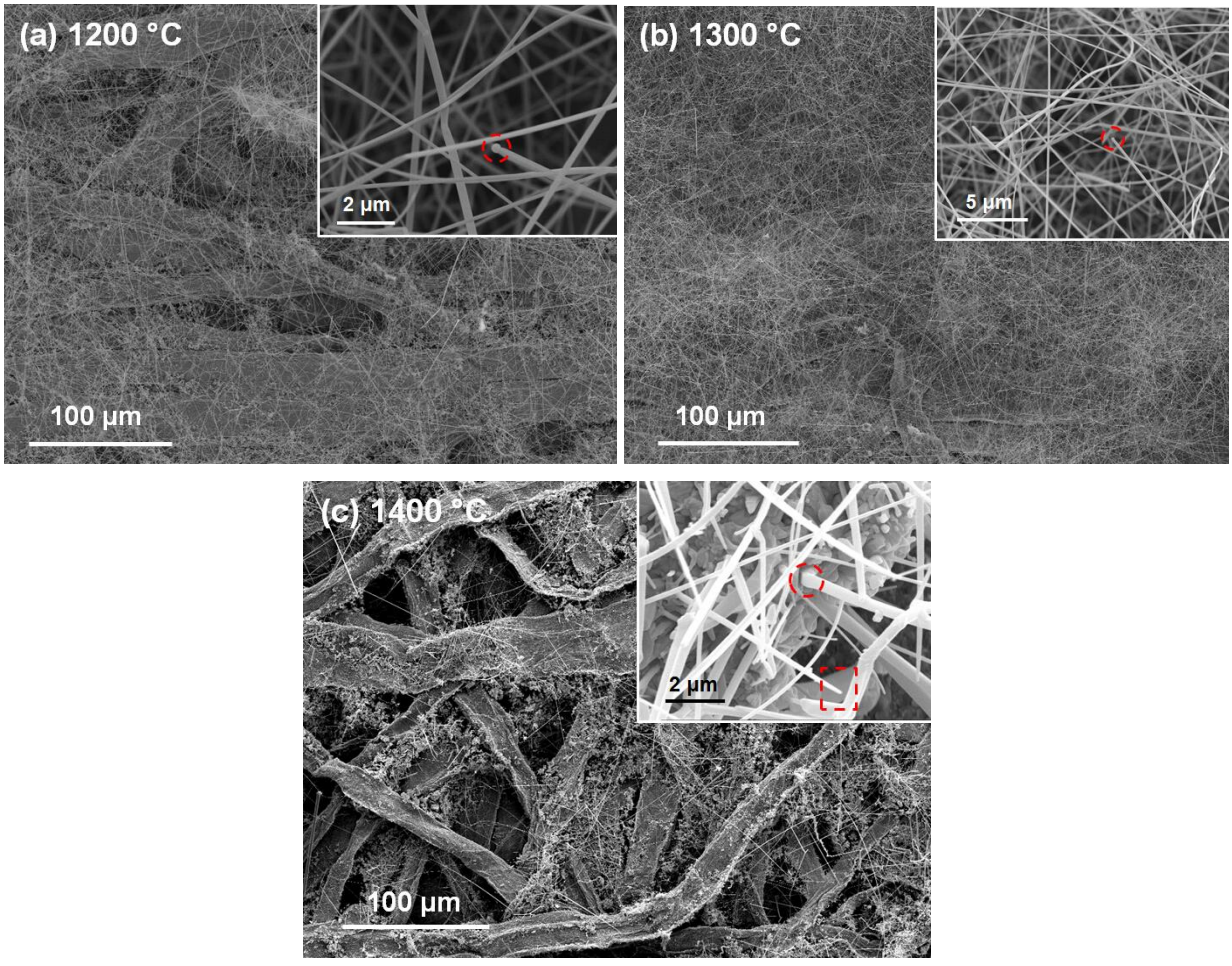

Fig. 4-34. SEM micrographs taken from the surfaces of sample Paper-SiFeN(O)50 pyrolyzed at different temperatures under N_2: (a) 1200 ℃, (b) 1300 ℃, (c) 1400 ℃. Insets show high-magnification images of the 1D nanostructures.

XRD patterns of the ceramic paper obtained at different temperatures are shown in Fig. 4-35(a). The strong diffraction peaks of Fe_3Si can be easily observed, accompanied by the α- and β-Si_3N_4 crystallites, and a broad peak at 2θ=11.8 ° can be assigned to carbon. However, there is no significant difference between the three samples. Raman spectroscopy was also used here to investigate the structural evolution of the free carbon phase in the Paper-SiFeN(O)50 prepared at different temperatures. In Fig. 4-35(b), the ceramic paper obtained at 1200 ℃ exhibits a typical spectrum of amorphous carbon, with a small and broad D band (1350 cm^{-1}), a sharp and intensive G band (1577 cm^{-1}) and a strong 2D band (2701 cm^{-1}), suggesting that the filter paper substrate converted into carbon (partially graphite) at high temperature. As the heating temperature increased, no significant change in the Raman spectra was found, meaning that higher temperature had less effect on the carbonized paper substrate. Raman spectra proved the existence of carbon in the ceramic paper at high temperature, in accordance with the above XRD result.

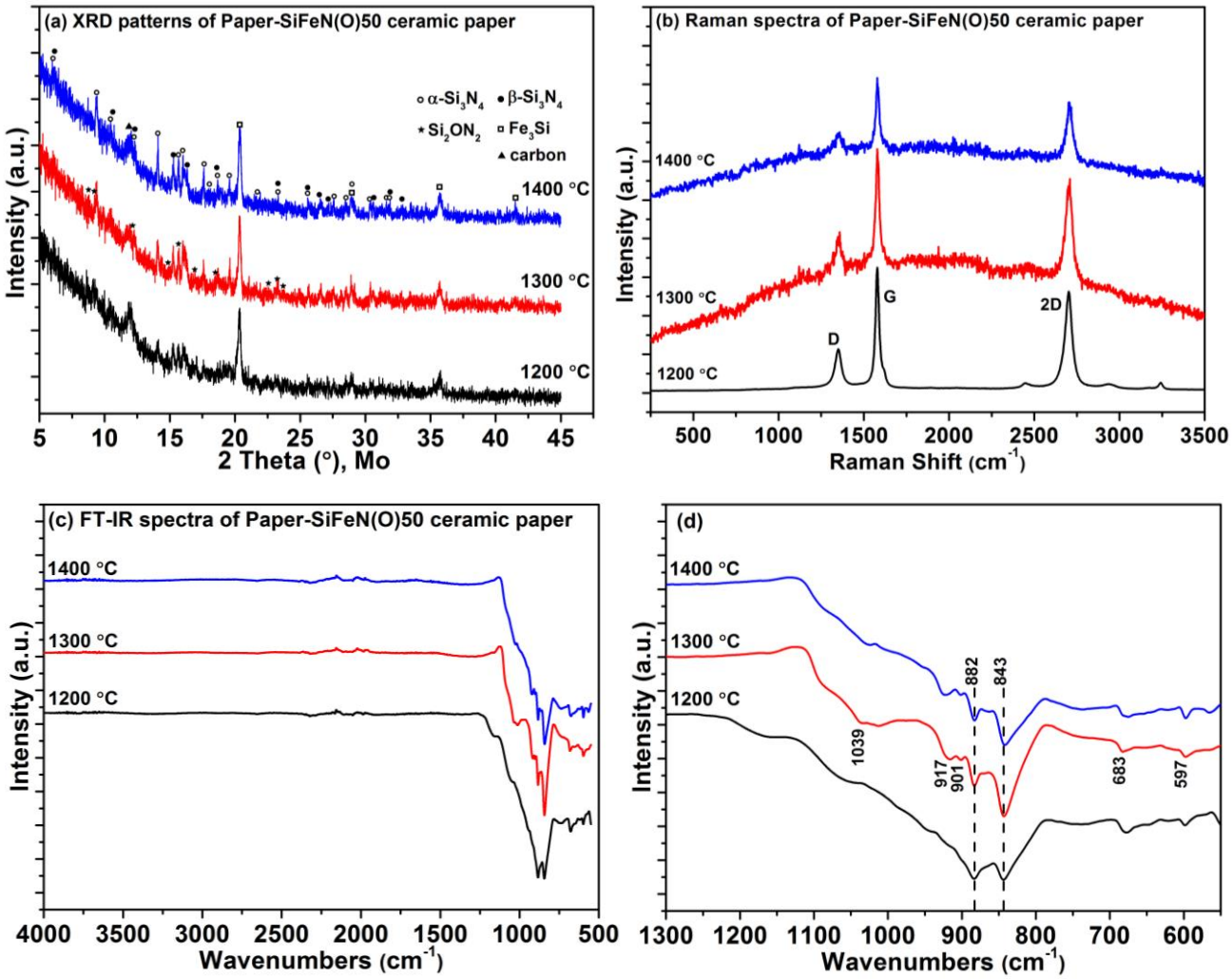

Fig. 4-35. XRD patterns (a), Raman (b) and FT-IR (c, d) spectra of Paper-SiFeN(O)50 pyrolyzed at different temperatures.

FT-IR spectroscopy was also used to analyze the ceramic paper. In the FT-IR spectra [Fig. 4-35(d)], a series of absorption peaks centered at 1039, 917, 901, 882, 843, 683 and 597 cm^{-1} are observed and usually attributed to

the characteristic absorption of Si-N[220]. The absorption peak at 917 cm^{-1} corresponds to the antisymmetrical stretching vibration of Si-N-Si, and the peak at 843 cm^{-1} is assigned to the antisymmetrical mode of N-Si-N[247, 248]. Compared with powdery Si_3N_4 (ca. 935 and 854 cm^{-1}), the stretching vibration absorption peaks have a red-shift of about 10 cm^{-1}, which may be caused by the nanosize effect[249, 250] or the influence of tensile and compressive stress[251].

On the basis of the above results, it can be pointed out that 1300 ℃ was the optimal temperature for the formation of α-Si_3N_4. This is possibly because that, in the present research, the formation of nanowires was based on the reaction of SiO, CO and N_2, which were derived from the decomposition of Si_2ON_2 (This part will be discussed in details in Section 4.3.5). Therefore, 1200 ℃ may be not sufficient for the decomposition of SiFeN(O) ceramic matrix and the formation of 1D nanostructures. By increasing the temperature to 1300 ℃, the decomposition of ceramics and the release of gaseous byproducts can be accelerated, then, the yield of nanowires improved. But when the temperature reached 1400 ℃, the yield of nanowires decreased drastically, and this result could be attributed to the fast decomposition of ceramics and the resulting rapid escape of SiO, CO and N_2 gaseous byproducts.

(b) Influence of dipping times

Dipping time is another factor that affected the formation of 1D nanostructures. In order to investigate the influence of dipping time, a comparison experiment was made: dry filter paper was dipped into the SiFeN(O)-50 precursor toluene solution for 1 second, and then the solvent was removed under an argon atmosphere. This process was repeated up to 5 times. At last, the 5-times dipping sample was heat-treated under the same conditions to fabricate the ceramic paper; as a result, a black and stiff sample was obtained. The resulting sample was observed by SEM, and the result is shown in Fig. 4-36. In Fig. 4-36(a), it can be seen that the whole paper is wrapped by the SiFeN(O) ceramic and becomes a monolithic sheet with cracks all over the surface. Almost no 1D nanostructures could be found on the surface of the ceramic paper, and only a small quantity of nanowires are found around the cracks [Fig. 4-36(b)]. One reasonable explanation for this phenomenon was that the whole paper was covered by the SiFeN(O)50 precursor due to dipping 5 times, and most of the macro-pores in the paper were also filled up and caused no space for the formation of 1D nanostructures during the pyrolysis. Finally, the gaseous products such as SiO and CO derived from the decomposition of SiFeN(O)50 can only escape from the cracks, resulting in the formation of nanowires around the cracks. In this situation, the cracks acted like the macro-pores in the paper, and the results highlighted the indispensable role the macro-pores played in the formation of 1D nanostructures.

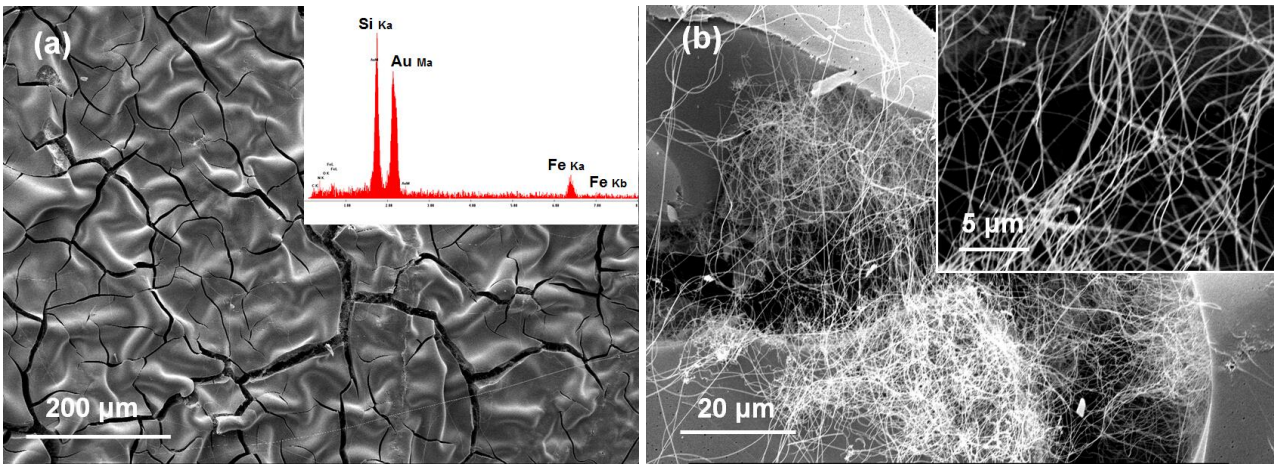

Fig. 4-36. SEM micrographs taken from the Paper-SiFeN(O)50 (dipping 5 times) pyrolyzed at 1300 ℃ under N_2: (a) low-magnification SEM overview of the surface of the sample with the EDX profile; (b) SEM image of the nanowires grown around the cracks.

(c) Influence of the addition of $Fe(acac)_2$

SiFeN(O) ceramic paper decorated with α-Si_3N_4 nanowires could be fabricated by using the filter paper impregnated by a SiFeN(O) precursor. In order to illustrate the role of iron in the formation of these one-dimensional structures, comparison experiments with low content of $Fe(acac)_2$ and without using $Fe(acac)_2$ were performed.

In this case, only 5 wt.% $Fe(acac)_2$ was used to modify PHPS, and the as-obtained paper-ceramic hybrid sample was named Paper-SiFeN(O)5. Heat-treatment was performed on the sample under N_2, and the resultant Paper-SiFeN(O)5 ceramic paper was investigated by SEM. In Fig. 4-37(a), very few α-Si_3N_4 nanowires were generated on the surface of the ceramic paper, and the thick carbonized paper fibers as well as the macro-pores between the paper fibers can easily be observed. These nanowires are curly and intertwined with each other, and no spherical tips are found to be present at the end of nanowires, indicating that the growth of the 1D nanostructures occurred via a different mechanism. The signal of iron was not detected by EDS due to the low iron content. This result indicates that the catalyst iron plays a very important role in the growth of 1D nanostructures. The iron content not only affected the yield of nanowires but also the growth mechanism of 1D nanostructures.

To further verify this assumption, the filter paper impregnated with PHPS (abbreviated as Paper-PHPS) was also pyrolyzed at 1300 ℃ under a N_2 atmosphere. The SEM images [Fig. 4-37(b)] exhibited that the structure of the filter paper has been retained after the impregnation and pyrolysis, but no 1D nanostructures were observed on the surface or in the pores of the paper substrate, meaning that 1D nanostructures were difficult to generate without the catalysis of iron.

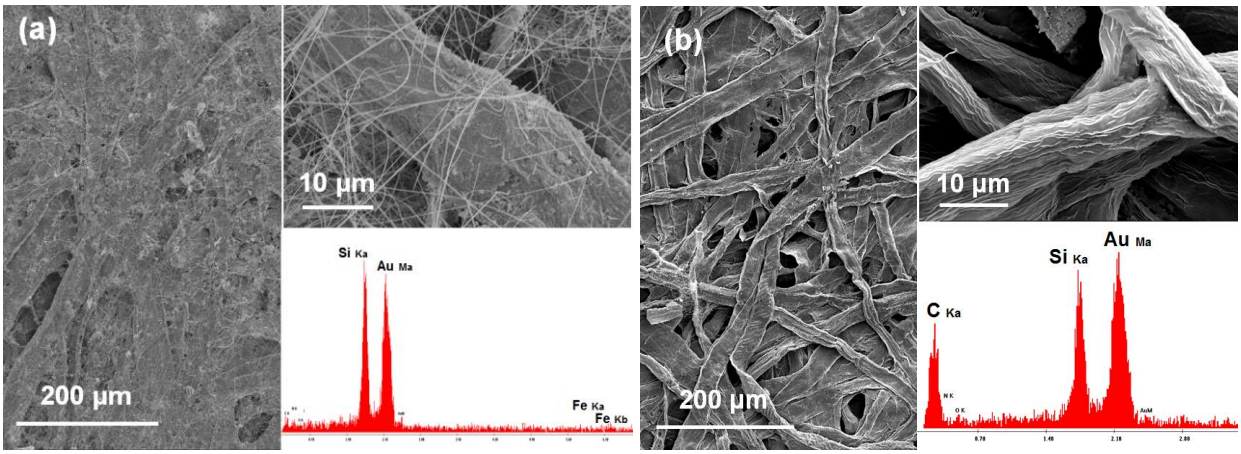

Fig. 4-37. SEM micrographs of the samples pyrolyzed at 1300 ℃ under N_2. (a) Paper-SiFeN(O)5 and (b) Paper-PHPS. Insets show high-magnification images and EDX profiles.

Based on these data, it can be deduced that iron has acted as a catalyst center for the nucleation of the α-Si_3N_4 nanowires. Furthermore, by comparing with the results from Paper-SiFeN(O)5 and Paper-PHPS, it can be concluded that high content of Fe could promote the formation of ultra-long nanowires and improve the yield of 1D nanostructures.

4.3.5 Growth mechanisms of one-dimensional structures

In order to further understand the growth mechanism of the 1D nanostructures, TGA measurement was applied to the Paper-SiFeN(O)50 ceramic paper obtained via ammonolysis at 1000 ℃ and shown in Fig. 4-38. In Fig. 4-38(a), the TGA curve displayed a slow mass loss at temperature < 1000 ℃ even though the sample had already been pyrolyzed at 1000 ℃ in ammonia. The weight loss at 1000 ℃ was about 8 wt.%, by a combination of *in situ* TGA-MS data, the mass loss was predominantly caused by the release of volatile matter such as CO and CO_2, NH_3 and H_2O, as shown in Fig. 4-38(b), which were from the decomposition of Paper-SiFeN(O)50 ceramic paper at high temperature. By further increasing the temperature, it was observed that the introduction of $Fe(acac)_2$ significantly affected the high-temperature stability (with respect to decomposition) of the resultant ceramic paper, leading to an additional mass loss (*ca.* 35 wt.%) at high temperature range from 1100 to 1400 ℃. With the assistance of *in situ* TGA-MS and FT-IR measurements, it was detected that this decomposition occurred with the release of gaseous by-products CO, CO_2 and SiO, which is in agreement with other published studies [23, 252, 253]. Obviously, the massive release of gaseous CO, CO_2 and SiO in the temperature range from 1000 to 1400 ℃ is responsible for the formation of the Si_3N_4 nanowires.

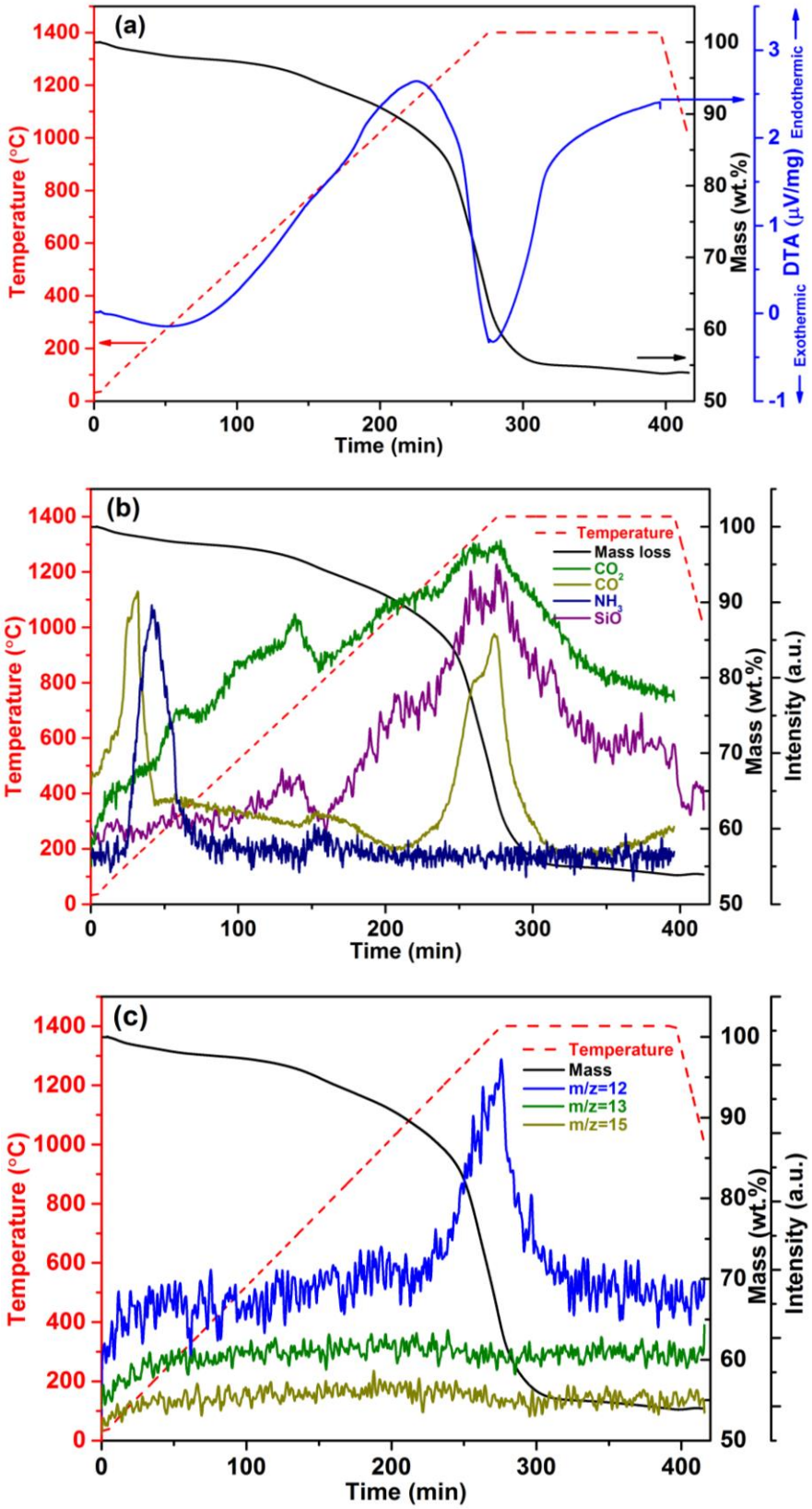

Fig. 4-38. TG, DTA (a) and ion current curves (*in situ* mass spectrometry, quasi multiple ion detection QMID) [as for SiO, NH_3, CO and CO_2 in (b) and for CH_4 in (c)] for the ceramic paper heat-treated in nitrogen atmosphere.

Additionally, the HT annealing of the SiFeN(O)-50 based ceramic paper leads to the release of hydrocarbons (Fig. 4-38(c), as for CH_4) which are considered to be responsible for the formation of the turbostratic carbon present on the surface of the Fe_3Si tips of the α-Si_3N_4 nanowires. There have been numerous studies in the literature reporting on the catalytic formation of carbon-based 1D structures. Interestingly, it has been reported that the Si content in iron-silicon alloy as well as the contact angle of the alloy on the carbon phase significantly affect the morphology of the in situ generated carbon [254, 255]. Thus, typically iron-silicon alloys containing low amounts of dissolved silicon (*e.g.*, < 10at% [255]) catalyze the generation of carbon-based 1D nanostructures; whereas in the case of Fe-Si alloys with larger amounts of silicon two concurrent processes occur, *i.e.* 1D nanostructure growth as well as etching of the formed carbon phase [255]. It has been stated that the Fe-Si alloy catalyst is encapsulated by the carbon phase in the case that the etching process of the carbon phase predominates [254]. It is considered that this effect also being the reason for the presence of the turbostratic carbon phase on the surface of the Fe_3Si tips in the SiFeN(O)-50 based ceramic paper.

Whereas the presence of the Fe_3Si tips at the ends of the in situ generated α-Si_3N_4 nanowires can be explained as a consequence of VLS growth of the nanowires, this mechanism cannot be the reason of the in-situ precipitation of the Fe_3Si nanoparticles within the ceramic matrix (see Fig. 4-30). Here, a SLS mechanism for the nucleation and growth of Fe_3Si is assumed and agrees with previous studies related to the crystallization behavior of SiFeCN ceramics prepared from iron-filled polysilazanes [256].

The presence of Fe_3Si catalyst round particles at the end of the Si_3N_4 nanowires, together with the experimental phenomenon that nanowires were only prepared when $Fe(acac)_2$ was added, suggested that the iron catalyst can promote the formation of Si_3N_4 nanowires and the growth proceeded via a VLS mechanism. The preparation of 1D nanowires in the present case was effected by three basic conditions: (i) the filter paper substrate was constituted by many cellulose-based paper fibers; these paper fibers intertwined loosely and a lot of macro-pores were present in the filter paper, which are responsible for the entrapment and enrichment of the released gaseous species such as SiO and CO, which acted as reaction micro-chambers for the formation of 1D nanostructures. Moreover, it is considered that the presence of the macro-pores in the template also avoids the gas-phase transport of the evaporated iron away from the sample, and consequently the growth of the Si_3N_4 1D nanostructures takes place on the surface and within the pores of the template and not at other places, as it was observed in the case of the high-temperature annealing of the SiFeN(O) ceramic powder without template.

(ii) Temperature also plays a critical role in the formation of one-dimensional nanostructures. It was reported that SiO and CO were the dominant gaseous by-products that formed during the pyrolysis of a polysiloxane precursor at temperatures > 1000 ℃[257]. Similarly, the decomposition of SiFeN(O) gave rise to the release of gaseous CO and SiO in the temperature range from 1000 to 1400 ℃, and these gaseous byproducts acted as raw materials for the formation of the Si_3N_4 nanowires. It was assumed that Si_3N_4 crystallites can nucleate on account of the reaction between SiO, CO, N_2 and free carbon (in our case, carbon was from the paper substrate) according to the reaction shown in Equation 6. However, this reaction was not enough to explain the growth

mechanism of the Si_3N_4 nanowires as well as the decrease in CO concentration, because the increased CO concentration around the reaction zone, which was from the by-product of Equation 6, and the decomposition of SiFeN(O) ceramic caused the reaction difficult to proceed[258]. As a result, another reaction was proposed, as shown in Equation 7, which was supported by other studies [243, 259, 260]. In this reaction, CO was consumed in the reaction with SiO and N_2, and then produced Si_3N_4 and CO_2 byproducts. In fact, crystalline SiC may also be produced by a reaction between SiO and CO gases or by a solid-gas reaction between SiO and C. However, no evidence of SiC was observed in previous investigations, indicating that these two reactions were not thermodynamically favored in the annealing conditions of the present study. Besides, it is well known that α-Si_3N_4 is the low-temperature stable polymorph of silicon nitride, and the carbothermal reaction of Si_3N_4 with carbon usually occurs at around 1450 ℃ under N_2, which is higher than the annealing temperature adopted in the present research.

$$3SiO(g) + 3C(s) + 2N_2(g) \rightarrow Si_3N_4(s) + 3CO(g) \quad \text{(Equation 6)}$$

$$3SiO(g) + 3CO(g) + 2N_2(g) \rightarrow Si_3N_4(s) + 3CO_2(g) \quad \text{(Equation 7)}$$

(iii) As evidenced by the XRD data, residual $Fe(acac)_2$ in the precursor and the Si-O-Fe bond were reduced to α-Fe firstly during the heat-treatment, and then a Fe-Si solution can be formed at higher temperatures. Because Fe and Si can form Fe-Si binary phase and show eutectic points at ca. 1200 ℃[261], the liquid Fe-Si alloys were considered to be formed under our experimental conditions at the annealing temperatures (Fe-Si alloys with a broad range of composition, *i.e.*, with Si contents increasing from 25 to 50 at.%; the melting point increased gradually from $Tm_{(Fe_3Si)}$ = 1200 ℃ to $Tm_{(FeSi)}$ = 1400 ℃ [262, 263]). As shown in the above XRD patterns, from 1200 to 1400 ℃, Fe_3Si crystallite was observed [Fig. 4-39(a)]. Furthermore, the surface of the liquid droplets had a large accommodation coefficient, which made the droplets become a preferred deposition site for SiO, CO and N_2 gases[245, 264]. Upon the reaction of SiO, CO and N_2 in the Fe-Si alloy liquid droplets, α-Si_3N_4 seeds began to precipitate from the supersaturated droplets [Fig. 4-39(a2, b2)]. With the continuous growth of the 1D crystal, it lifted the liquid catalyst up and finally grew up to a straight nanowire, as shown in Fig. 4-39(a2) and (b3).

Based on the above results and discussion, schematical descriptions of the high-temperature evolution of SiFeN(O)-50 powder and ceramic paper are presented in Fig. 4-39(a) and Fig. 4-39(b), respectively. In both samples, the formation of the α-Si_3N_4 nanowires relies on a VLS mechanism: in a first step, iron evaporation from SiFeN(O) takes place; the condensation of the iron vapors occurs subsequently on the surface of the crucible in the case of the ceramic powder [see Fig. 4-39(a2)]; whereas in the case of the ceramic paper, the condensation of iron occurs onto the surface of the ceramic paper as well as on the macro-pores surface [see Fig. 4-39(b1)]. Upon high-temperature annealing of the sample in a nitrogen atmosphere, gaseous SiO and CO are released in both SiFeN(O)-50 powder and ceramic paper. Thus, the main process responsible for the VLS growth of the α-Si_3N_4 nanowires involves the catalytic reaction of gaseous SiO, CO and N_2 to furnish Si_3N_4 and gaseous CO_2 as a side product [257, 258]. Due to the fact that the high-temperature annealing SiFeN(O)-50-based ceramic paper leads to the release of significant amounts of hydrocarbons, the Fe_3Si tips show the presence of a

turbostratic carbon phase on their surface [Fig. 4-39(a2)], unlike those observed while annealing the SiFeN(O)-50 ceramic powder.

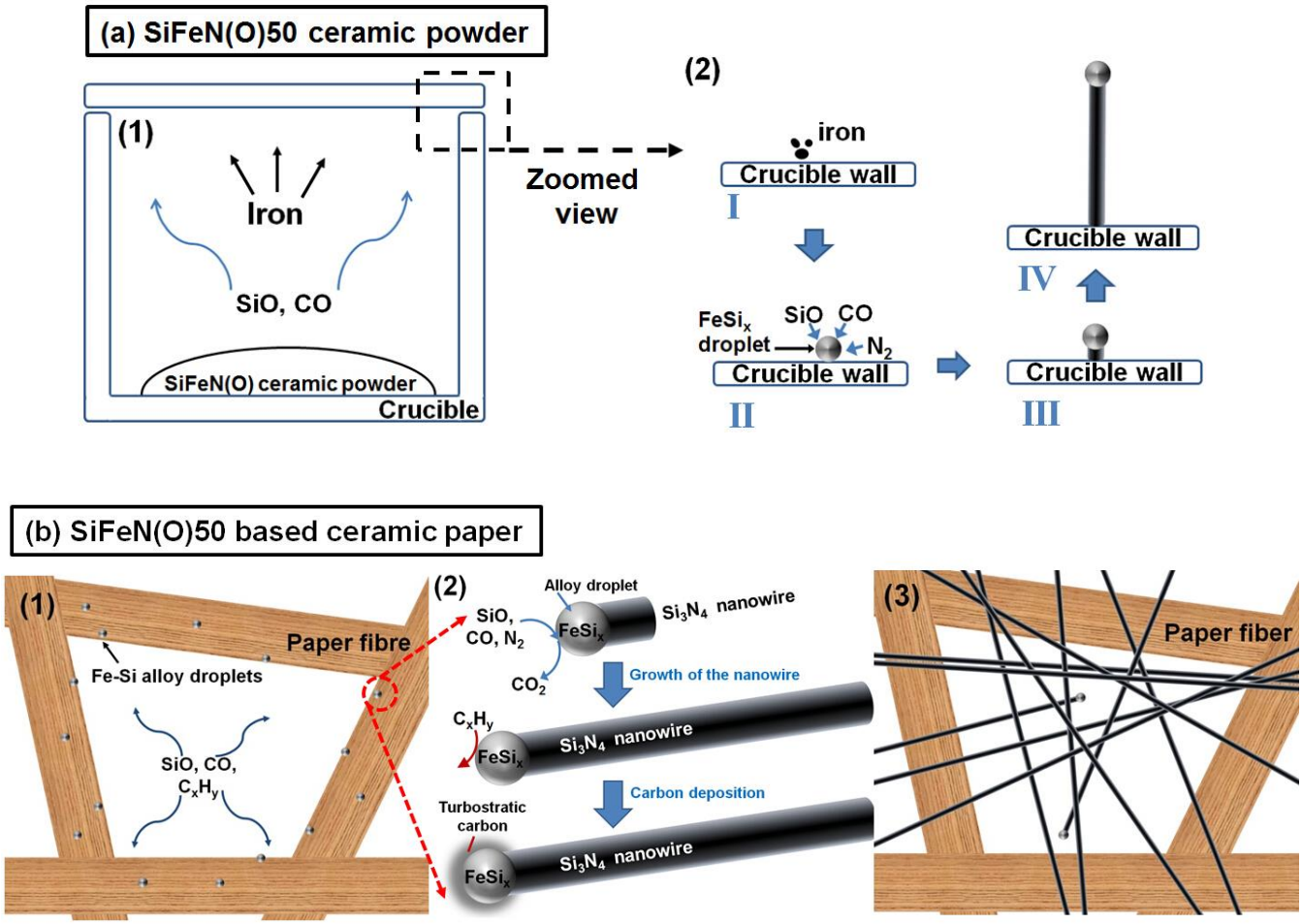

Fig. 4-39. Schematic description of the growth process of the Si_3N_4-based 1D nanostructures via a VLS mechanism. (a) formation mechanism of 1D nanostructures on the surface of SiC crucible when SiFeN(O) ceramic powder was annealed (*i.e.*, without paper template): (a1), the SiFeN(O)50 ceramic powder was annealed at high temperature (*e.g.*, 1400 ℃) under nitrogen; (a2-I), the evaporation and re-condensation of iron on the crucible surface; (a2-II), formation of $FeSi_x$ alloy droplet by diffusion of SiO, CO and N_2 vapours into iron; (a2-III), formation of α-Si_3N_4 seed based on the VLS mechanism; (a2-IV), final long α-Si_3N_4 nanowire with a round tip. (b) VLS growth mechanism for the generation of 1D nanostructures in SiFeN(O)-based ceramic paper: (b1), the formation of Fe-Si alloy droplets and the decomposition of SiFeN(O)-based ceramic paper when it was annealed at high temperature under nitrogen; (b2), from top to bottom: formation of α-Si_3N_4 seed based on the VLS mechanism, growth of α-Si_3N_4 nanowire, formation of turbostratic carbon around the $FeSi_x$ tip; (b3), final ceramic paper decorated with ultra-long α-Si_3N_4 nanowires.

4.3.6 Summary

In the present work, the SiFeN(O) single-source precursor was synthesized and a SiFeN(O)-based ceramic paper was successfully prepared by pyrolyzing the SiFeN(O) precursor infiltrated filter paper, and the results are summarized below.

(1) A SiFeN(O) precursor was synthesized by the chemical modification of PHPS with $Fe(acac)_2$. FT-IR measurement proved that $Fe(acac)_2$ can react with Si-H groups of PHPS and formed a Si-O-Fe bond, and then metallic iron was linked to the skeleton of the polymer precursor.

(2) In contrast to the PHPS-derived sample, the introduction of small amounts of $Fe(acac)_2$ had little influence on the crystallization behavior of the SiFeN(O)-5 ceramic powder. However, SiFeN(O)-50 pyrolyzed at 600 ℃ induced a phase separation process accompanied with the formation of iron nitride. By increasing the temperature, Fe_2N decomposed into α-Fe, which could react with silicon in the matrix when the SiFeN(O)-50 sample was annealed at higher temperatures from 1200 to 1400 ℃, crystalline Fe_3Si and Si_2ON_2 were observed in the final ceramics. 1D nanostructures was found on the surface of the crucible after 1400 ℃ annealing.

(3) SiFeN(O)-based ceramic paper was prepared by pyrolyzing the filter paper impregnated by SiFeN(O) precursors. When the sample was heat-treated at 1000 ℃ under ammonia, ceramic paper with α-Fe crystallite was obtained, and it was obvious that this ceramic paper had magnetic property. When it was annealed at higher temperatures, ceramic paper decorated with a large amount of 1D Si_3N_4 nanowires with high aspect ratio was prepared. Fe_3Si round tips were observed at the end of the nanowires and embedded within a “skin” of turbostratic carbon.

(4) This study confirmed that the combination of Fe-based catalyst, single-source precursor and porous template can extremely promote the formation of 1D nanostructures. The characteristics of the 1D nanostructures were affected by multiple conditions, including heating temperature, dipping times and iron content. In addition, the investigations and discussion confirmed that the growth of the 1D nanostructures occurred via a VLS mechanism.

5. CONCLUSION

Si-M-N material is a promising candidate for different challenging applications in the future. Based on the PDCs route, metal modified single-source precursors were synthesized, and then ternary Si-M-N nanocomposite materials were produced by subsequent heat-treatment. The results in this thesis suggest that chemical modification of the raw preceramic polymers using metallic complex is one of the best strategies, a bottom-up approach, and it offers the opportunity to tailor and design the type, size and dispersity of the as-formed metal nanoparticles in the nanocomposites. In the present research, PHPS was used for the fabrication of Si_3N_4 ceramic matrix, while TDMAH, $VO(acac)_2$ and $Fe(acac)_2$ were introduced for the modification, and then three different Si-M-N nanocomposite materials were fabricated by pyrolyzing corresponding metal-containing single-source precursors, which were synthesized by the chemical modification of perhydropolysilazane with different transition metal compounds. For the ternary Si-M-N ceramics, numerous characterization techniques are employed to acquire information of the structures, compositions, morphologies and functional properties of both ceramic matrix and metal nanoparticles. The detailed results of this dissertation are now summarized here.

In the case of the synthesis of a Si-Hf-N single-source precursor, the commercially available precursor PHPS reacted with TDMAH through a substitution reaction between both Si-H/N-H and ≡Hf-NMe_2, and N-H groups showed higher reactivity than Si-H. The subsequent ^{29}Si NMR further confirmed that the reaction occurred through Hf-N-Si linkages, and no Hf-Si bond was formed. Further investigation of the polymer-to-ceramic transformation of Si-Hf-N precursors suggested that the single-source precursor converted to amorphous single-phase ceramics after pyrolysis in ammonia. The modification of PHPS with TDMAH improved the cross-linking degree of the single-source precursors and resulted in high ceramic yield, which was improved from 82.7 wt.% (PHPS) to 92.3 wt.% (SiHfN-3), leading to the formation of amorphous Si-Hf-N ceramic with the composition of $Si_1Hf_{0.056}N_{1.32}$ at 1000 ℃. This SiHfN-3 ceramic remained X-ray amorphous up to 1400 ℃, while PHPS-derived ceramic highly crystallized at 1300 ℃, suggesting that the obtained single-phase SiHfN ceramic has outstanding resistance against crystallization. Further annealing at 1300 ℃ induced a phase separation process of hafnium nitride proved by solid NMR, and then the single-phase SiHfN ceramic converted into an amorphous HfN_x/SiN_x nanocomposite. Annealing of the Si-Hf-N ceramic at higher temperatures above 1600 ℃ induced the generation of crystalline HfN together with α- and β-Si_3N_4, and their grain coarsening was greatly inhibited in comparison to the PHPS-derived sample. Moreover, the Si-Hf-N ceramics exhibited excellent high-temperature stability with respect to α- to β-Si_3N_4 phase transformation: the volume fraction of α-Si_3N_4 was increased from 6.9% (PHPS) to 54.2% (SiHfN-3) at 1800 ℃ in a N_2 atmosphere.

Secondly, a SiVN(O) single-source precursor was successfully synthesized using PHPS and $VO(acac)_2$. The formation of Si-O-V bonds confirmed the reaction between Si-H and $VO(acac)_2$, and the $–NH_2$ groups were consumed in the condensation reaction with $VO(acac)_2$. Single-phase SiVN(O) ceramics were prepared by the subsequent ammonolysis at 1000 ℃ in NH_3, and they showed outstanding resistance with respect to crystallization up to 1300 ℃. Annealing at 1400 ℃ induced a phase separation of the ceramic, and the

diffraction peaks of crystalline VN could be observed in the XRD patterns. Further increases of the heating temperature resulted in a Si-V-N nanocomposite composed of VN, α- and β-Si_3N_4 at 1600 ℃. It is worth mentioning that the introduction of $VO(acac)_2$ changed the ratio of α/β-Si_3N_4 in the final ceramic nanocomposites, and only the β-Si_3N_4 phase was found in the 1600 ℃-annealed SiVN(O)-3 ceramic; therefore, the proportion of β-Si_3N_4 can be controlled by tuning the $VO(acac)_2$ in the feed. Afterwards, mesoporous SiVN(O)-3 ceramics with high SSA were successfully prepared by using polystyrene as a self-sacrificial template in a one-pot synthesis. Both the SSA and pore size distribution can be adjusted by the content of PS template used in the feed, and mesoporous SiVN(O)-3 ceramics with the maximum SSA (506 m^2/g) was obtained at 1000 ℃ in NH_3 when the weight ratio of PS/SiVN(O)-3 was 2/1. In addition, more than half of the mesopores can survive up to 1300 ℃, suggesting the structural stability of the mesoporous SiVN(O) ceramic nanocomposites.

A SiFeN(O) precursor was synthesized by the chemical modification of PHPS with $Fe(acac)_2$ through the formation of Si-O-Fe bonds proved by FT-IR measurement. The following pyrolysis of SiFeN(O)-50 in ammonia induced a phase separation with the formation of iron nitride at low temperature (600 ℃), and then Fe_2N decomposed into α-Fe by further increasing the temperature and resulted in the α-Fe/a-Si_3N_4 nanocomposite. When the SiFeN(O)-50 ceramic nanocomposite was annealed at high temperatures ranging from 1200 to 1400 ℃, Fe_3Si and Si_2ON_2 crystallites were observed in the products, revealing that the introduction of $Fe(acac)_2$ caused considerable influence on the phase separation and crystallization behavior of the ceramic, and Fe_3Si was obtained in the end. Subsequently, filter paper was infiltrated by SiFeN(O) precursors and heat-treated at 1000 ℃ under ammonia. SiFeN(O)-based ceramic paper with crystalline α-Fe was obtained. Further annealing the ceramic paper at higher temperatures, a ceramic paper decorated with a huge amount of 1D Si_3N_4 nanowires with high aspect ratios was prepared. The formation of 1D nanostructures in the sample occurred via a VLS mechanism, and it was promoted remarkably by the combination of the SiFeN(O) precursor, porous template and Fe-based catalyst in a one-step synthesis.

In the present thesis, different transition metals modified PHPS precursors were successfully synthesized using PDC route and corresponding Si-M-N ceramic nanocomposites were produced by subsequent heat-treatment. These transition metals converted to different crystallites (HfN, VN or Fe_3Si) at high temperature and dispersed in the Si_3N_4 matrix homogeneously. The modification with transition metals showed significant effects on the phase separation and crystallization behavior of the silicon nitride matrix, and the introduction of different metals caused the formation of PDC-NCs with different structures and compositions and provided the materials various intriguing properties, making the Si-M-N nanocomposites promising candidates in various applications, such as catalysts, ultra-high temperature materials and microelectronics.

6. OUTLOOK

This Ph.D. thesis presents a study of Si-M-N ceramics that were derived from novel metal-modified PHPS single-source precursors. The detailed results of the chemical synthesis reactions, chemical compositions, phase revolution and nanostructures of the as-obtained Si-M-N ceramic composites can provide some guidance and inspiration for future studies. An outline of future investigations is recommended below.

1. The use of metallic amido complexes was very successful in this research. This series of non-oxide metallic compounds act as metal transfer reagents towards the functional groups of preceramic polymers, and the formation of a Si-N-Metal bond is a mild reaction and can be easily confirmed by spectroscopy. Active metal nanoparticles can be highly dispersed into the ceramic matrix by simple chemical modification, and the ceramic nanocomposites demonstrate considerable advantages over conventional processes. Moreover, these metallic amido compounds are available for most transition metals. It can be speculated that corresponding modification is possible, and plenty of choices are provided. Therefore, a variety of metal-modified ceramic nanocomposites like Si-M-N can be produced via a PDC approach, and the research should be focused on the structures and properties of the nanocomposites. The applications of metal-modified ceramics in catalysis, ultra-high temperature materials and microelectronic should also be deeply studied.

2. The use of polyolefin as soft sacrificial templates demonstrated a good effect in the synthesis of porous ceramics. The template can be simply mixed with the preceramic polymers in a one-pot synthesis and is easily removed during the following heat-treatment. This method can be also applied in the preparation of other porous PDCs, and the specific surface areas and pore sizes are controllable. The relationship between pore parameters (specific surface area and pore size) and the properties of polymer sacrificial templates (such as molecular weight, molecular morphology and composition) should be further investigated.

3. The Si_3N_4 ceramic matrix is a promising support for catalysts due to its excellent chemical and mechanical stability. Additionally, VN has shown catalytic performance in propane and butane dehydrogenation[265, 266]. The catalytic property of the mesoporous SiVN(O) ceramics should be investigated, and it is believed that the homogeneous dispersion of VN nanoparticles in the Si_3N_4 matrix together with the high surface area can improve the catalytic efficiency.

4. The combination of polymeric precursors, porous template and metal-based catalyst enable the decoration of a ceramic surface with one-dimensional nanostructures via a simple approach. In order to improve the yield of 1D nanostructures, the experimental conditions should be further optimized.

5. Most of the research focused on the preparation and characterization of 1D nanostructures, while the properties and applications of these as-obtained 1D nanostructures have been rarely reported. More effort should be made to study the functional properties of 1D nanostructures like photoluminescence and semiconducting performance.

REFERENCES

1. Reid, J., et al., *Evaluation of amorphous (Mo, Ta, W)-Si-N diffusion barriers for Si/Cu metallizations.* Thin Solid Films, 1993. **236**(1): p. 319-324.
2. Kim, K.H., S.-r. Choi, and S.-y. Yoon, *Superhard Ti–Si–N coatings by a hybrid system of arc ion plating and sputtering techniques.* Surface and Coatings Technology, 2002. **161**(2): p. 243-248.
3. Löffelholz, J., J. Engering, and M. Jansen, *Sol-Gel-Process in the Ammono-System–a Novel Access to Silicon Based Nitrides.* Zeitschrift für anorganische und allgemeine Chemie, 2000. **626**(4): p. 963-968.
4. Kim, D.J., Y.T. Kim, and J.-W. Park, *Nanostructured Ta-Si-N diffusion barriers for Cu metallization.* Journal of applied physics, 1997. **82**(10): p. 4847-4851.
5. Orlov, A. and J. Grabis, *Plasma chemical synthesis of fine $MoSi_2$ and $MoSi_2$-Si_3N_4 composite powders.* High Temperature Material Processes: An International Quarterly of High-Technology Plasma Processes, 2011. **15**(4).
6. Cheng, F., et al., *Ammonothermal synthesis of a mesoporous Si-Ti-N composite material from a single-source precursor.* Chemistry of materials, 2005. **17**(22): p. 5594-5602.
7. Hafiz, J., et al., *Hypersonic plasma particle deposition of Si–Ti–N nanostructured coatings.* Surface and Coatings Technology, 2004. **188**: p. 364-370.
8. Mikula, M., et al., *Thermal stability and high-temperature oxidation behavior of Si–Cr–N coatings with high content of silicon.* Surface and Coatings Technology, 2013. **232**: p. 349-356.
9. Wu, Z., et al., *Understanding hardness evolution of Zr–Si–N nanocomposite coatings via investigating their deformation behaviors.* Journal of the European Ceramic Society, 2016. **36**(14): p. 3329-3339.
10. Wen, H.-C., et al. *Systematic investigation of amorphous transition-metal-silicon-nitride electrodes for metal gate CMOS applications*. in *VLSI Technology, 2005. Digest of Technical Papers. 2005 Symposium on*. 2005. IEEE.
11. Ionescu, E., et al., *Thermodynamic Control of Phase Composition and Crystallization of Metal-Modified Silicon Oxycarbides.* Journal of the American Ceramic Society, 2013. **96**(6): p. 1899-1903.
12. Ionescu, E., et al., *Polymer-Derived Silicon Oxycarbide/Hafnia Ceramic Nanocomposites. Part I: Phase and Microstructure Evolution During the Ceramization Process.* Journal of the American Ceramic Society, 2010. **93**(6): p. 1774-1782.
13. Kleebe, H.J., et al., *Decomposition-Coarsening Model of SiOC/HfO2 Ceramic Nanocomposites Upon Isothermal Anneal at 1300 °C.* Journal of the American Ceramic Society, 2012. **95**(7): p. 2290-2297.
14. Papendorf, B., et al., *Strong Influence of Polymer Architecture on the Microstructural Evolution of Hafnium-Alkoxide-Modified Silazanes upon Ceramization.* Small, 2011. **7**(7): p. 970-978.
15. Sujith, R., A.B. Kousaalya, and R. Kumar, *Synthesis and phase stability of precursor derived HfO_2/Si–C–N–O nanocomposites.* Ceramics International, 2012. **38**(2): p. 1227-1233.
16. Wen, Q., et al., *Microwave Absorption of SiC/HfC_xN_{1-x}/C Ceramic Nanocomposites with HfC_xN_{1-x}-Carbon Core–Shell Particles.* Journal of the American Ceramic Society, 2016.
17. Bechelany, M.C., et al., *In situ controlled growth of titanium nitride in amorphous silicon nitride: A general route toward bulk nitride nanocomposites with very high hardness.* Advanced Materials, 2014. **26**(38): p. 6548-6553.
18. Alonso, B., J. Maquet, and B. Viana, *Hybrid organic-inorganic polydimethylsiloxane–vanadium–oxo materials crosslinked at the molecular level.* New J. Chem., 1998. **22**(9): p. 935-939.
19. Alonso, B. and C. Sanchez, *Structural investigation of polydimethylsiloxane–vanadate hybrid materials.* Journal of Materials Chemistry, 2000. **10**(2): p. 377-386.
20. Borah, P., et al., *A vanadyl complex grafted to periodic mesoporous organosilica: a green catalyst for selective hydroxylation of benzene to phenol.* Angewandte Chemie International Edition, 2012. **51**(31): p. 7756-7761.
21. Gou, Y., et al., *The preparation and characterization of polymer-derived Fe/Si/C magnetoceramics.* Ceramics International, 2016. **42**(1): p. 681-689.
22. Yu, Z., et al., *Template-Free Synthesis of Porous Fe_3O_4/SiOC (H) Nanocomposites with Enhanced Catalytic Activity.* Journal of the American Ceramic Society, 2016.
23. Vakifahmetoglu, C., et al., *Growth of One-Dimensional Nanostructures in Porous Polymer-Derived Ceramics by Catalyst-Assisted Pyrolysis. Part I: Iron Catalyst.* Journal of the American Ceramic Society, 2010. **93**(4): p. 959-968.

24. Ainger, F. and J. Herbert, *The preparation of phosphorus-nitrogen compounds as non-porous solids.* Special Ceramics, 1960: p. 168-182.
25. Chantrell, P. and P. Popper, *Inorganic polymers and ceramics.* Special Ceramics, 1965: p. 67.
26. Verbeek, W., *Production of shaped articles of homogeneous mixtures of silicon carbide and nitride*. 1974, Google Patents.
27. Yajima, S., J. Hayashi, and M. Omori, *Continuous silicon carbide fiber of high tensile strength.* Chemistry Letters, 1975. **4**(9): p. 931-934.
28. Fritz, G. and B. Raabe, *Bildung siliciumorganischer Verbindungen. V. Die Thermische Zersetzung von Si (CH3) 4 und Si (C2H5) 4.* Zeitschrift für anorganische und allgemeine Chemie, 1956. **286**(3-4): p. 149-167.
29. Riedel, R., et al., *Silicon-Based Polymer-Derived Ceramics: Synthesis Properties and Applications-A Review Dedicated to Prof. Dr. Fritz Aldinger on the occasion of his 65th birthday.* Journal of the Ceramic Society of Japan, 2006. **114**(1330): p. 425-444.
30. Wang, Z.C., F. Aldinger, and R. Riedel, *Novel Silicon-Boron-Carbon-Nitrogen Materials Thermally Stable up to 2200 °C.* Journal of the American Ceramic Society, 2001. **84**(10): p. 2179-2183.
31. Toma, L., et al., *Correlation Between Intrinsic Microstructure and Piezoresistivity in a SiOC Polymer-Derived Ceramic.* Journal of the American Ceramic Society, 2012. **95**(3): p. 1056-1061.
32. Zhang, L., et al., *A silicon carbonitride ceramic with anomalously high piezoresistivity.* Journal of the American Ceramic Society, 2008. **91**(4): p. 1346-1349.
33. Komarneni, S., *Nanocomposites.* J. Mater. Chem., 1992. **2**(12): p. 1219-1230.
34. Gleiter, H., *Nanocrystalline materials.* Progress in materials science, 1989. **33**(4): p. 223-315.
35. Newnham, R., D. Skinner, and L. Cross, *Connectivity and piezoelectric-pyroelectric composites.* Materials Research Bulletin, 1978. **13**(5): p. 525-536.
36. Rayleigh, L., *Nitrogen, argon and neon in the earth's crust with applications to cosmology.* Proceedings of the Royal Society of London. Series A, Mathematical and Physical Sciences, 1939: p. 451-464.
37. Lee, M.R., et al., *Nierite (Si_3N_4), a new mineral from ordinary and enstatite chondrites.* Meteoritics, 1995. **30**(4): p. 387-398.
38. Nittler, L.R., et al., *Silicon nitride from supernovae.* The Astrophysical Journal Letters, 1995. **453**(1): p. L25.
39. Deville, H.S.-C. and F. Wöhler, *On the direct compound silicon nitride.* Liebigs Ann. Chem. Pharm., 1859. **110**: p. 248-250.
40. Melner, H., *Verfahren zür darstellung von nitriden.* Ger. Pat. No. 88999, Sept. 30, 1896.
41. Weiss, L. and T. Engelhardt, *Über die Stickstoffverbindungen des Siliciums.* Zeitschrift für anorganische Chemie, 1910. **65**(1): p. 38-104.
42. Wohler, L., *Silicon and nitrogen.* Z. Elektr. Chem, 1926. **32**: p. 420-23.
43. Collins, J. and R. Gerby, *New refractory uses for silicon nitride reported.* J. Metals, 1955. **7**.
44. Lenoe, E.M., R.N. Katz, and J.J. Burke, *Ceramics for High-Performance Applications III: Reliability*. Vol. 6. 2013: Springer Science & Business Media.
45. Deeley, G., J. Herbert, and N. Moore, *Dense silicon nitride.* Powder Metallurgy, 1961. **4**(8): p. 145-151.
46. Wild, S., et al., *The role of magnesia in hot-pressed silicon nitride.* Special Ceramics, 1972. **5**: p. 357-386.
47. Hardie, D. and K. Jack, *Crystal structures of silicon nitride.* 1957.
48. Priest, H., et al., *Oxygen content of alpha silicon nitride.* Journal of the American Ceramic Society, 1973. **56**(7): p. 395-395.
49. Zerr, A., et al., *Synthesis of cubic silicon nitride.* Nature, 1999. **400**(6742): p. 340-342.
50. Leger, J., et al., *Discovery of hardest known oxide.* Nature, 1996. **383**(6599): p. 401-401.
51. Zerr, A., et al., *Elastic moduli and hardness of cubic silicon nitride.* Journal of the American Ceramic Society, 2002. **85**(1): p. 86-90.
52. Kruger, M., et al., *Equation of state of α-Si_3N_4.* Physical Review B, 1997. **55**(6): p. 3456-3460.
53. Cartz, L. and J. Jorgensen, *The high-pressure behavior of α-quartz, oxynitride, and nitride structures.* Journal of Applied Physics, 1981. **52**(1): p. 236-244.
54. Soignard, E., et al., *High pressure-high temperature synthesis and elasticity of the cubic nitride spinel γ-Si_3N_4.* Journal of Physics: Condensed Matter, 2001. **13**(4): p. 557.
55. Schwarz, M., et al., *Spinel-Si_3N_4: Multi-Anvil Press Synthesis and Structural Refinement.* Advanced Materials, 2000. **12**(12): p. 883-887.
56. Sekine, T., et al., *Shock-induced transformation of beta-Si_3N_4 to a high-pressure cubic-spinel phase.* Applied Physics Letters, 2000. **76**: p. 3706.

57. Schlothauer, T., et al., *"Shock Wave" Synthesis of Oxygen-Bearing Spinel-Type Silicon Nitride γ-$Si_3(O, N)_4$ in the Pressure Range from 30 to 72 GPa with High Purity*, in *Minerals as Advanced Materials II*. 2012, Springer. p. 375-388.
58. Yunoshev, A., *Shock-Wave Synthesis of Cubic Silicon Nitride.* Combustion, Explosion and Shock Waves, 2004. **40**(3): p. 370-373.
59. Sekine, T., *Shock synthesis of cubic silicon nitride.* Journal of the American Ceramic Society, 2002. **85**(1): p. 113-116.
60. Leitch, S., et al., *Properties of non-equivalent sites and bandgap of spinel-phase silicon nitride.* Journal of Physics: Condensed Matter, 2004. **16**(36): p. 6469.
61. Boyko, T., et al., *Electronic Structure of Spinel-Type Nitride Compounds Si_3N_4, Ge_3N_4, and Sn_3N_4 with Tunable Band Gaps: Application to Light Emitting Diodes.* Physical review letters, 2013. **111**(9): p. 097402.
62. Washburn, M. and R. Love, *A silicon carbide refractory with a complex nitride bond containing silicon oxynitride.* Am. Ceram. Soc. Bull, 1962. **41**(7).
63. Popper, P. and S. Ruddlesden, *The preparation, properties and structure of silicon nitride.* Trans. Br. Ceram. Soc, 1961. **60**: p. 603-626.
64. Davidge, R., *Economic and energetic considerations for nitrogen ceramics. Nitrogen Cerara. Prac.* NATO Adv. Study Inst., Canterburu, 1976.
65. Fischer, T. and H. Tomizawa, *Interaction of tribochemistry and microfracture in the friction and wear of silicon nitride.* Wear, 1985. **105**(1): p. 29-45.
66. Wang, Y. and M. Hadfield, *The influence of ring crack location on the rolling contact fatigue failure of lubricated silicon nitride: fracture mechanics analysis.* Wear, 2000. **243**(1): p. 167-174.
67. Greskovich, C., S. Prochazka, and J. Rosolowski, *Sintering behavior of covalently bonded materials*, in *Nitrogen Ceramics*. 1977, Nordhoff Leyden. p. 351-357.
68. Doo, V., D. Nichols, and G. Silvey, *Preparation and properties of pyrolytic silicon nitride.* Journal of The Electrochemical Society, 1966. **113**(12): p. 1279-1281.
69. Appels, J., et al., *Local oxidation of silicon and its application in semiconductor-device technology.* PHILIPS RESEARCH REPORTS., 1970. **25**(2): p. 118-132.
70. Schaffer, P. and B. Swaroop, *Vapor phase growth and dc breakdown of silicon nitride films.* Amercian Ceramic Society Bulletin, 1970. **49**(5): p. 536-538.
71. Dalton, J. and J. Drobek, *Structure and sodium migration in silicon nitride films.* Journal of the Electrochemical Society, 1968. **115**(8): p. 865-868.
72. Gardeniers, J., H. Tilmans, and C. Visser, *LPCVD silicon-rich silicon nitride films for applications in micromechanics, studied with statistical experimental design.* Journal of Vacuum Science & Technology A, 1996. **14**(5): p. 2879-2892.
73. Chuang, W.-H., et al., *Mechanical property characterization of LPCVD silicon nitride thin films at cryogenic temperatures.* Microelectromechanical Systems, Journal of, 2004. **13**(5): p. 870-879.
74. Knight, T.J., et al., *Real-time multivariable control of PECVD silicon nitride film properties.* Semiconductor Manufacturing, IEEE Transactions on, 1997. **10**(1): p. 137-146.
75. Ikeda, K., et al., *Thermal and Kerr nonlinear properties of plasma-deposited silicon nitride/silicon dioxide waveguides.* Optics express, 2008. **16**(17): p. 12987-12994.
76. Monro, T.M. and H. Ebendorff-Heidepriem, *Progress in microstructured optical fibers.* Annu. Rev. Mater. Res., 2006. **36**: p. 467-495.
77. Cazzanelli, M., et al., *Second-harmonic generation in silicon waveguides strained by silicon nitride.* Nature materials, 2012. **11**(2): p. 148-154.
78. Sekaric, L., et al., *Nanomechanical resonant structures in silicon nitride: fabrication, operation and dissipation issues.* Sensors and Actuators A: Physical, 2002. **101**(1): p. 215-219.
79. Yu, P.-L., T. Purdy, and C. Regal, *Control of material damping in high-Q membrane microresonators.* Physical review letters, 2012. **108**(8): p. 083603.
80. Biswas, T.S., et al., *High-Q gold and silicon nitride bilayer nanostrings.* Applied Physics Letters, 2012. **101**(9): p. 093105.
81. Váez-Fort, E., et al., *Single step fabrication of N-doped graphene/Si_3N_4/SiC heterostructures.* Nano Research, 2014. **7**(6): p. 835-843.
82. Sun, J., et al., *Large-area uniform graphene-like thin films grown by chemical vapor deposition directly on silicon nitride.* Applied Physics Letters, 2011. **98**(25): p. 252107.

83. Ramirez, C., et al., *Graphene nanoplatelet/silicon nitride composites with high electrical conductivity.* Carbon, 2012. **50**(10): p. 3607-3615.
84. Lee, S., et al., *Graphene metallization of high-stress silicon nitride resonators for electrical integration.* Nano letters, 2013. **13**(9): p. 4275-4279.
85. Howlett, C., E. McCartney, and W. Ching, *The Effect of Silicon Nitride Ceramic on Rabbit Skeletal Cells and Tissue: An In Vitro and In Vivo Investigation.* Clinical orthopaedics and related research, 1989. **244**: p. 293-304.
86. Neumann, A., et al., *[Biocompatibilty of silicon nitride ceramic in vitro. A comparative fluorescence-microscopic and scanning electron-microscopic study]*. Laryngo-rhino-otologie, 2004. **83**(12): p. 845-851.
87. Taylor, R., et al., *Silicon nitride: a new material for spinal implants.* Journal of Bone & Joint Surgery, British Volume, 2010. **92**(SUPP I): p. 133-133.
88. Bal, B.S., et al., *Testing of silicon nitride ceramic bearings for total hip arthroplasty.* Journal of Biomedical Materials Research Part B: Applied Biomaterials, 2008. **87**(2): p. 447-454.
89. Riley, F.L., *Silicon nitride and related materials.* Journal of the American Ceramic Society, 2000. **83**(2): p. 245-265.
90. Hofmann, H., et al. *Silicon nitride powder from carbothermal reaction*. in *MRS Proceedings*. 1992. Cambridge Univ Press.
91. *Silicon nitride-bonded refractory oxide bodies and method of making*. 1953, Google Patents.
92. Atkinson, A., A.J. Moulson, and E. Roberts, *Nitridation of High-Purity Silicon.* Journal of the American Ceramic Society, 1976. **59**(7-8): p. 285-289.
93. Mazdiyasni, K.S. and C.M. COOKE, *Synthesis, characterization, and consolidation of Si_3N_4 obtained from ammonolysis of $SiCl_4$.* Journal of the American Ceramic Society, 1973. **56**(12): p. 628-633.
94. Rovai, R., C.W. Lehmann, and J.S. Bradley, *Non-Oxide Sol–Gel Chemistry: Preparation from Tris(dialkylamino)silazanes of a Carbon-Free, Porous, Silicon Diimide Gel.* Angewandte Chemie International Edition, 1999. **38**(13-14): p. 2036-2038.
95. Cannon, W.R., et al., *Sinterable Ceramic Powders from Laser-Driven Reactions: I, Process Description and Modeling.* Journal of the American Ceramic Society, 1982. **65**(7): p. 324-330.
96. Cannon, W.R., et al., *Sinterable Ceramic Powders from Laser-Driven Reactions: II, Powder Characteristics and Process Variables.* Journal of the American Ceramic Society, 1982. **65**(7): p. 330-335.
97. Schutzenberger, P. and A. Colson, *"Silicon," Comptes Rendus Hebdomadaires des Seances.* de l'Academie des Sciences, 1885. **93**: p. 1508-1511.
98. Brewer, S.D. and C.P. Haber, *Alkylsilazanes1 and Some Related Compounds.* Journal of the American Chemical Society, 1948. **70**(11): p. 3888-3891.
99. Hörz, M., et al., *Novel polysilazanes as precursors for silicon nitride/silicon carbide composites without "free" carbon.* Journal of the European Ceramic Society, 2005. **25**(2): p. 99-110.
100. Krüger, C.R. and E.G. Rochow, *Polyorganosilazanes.* Journal of Polymer Science Part A: General Papers, 1964. **2**(7): p. 3179-3189.
101. Verbeek, W. and G. Winter, *Silicon Carbide-Shaped Article and Process for the Manufacture Thereof.* Ger. Pat, 1974(02236078).
102. Fleischer, H., et al., *Bis(chloromethylsilyl) amine and bis(chloromethylsilyl) methylamine; preparation, reactivity and spectroscopic studies of their stereoisomers and conformers.* Journal of the Chemical Society, Dalton Transactions, 1998(4): p. 585-592.
103. Blum, Y.D., R.M. Platz, and E.J. Crawford, *Glass Strengthening by Polymer-Derived Ceramic Coatings.* Journal of the American Ceramic Society, 1990. **73**(1): p. 170-172.
104. He, J., M. Scarlete, and J.F. Harrod, *Silicon nitride and silicon carbonitride by the pyrolysis of poly (methylsiladiazane).* Journal of the American Ceramic Society, 1995. **78**(11): p. 3009-3017.
105. Blum, Y.D., K.B. Schwartz, and R.M. Laine, *Preceramic polymer pyrolysis.* Journal of materials science, 1989. **24**(5): p. 1707-1718.
106. Seyferth, D., J.M. Schwark, and R.M. Stewart, *Stoichiometric and catalytic ring opening of hexaalkylcyclodisilazanes by organoalkali reagents.* Organometallics, 1989. **8**(8): p. 1980-1986.
107. Tang, H., et al., *Solid-state characterization and properties of poly (N-methylcyclodisilazanes).* Macromolecules, 1997. **30**(5): p. 1400-1407.
108. Kroke, E., et al., *Silazane derived ceramics and related materials.* Materials Science and Engineering: R: Reports, 2000. **26**(4): p. 97-199.

109. Blum, Y. and R. Laine, *Catalytic methods for the synthesis of oligosilazanes.* Organometallics, 1986. **5**(10): p. 2081-2086.
110. Colombo, P., et al., *Polymer-Derived Ceramics: 40 Years of Research and Innovation in Advanced Ceramics.* Journal of the American Ceramic Society, 2010. **93**(7): p. 1805-1837.
111. Babonneau, F., et al., *Chemical Characterization of Si-Al-C-O Precursor and Its Pyrolysis.* Journal of the American Ceramic Society, 1991. **74**.
112. Thorne, K., E. Liimatta, and J.D. Mackenzie, *Synthesis of SiC/TaC ceramics from tantalum alkoxide modified polycarbosilane.* Journal of materials research, 1991. **6**(10): p. 2199-2207.
113. Ishikawa, T., Y. Kohtoku, and K. Kumagawa, *Production mechanism of polyzirconocarbo-silane using zirconium(IV) acetylacetonate and its conversion of the polymer into inorganic materials.* Journal of materials science, 1998. **33**(1): p. 161-166.
114. Ishikawa, T., et al., *A tough, thermally conductive silicon carbide composite with high strength up to 1600 ℃ in air.* Science, 1998. **282**(5392): p. 1295-1297.
115. Ionescu, E., et al., *Polymer-Derived SiOC/ZrO_2 Ceramic Nanocomposites with Excellent High-Temperature Stability.* Journal of the American Ceramic Society, 2010. **93**(1): p. 241-250.
116. Iwamoto, Y., K. Kikuta, and S. Hirano, *Synthesis of poly-titanosilazanes and conversion into Si_3N_4-TiN ceramics.* Journal of the Ceramic Society of Japan, 2000. **108**(4): p. 350-356.
117. Seyferth, D., et al., *Chemical modification of preceramic polymers: Their reactions with transition metal complexes and transition metal powders.* Journal of Inorganic and Organometallic Polymers, 1992. **2**(1): p. 59-77.
118. Seyferth, D., C.A. Sobon, and J. Borm, *A new procedure for up-grading the nicalon polycarbosilane and related Si-H containing organosilicon polymers.* New journal of chemistry, 1990. **14**(6-7): p. 545-547.
119. Hauser, R., et al., *Processing and magnetic properties of metal-containing SiCN ceramic micro-and nano-composites.* Journal of Materials Science, 2008. **43**(12): p. 4042-4049.
120. Greenberg, S., et al., *Synthesis and lithographic patterning of polycarbosilanes with pendant cobalt carbonyl clusters.* Macromolecules, 2005. **38**(6): p. 2023-2026.
121. Chen, X., et al., *Iron Nanoparticle-Containing Silicon Carbide Fibers Prepared by Pyrolysis of $Fe(CO)_5$-Doped Polycarbosilane Fibers.* Journal of the American Ceramic Society, 2010. **93**(1): p. 89-95.
122. Seifollahi Bazarjani, M., et al., *Nanoporous silicon oxycarbonitride ceramics derived from polysilazanes in situ modified with nickel nanoparticles.* Chemistry of Materials, 2011. **23**(18): p. 4112-4123.
123. Li, Y., et al., *Preparation of Si–C–N–Fe magnetic ceramics from iron-containing polysilazane.* Applied organometallic chemistry, 2003. **17**(2): p. 120-126.
124. Park, J.H., K.H. Park, and D.P. Kim, *Superparamagnetic Si_3N_4-Fe-containing ceramics prepared from a polymer-metal complex.* Journal of Industrial and Engineering Chemistry, 2007. **13**(1): p. 27-32.
125. Tsirlin, A., et al., *Nano-structured metal-containing polymer precursors for high temperature non-oxide ceramics and ceramic fibers—syntheses, pyrolyses and properties.* Journal of the European Ceramic Society, 2002. **22**(14): p. 2577-2585.
126. Amoros, P., et al., *Synthesis and characterization of SiC/MC/C Ceramics (M= Ti, Zr, Hf) starting from totally non-oxidic precursors.* Chemistry of materials, 2002. **14**(4): p. 1585-1590.
127. Yu, Z., et al., *Preparation, cross-linking and ceramization of AHPCS/Cp_2ZrCl_2 hybrid precursors for SiC/ZrC/C composites.* Journal of the European Ceramic Society, 2012. **32**(6): p. 1291-1298.
128. Yu, Z., et al., *Single-source-precursor synthesis of high temperature stable SiC/C/Fe nanocomposites from a processable hyperbranched polyferrocenylcarbosilane with high ceramic yield.* Journal of Materials Chemistry C, 2014. **2**(6): p. 1057-1067.
129. Toyoda, R., S. Kitaoka, and Y. Sugahara, *Modification of perhydropolysilazane with aluminum hydride: Preparation of poly (aluminasilazane) s and their conversion into Si–Al–N–C ceramics.* Journal of the European Ceramic Society, 2008. **28**(1): p. 271-277.
130. Wagner, O., M. Jansen, and H.P. Baldus, *N(B(NMe_2)$_2$)(Si(NMe_2)$_3$)(Ti(NMe_2)$_3$), [N(Si(NMe_2)$_3$)(Ti(NMe_2)$_2$)]$_2$ und N($SiMe_3$)(Si(NMe_2)$_3$)(Ti(NMe_2)$_3$)-Synthese und Charakterisierung neuer molekularer Einkomponentenvorläufer für nitridische und carbonitridische Keramiken.* Zeitschrift für anorganische und allgemeine Chemie, 1994. **620**(2): p. 366-370.
131. Hapke, J. and G. Ziegler, *Synthesis and pyrolysis of liquid organometallic precursors for advanced Si-Ti-C-N composites.* Advanced Materials, 1995. **7**(4): p. 380-384.
132. Yuan, J., et al., *Single-source-precursor synthesis of hafnium-containing ultrahigh-temperature ceramic nanocomposites (UHTC-NCs).* Inorganic chemistry, 2014. **53**(19): p. 10443-10455.

133. Glatz, G., et al., *Copper-Containing SiCN Precursor Ceramics (Cu@SiCN) as Selective Hydrocarbon Oxidation Catalysts Using Air as an Oxidant.* Chemistry-A European Journal, 2010. **16**(14): p. 4231-4238.
134. Zaheer, M., G. Motz, and R. Kempe, *The generation of palladium silicide nanoalloy particles in a SiCN matrix and their catalytic applications.* Journal of Materials Chemistry, 2011. **21**(46): p. 18825-18831.
135. Kamperman, M., et al., *Integrating structure control over multiple length scales in porous high temperature ceramics with functional platinum nanoparticles.* Nano letters, 2009. **9**(7): p. 2756-2762.
136. Schmalz, T., et al., *Catalytic formation of carbon phases in metal modified, porous polymer derived SiCN ceramics.* Carbon, 2011. **49**(9): p. 3065-3072.
137. Studart, A.R., et al., *Processing routes to macroporous ceramics: a review.* Journal of the American Ceramic Society, 2006. **89**(6): p. 1771-1789.
138. Zhu, X., D. Jiang, and S. Tan, *Preparation of silicon carbide reticulated porous ceramics.* Materials Science and Engineering: A, 2002. **323**(1): p. 232-238.
139. Fitzgerald, T., V. Michaud, and A. Mortensen, *Processing of microcellular SiC foams.* Journal of materials science, 1995. **30**(4): p. 1037-1045.
140. Colombo, P. and E. Bernardo, *Macro-and micro-cellular porous ceramics from preceramic polymers.* Composites Science and Technology, 2003. **63**(16): p. 2353-2359.
141. Zeschky, J., et al., *Preceramic polymer derived cellular ceramics.* Composites Science and Technology, 2003. **63**(16): p. 2361-2370.
142. Colombo, P., E. Bernardo, and L. Biasetto, *Novel microcellular ceramics from a silicone resin.* Journal of the American Ceramic Society, 2004. **87**(1): p. 152-154.
143. Yoon, T.-H., et al., *Fabrication of SiC-based ceramic microstructures from preceramic polymers with sacrificial templates and lithographic techniques-A review.* Journal of the Ceramic Society of Japan, 2006. **114**(1330): p. 473-479.
144. Dismukes, J.P., et al., *Chemical synthesis of microporous nonoxide ceramics from polysilazanes.* Chemistry of materials, 1997. **9**(3): p. 699-706.
145. Bradley, J.S., et al., *High surface area silicon imidonitrides: A new class of microporous solid base.* Advanced Materials, 1998. **10**(12): p. 938-942.
146. Kaskel, S., D. Farrusseng, and K. Schlichte, *Synthesis of mesoporous silicon imido nitride with high surface area and narrow pore size distribution.* Chemical Communications, 2000(24): p. 2481-2482.
147. Kaskel, S., K. Schlichte, and B. Zibrowius, *Pore size engineering of mesoporous silicon nitride materials.* Physical Chemistry Chemical Physics, 2002. **4**(9): p. 1675-1681.
148. Parmentier, J., et al., *Formation of SiC via carbothermal reduction of a carbon-containing mesoporous MCM-48 silica phase: a new route to produce high surface area SiC.* Ceramics International, 2002. **28**(1): p. 1-7.
149. Shi, Y., et al., *Highly ordered mesoporous silicon carbide ceramics with large surface areas and high stability.* Advanced Functional Materials, 2006. **16**(4): p. 561-567.
150. Majoulet, O., et al., *Preparation, characterization, and surface modification of periodic mesoporous silicon–aluminum–carbon–nitrogen frameworks.* Chemistry of Materials, 2013. **25**(20): p. 3957-3970.
151. Sung, I.K., et al., *Tailored Macroporous SiCN and SiC Structures for High-Temperature Fuel Reforming.* Advanced Functional Materials, 2005. **15**(8): p. 1336-1342.
152. Schmalz, T., et al., *Analysis of polyethylene-particle filled SiCN precursor and the resulting porous ceramics with emphasis on using micro computed tomography.* Journal of the Ceramic Society of Japan, 2011. **119**(1390): p. 477-482.
153. Biasetto, L., et al., *Gas permeability of microcellular ceramic foams.* Industrial & engineering chemistry research, 2007. **46**(10): p. 3366-3372.
154. Kim, Y.-W., C. Wang, and C.B. Park, *Processing of porous silicon oxycarbide ceramics from extruded blends of polysiloxane and polymer microbead.* Journal of the Ceramic Society of Japan, 2007. **115**(1343): p. 419-424.
155. Malenfant, P.R., et al., *Self-assembly of an organic–inorganic block copolymer for nano-ordered ceramics.* Nature nanotechnology, 2007. **2**(1): p. 43-46.
156. Yu, Y., et al., *Synthesis of nanostructured silicon carbide at ultralow temperature using self-assembled polymer micelles as a precursor.* Journal of Materials Chemistry, 2011. **21**(44): p. 17619-17622.
157. Nghiem, Q.D., D. Kim, and D.P. Kim, *Synthesis of inorganic–organic diblock copolymers as a precursor of ordered mesoporous SiCN ceramic.* Advanced Materials, 2007. **19**(17): p. 2351-2354.

158. Nghiem, Q.D. and D.-P. Kim, *Direct preparation of high surface area mesoporous SiC-based ceramic by pyrolysis of a self-assembled polycarbosilane-block-polystyrene diblock copolymer.* Chemistry of Materials, 2008. **20**(11): p. 3735-3739.
159. Ewert, J.-K., et al., *Meso-Structuring of SiCN Ceramics by Polystyrene Templates.* Nanomaterials, 2015. **5**(2): p. 425-435.
160. Leutwyler, W.K., S.L. Bürgi, and H. Burgl, *Semiconductor clusters, nanocrystals, and quantum dots.* Science, 1996. **271**(5251): p. 933-937.
161. Brus, L., *Luminescence of silicon materials: chains, sheets, nanocrystals, nanowires, microcrystals, and porous silicon.* The Journal of Physical Chemistry, 1994. **98**(14): p. 3575-3581.
162. Krans, J., et al., *The signature of conductance quantization in metallic point contacts.* Nature, 1995. **375**(6534): p. 767-769.
163. Likharev, K.K., *Correlated discrete transfer of single electrons in ultrasmall tunnel junctions.* IBM Journal of Research and Development, 1988. **32**(1): p. 144-158.
164. Markovich, G., et al., *Architectonic quantum dot solids.* Accounts of Chemical Research, 1999. **32**(5): p. 415-423.
165. Ross, C.A., *Patterned magnetic recording media.* Annual Review of Materials Research, 2001. **31**(1): p. 203-235.
166. Kingon, A.I., J.-P. Maria, and S. Streiffer, *Alternative dielectrics to silicon dioxide for memory and logic devices.* Nature, 2000. **406**(6799): p. 1032-1038.
167. Chen, J., B.J. Wiley, and Y. Xia, *One-dimensional nanostructures of metals: large-scale synthesis and some potential applications.* Langmuir, 2007. **23**(8): p. 4120-4129.
168. Xia, Y., et al., *One-dimensional nanostructures: synthesis, characterization, and applications.* Advanced materials, 2003. **15**(5): p. 353-389.
169. Wan, C., G. Guo, and Q. Zhang, *SiOC ceramic nanotubes of ultrahigh surface area.* Materials Letters, 2008. **62**(17): p. 2776-2778.
170. Wang, H., et al., *Inorganic polymer-derived tubular SiC arrays from sacrificial alumina templates.* Applied Physics Letters, 2005. **86**(17): p. 173104.
171. Cai, K., Q. Lei, and L. Zhang, *Ultra long SiC/SiO_2 core-shell nanocables from organic precursor.* Journal of nanoscience and nanotechnology, 2005. **5**(11): p. 1925-1928.
172. Xu, Y., et al., *Microstructure and Microchemistry of Polymer-Derived Crystalline SiC Fibers.* Journal of the American Ceramic Society, 1993. **76**(12): p. 3034-3040.
173. Jayaseelan, D.D., et al., *In situ formation of silicon carbide nanofibers on cordierite substrates.* Journal of the American Ceramic Society, 2007. **90**(5): p. 1603-1606.
174. Martin, C.R., *Membrane-based synthesis of nanomaterials.* Chemistry of Materials, 1996. **8**(8): p. 1739-1746.
175. Jou, S. and C.K. Hsu, *Preparation of carbon nanotubes from vacuum pyrolysis of polycarbosilane.* Materials Science and Engineering: B, 2004. **106**(3): p. 275-281.
176. Haberecht, J., et al., *Carbon nanostructures on high-temperature ceramics–a novel composite material and its functionalization.* Catalysis today, 2005. **102**: p. 40-44.
177. Yang, W., et al., *Synthesis of ceramic nanocomposite powders with in situ formation of nanowires/nanobelts.* Journal of the American Ceramic Society, 2008. **91**(4): p. 1312-1315.
178. Cai, K., A. Zhang, and J. Yin, *Ultra thin and ultra long SiC/SiO_2 nanocables from catalytic pyrolysis of poly(dimethylsiloxane).* Nanotechnology, 2007. **18**(48): p. 485601.
179. Cai, K., et al., *Ultra long SiCN nanowires and SiCN/SiO_2 nanocables: synthesis, characterization, and electrical property.* Journal of nanoscience and nanotechnology, 2008. **8**(12): p. 6338-6343.
180. Sing, K.S., *Reporting physisorption data for gas/solid systems with special reference to the determination of surface area and porosity (Recommendations 1984).* Pure and applied chemistry, 1985. **57**(4): p. 603-619.
181. De Boer, J., et al., *Studies on pore systems in catalysts: VII. Description of the pore dimensions of carbon blacks by the t method.* Journal of Catalysis, 1965. **4**(6): p. 649-653.
182. Widjaja, Y. and C.B. Musgrave, *Atomic layer deposition of hafnium oxide: A detailed reaction mechanism from first principles.* Journal of Chemical Physics, 2002. **117**(5): p. 1931-1934.
183. Seyferth, D., G.H. Wiseman, and C. Prud'homme, *A liquid silazane precursor to silicon nitride.* Journal of the American Ceramic Society, 1983. **66**(1): p. 13-14.

184. Qi, G.-J., et al., *Preparation of three-dimensional silica fiber reinforced silicon nitride composites using perhydropolysilazane as precursor.* Materials Letters, 2005. **59**(26): p. 3256-3258.
185. Yamano, A. and H. Kozuka, *Perhydropolysilazane-derived silica–polymethylmethacrylate hybrid thin films highly doped with spiropyran: Effects of polymethylmethacrylate on the hardness, chemical durability and photochromic properties.* Thin Solid Films, 2011. **519**(6): p. 1772-1779.
186. Prager, L., et al., *Conversion of perhydropolysilazane into a SiO_x network triggered by vacuum ultraviolet irradiation: Access to flexible, transparent barrier coatings.* Chemistry-A European Journal, 2007. **13**(30): p. 8522-8529.
187. Hu, L., et al., *Perhydropolysilazane derived silica coating protecting Kapton from atomic oxygen attack.* Thin Solid Films, 2011. **520**(3): p. 1063-1068.
188. Li, K., et al., *Tetrakis (dimethylamido) hafnium adsorption and reaction on hydrogen terminated Si (100) surfaces.* The Journal of Physical Chemistry C, 2010. **114**(33): p. 14061-14075.
189. Beaudoin, M. and S.L. Scott, *Spontaneous Evolution of Silica-Supported Ti Amide Fragments to Imine and Imido Complexes.* Organometallics, 2001. **20**(2): p. 237-239.
190. Cundari, T.R. and J.M. Morse, *Decomposition pathways for a model TiN chemical vapor deposition precursor.* Chemistry of materials, 1996. **8**(1): p. 189-196.
191. Weiller, B.H., *Chemical vapor deposition of TiN from tetrakis (dimethylamido) titanium and ammonia: kinetics and mechanistic studies of the gas-phase chemistry.* Journal of the American Chemical Society, 1996. **118**(21): p. 4975-4983.
192. Rodríguez-Reyes, J.C.F. and A.V. Teplyakov, *Surface transamination reaction for tetrakis (dimethylamido) titanium with NH_X-terminated Si(100) surfaces.* The Journal of Physical Chemistry C, 2007. **111**(44): p. 16498-16505.
193. Killampalli, A.S., P.F. Ma, and J.R. Engstrom, *The reaction of tetrakis(dimethylamido)titanium with self-assembled alkyltrichlorosilane monolayers possessing-OH,-NH_2, and-CH_3 terminal groups.* Journal of the American Chemical Society, 2005. **127**(17): p. 6300-6310.
194. Wen, Q., et al., *Single-source-precursor synthesis of dense SiC/HfC_xN_{1-x}-based ultrahigh-temperature ceramic nanocomposites.* Nanoscale, 2014. **6**(22): p. 13678-13689.
195. Funayama, O., et al., *Conversion mechanism of perhydropolysilazane into silicon nitride-based ceramics.* Journal of materials science, 1994. **29**(18): p. 4883-4888.
196. Funayama, O., et al., *Synthesis of a polyborosilazane and its conversion into inorganic compounds.* Journal of the American Ceramic Society, 1993. **76**(3): p. 717-723.
197. Baxter, D.V., et al., *Molecular routes to metal Carbides, nitrides, and oxides. 2. Studies of the ammonolysis of metal Dialkylamides and Hexamethyldisilylamides.* Chemistry of materials, 1996. **8**(6): p. 1222-1228.
198. Li, J., et al., *Synthesis of nanocrystalline Zr_3N_4 and Hf_3N_4 powders from metal dialkylamides.* Zeitschrift für anorganische und allgemeine Chemie, 2005. **631**(8): p. 1449-1455.
199. Liu, Q., et al., *Investigation of the pyrolytic conversion of poly (silylenemethylene) to silicon carbide.* Chemistry of materials, 1999. **11**(8): p. 2038-2048.
200. Li, R., et al., *Synthesis and polymer-to-ceramic conversion of tailorable copolysilazanes.* Journal of Applied Polymer Science, 2011. **122**(2): p. 1286-1292.
201. Seitz, J., et al., *Structural investigations of Si/C/N-ceramics from polysilazane precursors by nuclear magnetic resonance.* Journal of the European Ceramic Society, 1996. **16**(8): p. 885-891.
202. Mizutani, U., *Hume-Rothery rules for structurally complex alloy phases*. 2010: CRC Press.
203. Córdoba, J.M., et al., *Monophasic Nanostructured Powders of Niobium, Tantalum, and Hafnium Carbonitrides Synthesized by a Mechanically Induced Self-Propagating Reaction.* Journal of the American Ceramic Society, 2007. **90**(2): p. 381-387.
204. Blanchard, C.R. and S.T. Schwab, *X-ray Diffraction Analysis of the Pyrolytic Conversion of Perhydropolysilazane into Silicon Nitride.* Journal of the American Ceramic Society, 1994. **77**(7): p. 1729-1739.
205. Messier, D.R., F. Riley, and R. Brook, *The α/β silicon nitride phase transformation.* Journal of Materials Science, 1978. **13**(6): p. 1199-1205.
206. Park, J.Y. and C.H. Kim, *The α-to β-Si_3N_4 transformation in the presence of liquid silicon.* Journal of materials science, 1988. **23**(9): p. 3049-3054.
207. Fujimori, H., et al., *^{29}Si MASNMR Spin-Lattice Relaxation Study of α-, β-, and Amorphous Silicon Nitride.* Journal of the American Ceramic Society, 2000. **83**(9): p. 2251-2254.

208. Ionescu, E., et al., *Phase separation of a hafnium alkoxide-modified polysilazane upon polymer-to-ceramic transformation—A case study.* Journal of the European Ceramic Society, 2012. **32**(9): p. 1873-1881.
209. Carduner, K.R., et al., *Determination of phase composition of silicon nitride powders by silicon-29 magic angle spinning nuclear magnetic resonance spectroscopy.* Analytical Chemistry, 1987. **59**(23): p. 2794-2797.
210. Carduner, K.R., et al., *Silicon-29 magic angle spinning nuclear magnetic resonance spectroscopy of sintered silicon nitride ceramics.* Chemistry of Materials, 1989. **1**(3): p. 302-307.
211. Ionescu, E., et al., *Polymer-Derived Silicon Oxycarbide/Hafnia Ceramic Nanocomposites. Part II: Stability Toward Decomposition and Microstructure Evolution at $T \gg 1000\,^{\circ}C$.* Journal of the American Ceramic Society, 2010. **93**(6): p. 1783-1789.
212. Colombo, P., et al. *Preparation of Ceramic Composites by Active-Ftller-Controlled-Polymer-Pyrolysis*. in *MRS Proceedings*. 1994. Cambridge Univ Press.
213. Batha, H. and E. Whitney, *Kinetics and mechanism of the thermal decomposition of Si_3N_4.* Journal of the American Ceramic Society, 1973. **56**(7): p. 365-369.
214. Fedorova, E., et al., *Synthesis and structure of oxovanadium(IV) complexes [$VO(Acac)_2$] and [VO(Sal: L-alanine)(H_2O)]*. Crystallography Reports, 2005. **50**(2): p. 224-229.
215. Nenashev, R., et al., *Thermal decomposition of vanadyl acetylacetonate.* Inorganic Materials, 2015. **51**(9): p. 891-896.
216. Jeragh, B.J. and A. El-Dissouky, *Synthesis and spectroscopic studies of oxovanadium (IV) and dichlorovanadium (IV) complexes of pX-phenyl-2-picolylketones.* Transition metal chemistry, 2004. **29**(6): p. 579-585.
217. Kaur, S., et al., *Single-source-precursor synthesis of novel V_8C_7/SiC (O)-based ceramic nanocomposites.* Journal of the European Ceramic Society, 2016.
218. Jarrais, B., A.R. Silva, and C. Freire, *Anchoring of Vanadyl Acetylacetonate onto Amine-Functionalised Activated Carbons: Catalytic Activity in the Epoxidation of an Allylic Alcohol.* European journal of inorganic chemistry, 2005. **2005**(22): p. 4582-4589.
219. Van Der Voort, P., M.G. White, and E.F. Vansant, *Thermal decomposition of $VO(acac)_2$ deposited on the surfaces of silica and alumina.* Langmuir, 1998. **14**(1): p. 106-112.
220. Wada, N., et al., *Raman and IR absorption spectroscopic studies on α, β, and amorphous Si_3N_4.* Journal of Non-Crystalline Solids, 1981. **43**(1): p. 7-15.
221. Choi, D., G.E. Blomgren, and P.N. Kumta, *Fast and reversible surface redox reaction in nanocrystalline vanadium nitride supercapacitors.* Advanced Materials, 2006. **18**(9): p. 1178-1182.
222. Lee, J.M., et al., *Effect of silver co-sputtering on amorphous V_2O_5 thin-films for microbatteries.* Journal of power sources, 2004. **136**(1): p. 122-131.
223. Fateh, N., et al., *The beneficial effect of high-temperature oxidation on the tribological behaviour of V and VN coatings.* Tribology letters, 2007. **28**(1): p. 1-7.
224. Fateh, N., et al., *Influence of high-temperature oxide formation on the tribological behaviour of TiN and VN coatings.* Wear, 2007. **262**(9): p. 1152-1158.
225. Wang, X., et al., *XRD and Raman study of vanadium oxide thin films deposited on fused silica substrates by RF magnetron sputtering.* Applied Surface Science, 2001. **177**(1): p. 8-14.
226. Ghimbeu, C.M., et al., *Vanadium nitride/carbon nanotube nanocomposites as electrodes for supercapacitors.* Journal of Materials Chemistry, 2011. **21**(35): p. 13268-13275.
227. Forberg, D., et al., *The synthesis of pyrroles via acceptorless dehydrogenative condensation of secondary alcohols and 1, 2-amino alcohols mediated by a robust and reusable catalyst based on nanometer-sized iridium particles.* Catalysis Science & Technology, 2014. **4**(12): p. 4188-4192.
228. Konegger, T., L.F. Williams, and R.K. Bordia, *Planar, Polysilazane-Derived Porous Ceramic Supports for Membrane and Catalysis Applications.* Journal of the American Ceramic Society, 2015. **98**(10): p. 3047-3053.
229. Vakifahmetoglu, C., et al., *Highly porous macro-and micro-cellular ceramics from a polysilazane precursor.* Ceramics International, 2009. **35**(8): p. 3281-3290.
230. Ionescu, E., H.-J. Kleebe, and R. Riedel, *Silicon-containing polymer-derived ceramic nanocomposites (PDC-NCs): preparative approaches and properties.* Chemical Society Reviews, 2012. **41**(15): p. 5032-5052.
231. Yamaoka, H., T. Ishikawa, and K. Kumagawa, *Excellent heat resistance of Si-Zr-CO fibre.* Journal of materials science, 1999. **34**(6): p. 1333-1339.

232. Hojamberdiev, M., et al., *Single-source-precursor synthesis of soft magnetic Fe_3Si-and Fe_5Si_3-containing SiOC ceramic nanocomposites.* Journal of the European Ceramic Society, 2013. **33**(13): p. 2465-2472.
233. Zhou, C., et al., *Synthesis and high-temperature evolution of single-phase amorphous Si–Hf–N ceramics.* Journal of the European Ceramic Society, 2015. **35**(7): p. 2007-2015.
234. Wriedt, H., N. Gokcen, and R. Nafziger, *The Fe-N (iron-nitrogen) system.* Bulletin of Alloy Phase Diagrams, 1987. **8**(4): p. 355-377.
235. Jiang, L. and L. Gao, *Fabrication and characterization of Fe_3O_4/CNTs and Fe_2N/CNTs composites.* Journal of electroceramics, 2006. **17**(1): p. 87-90.
236. Han, Y., et al., *Low-temperature approach to synthesize iron nitride from amorphous iron.* Inorganic chemistry, 2008. **47**(4): p. 1261-1263.
237. Choi, J. and E.G. Gillan, *Solvothermal metal azide decomposition routes to nanocrystalline metastable nickel, iron, and manganese nitrides.* Inorganic chemistry, 2009. **48**(10): p. 4470-4477.
238. Feyen, M., et al., *High-Temperature Stable, Iron-Based Core–Shell Catalysts for Ammonia Decomposition.* Chemistry–A European Journal, 2011. **17**(2): p. 598-605.
239. Kopcewicz, M., et al., *Phase transformations in nitrogen-implanted-a-iron.* Journal of applied physics, 1992. **71**(9): p. 4217-4226.
240. Kardonina, N., A. Yurovskikh, and A. Kolpakov, *Transformations in the Fe–N system.* Metal Science and Heat Treatment, 2011. **52**(9): p. 457-467.
241. Alexander, A.-M., J. Hargreaves, and C. Mitchell, *The denitridation of nitrides of iron, cobalt and rhenium under hydrogen.* Topics in Catalysis, 2013. **56**(18-20): p. 1963-1969.
242. Siddiqi, S. and A. Hendry, *The influence of iron on the preparation of silicon nitride from silica.* Journal of materials science, 1985. **20**(9): p. 3230-3238.
243. Durham, S.J., K. Shanker, and R.A. Drew, *Carbothermal synthesis of silicon nitride: effect of reaction conditions.* Journal of the American Ceramic Society, 1991. **74**(1): p. 31-37.
244. Wagner, R. and W. Ellis, *Vapor-liquid-solid mechanism of single crystal growth.* Applied Physics Letters, 1964. **4**(5): p. 89-90.
245. Huang, J., et al., *Fe-catalyzed growth of one-dimensional α-Si_3N_4 nanostructures and their cathodoluminescence properties.* Scientific reports, 2013. **3**: p. 3504.
246. Cui, J., et al., *Direct Synthesis of α-Silicon Nitride Nanowires from Silicon Monoxide on Alumina.* 2015.
247. Sunkara, M.K., et al., *Bulk synthesis of a-Si_xN_yH and a-Si_xO_y straight and coiled nanowires.* Journal of Materials Chemistry, 2004. **14**(4): p. 590-594.
248. Luongo, J., *Infrared Characterization of α-and β-Crystalline Silicon Nitride.* Journal of the Electrochemical Society, 1983. **130**(7): p. 1560-1562.
249. Ahmad, M., et al., *Ordered arrays of high-quality single-crystalline α-Si_3N_4 nanowires: synthesis, properties and applications.* Journal of Crystal Growth, 2009. **311**(20): p. 4486-4490.
250. Lin, L. and Y. He, *Synthesis and optical property of ultra-long alpha-Si_3N_4 nanowires under superatmospheric pressure conditions.* CrystEngComm, 2012. **14**(9): p. 3250-3256.
251. Tellez, G.M., *Infrared characterization of SiN films on Si for high speed electronics applications*. 2004, DTIC Document.
252. Vakifahmetoglu, C., et al., *Growth of One-Dimensional Nanostructures in Porous Polymer-Derived Ceramics by Catalyst-Assisted Pyrolysis. Part II: Cobalt Catalyst.* Journal of the American Ceramic Society, 2010. **93**(11): p. 3709-3719.
253. Segatelli, M.G., A.T.N. Pires, and I.V.P. Yoshida, *Synthesis and structural characterization of carbon-rich SiC_xO_y derived from a Ni-containing hybrid polymer.* Journal of the European Ceramic Society, 2008. **28**(11): p. 2247-2257.
254. Tsai, S., et al., *A novel technique for the formation of carbon-encapsulated metal nanoparticles on silicon.* Carbon, 2000. **38**(5): p. 781-785.
255. Kolel-Veetil, M.K., et al., *Carbon Nanocapsule-Mediated Formation of Ferromagnetic Fe_5Si_3 Nanoparticles.* The Journal of Physical Chemistry C, 2009. **113**(33): p. 14663-14671.
256. Francis, A., et al., *Crystallization behavior and controlling mechanism of iron-containing Si-C-N ceramics.* Inorganic chemistry, 2009. **48**(21): p. 10078-10083.
257. Wei, Q., et al., *Interfacial SiC formation in polysiloxane-derived Si–O–C ceramics.* Materials Chemistry and Physics, 2002. **73**(2): p. 281-289.
258. Zhang, S.C. and W.R. Cannon, *Preparation of silicon nitride from silica.* Journal of the American Ceramic Society, 1984. **67**(10): p. 691-695.

259. Li, J. and R. Riedel, *Carbothermal Reaction of Silica–Phenol Resin Hybrid Gels to Produce Silicon Nitride/Silicon Carbide Nanocomposite Powders.* Journal of the American Ceramic Society, 2007. **90**(12): p. 3786-3792.
260. Weimer, A.W., et al., *Mechanism and Kinetics of the Carbothermal Nitridation Synthesis of α-Silicon Nitride.* Journal of the American Ceramic Society, 1997. **80**(11): p. 2853-2863.
261. Neuer, G., *3.3. 1.7 Fe-based alloys*, in *Thermal Conductivity of Pure Metals and Alloys*. 1991, Springer. p. 220-229.
262. Kubaschewski, O., *Iron-Binary phase diagrams*. 2013: Springer Science & Business Media.
263. Clemens, P., et al., *Thermal Conductivity of Pure Metals and Alloys.* Subvol c, 1991.
264. Zhu, S., et al., *In Situ Growth of β-SiC Nanowires in Porous SiC Ceramics.* Journal of the American Ceramic Society, 2005. **88**(9): p. 2619-2621.
265. Krawiec, P., et al., *Oxide Foams for the Synthesis of High-Surface-Area Vanadium Nitride Catalysts.* Advanced Materials, 2006. **18**(4): p. 505-508.
266. Kwon, H., S. Choi, and L. Thompson, *Vanadium Nitride Catalysts: Synthesis and Evaluation forn-Butane Dehydrogenation.* Journal of Catalysis, 1999. **184**(1): p. 236-246.

ACKNOWLEDGEMENTS

This Ph.D. Thesis represents the research work performed at Technisch University Darmstadt from November 2012 to January 2017. I would like to give my sincere appreciation to the people who gave me help during the Ph.D. Work:

Firstly, many thanks to the supervisor, Prof. Dr. Ralf Riedel, who kindly gave the opportunity to study and work in his research group and on this interesting topic. Thanks for his supervision and mentorship during my research, for his help and support during my entire Ph.D. study period. In addition, I would like to thank him for his caring, patience and enthusiasm, and for his kind-hearted financial support in my difficult time. He is a very humorous professor and always helps his students with great eagerness not only on the research work but also on their daily life.

Secondly, thanks to my sub-supervisor PD Dr. Emmanuel Ionescu. He is very gentle and gives a lot of suggestions and guidance to my Ph.D. work when I run into obstacles on my research. He also helps me to modify the thesis and teaches me the knowledge of writing strategy. I appreciate that you have contributed a great deal to my PhD work.

Thanks to Prof. Dr. Zhaoju Yu for guiding me since I was a master student and recommended me to Prof. Riedel, for inspiring and supporting me during my Master and Ph.D. work. I feel very lucky being one of the students you supervised.

Thanks to Prof. Ikuhara Yuichi and Dr. Ishikawa Ryo for the high-resolution STEM measurement and warm reception during my visit at University of Tokyo.

Thanks to Prof. Dr. H.-J. Kleebe for the high-resolution TEM measurement.

Thanks to Dr. Yeping Xu for solid state CP/MAS NMR measurements.

Thanks to Dipl.-Ing. Claudia Fasel for the TG/MS measurements and a lot of technical supports in daily lab work.

Thanks to Dipl. Jean-Christophe Jaud for the assistance in XRD measurements.

Thanks to Dr. Koji Morita for the SPS experiments and the kind help during my visit at National Institute of Material Science (NIMS).

Thanks to Elmar Kersting for thesupport in UV-Visible absorption and photoluminescence measurements.

Thanks to M. Sc. Fangtong Xie and M. Sc. Benjamin Juretzka for translating the abstract of the thesis into German version.

Thanks to all the DF members who gave me lots of suggestions and help on my researches: Apl. Prof. Dr. Norbert Nicoloso, PD Dr. Leonore Wiehl, Dr. Gabriela Mera, Dr. Magdalena Joanna Graczyk-Zajac, Dr. Isabel Gonzalo de Juan, Dr. Jan Kaspar, Dr. Pradeep Vallachira Sasikumar, Dr. Sarabjeet Kaur, Dr. Cristina Schitco,

M. Sc. Dragoljub Vrankovic, M. Sc. Christina Stabler, Dipl.-Ing. Felix Rosenburg, Dipl.-Ing. Dario De Carolis, Dipl.-Ing. Alexander Uhl, Dipl.-Ing. Amon Klausmann.

Many thanks to Dr. Yan Gao, Dr. Jia Yuan, Dr. Wenjie Li, M. Eng. Qingbo Wen, M. Eng. Xingmin Liu, M. Sc. Nan Chai and M. Sc. Yao Feng for bring me my a lot of joy in the daily life. All of you are my best friends in Germany.

I would also like to acknowledge the China Scholarship Council (CSC) for my PhD career. Thanks for giving me the opportunity to study abroad as well as the financial support.

Thanks to the DAAD-JSPS (Deutscher Akademischer Austausch Dienst - Japan Society for the Promotion of Science) international project for supporting me to visit University of Tokyo and National Institute for Materials Science (NIMS).

Finally, a deep thanks to my parents. They supported me unconditionally all these years and always encouraged me with their best wishes and expectations.

CURRICULUM VITAE

PERSONAL INFORMATION

Name: Cong ZHOU

Date of Birth: June/18/1987

Citizenship: Chinese

Address: Jovanka-Bontschits-Strasse 2, L1|08 416

64287 Darmstadt, Germany

Tel: +49 6151 16-21627; Fax: +49 6151 16-21623

E-mail: zhou@materials.tu-darmstadt.de

Educational background

- **2012-2016, Ph.D. of Engineering.**

Disperse Feststoffe, Materials Science, Department of Materials and Earth Sciences, Technische Universität Darmstadt (TUD), Germany.

Thesis: Ternary Si-Metal-N Ceramics: Single-Source-Precursor Synthesis, Nanostructure and Properties Characterization.

Advisor: Prof. Dr. Ralf Riedel.

- **2009-2012, Master of Science in Polymer Physic and Chemistry.**

College of Materials, Key Laboratory of High Performance Ceramic Fibers, Ministry of Education, Xiamen University, Fujian, P.R.China.

Thesis: Modification of Polysilazanes and their Application in the Preparation of SiCN-based Ceramic Composites.

Advisor: Prof. Dr. Zhaoju Yu.

- **2005-2009, Bachelor of Engineering in Materials Science and Engineering.**

Department of Materials Science & Engineering, College of Materials, Xiamen University, Fujian, P.R.China.

Thesis: The modification and preparation of melamine-formaldehyde resin.

Advisor: Prof. Lei Li.

RESEARCH EXPERIENCES

- 2012-2016, Doctoral program/ Research Assistant, Technical University of Darmstadt.
  - Designed and synthesized metal-modified single-source precursors with systematically varied compositions and structures by the chemical modification of polysilazane with metallic compounds.
  - Investigated their compositions, nanostructures and crystallization behaviors upon heat treatment.

- Prepared mesoporous ceramics with high specific surface area using polystyrene as a self-sacrificial template in a one-pot synthesis. Studied the formation mechanism and stability of the mesoporous structures.
- Prepared a ceramic paper decorated with a huge amount of one-dimensional nanowires with high aspect ratios. Studied the formation mechanism of nanowires, optimized the experimental conditions.

● Nov.-Dec./2014 and Sep.-Oct./2015, Research Assistant, University of Tokyo and NIMS (National Institute for Materials Science), within the frame of a JSPS-DAAD funded exchange program for young researchers.

- Investigated the nanostructures of Si-Metal-N ceramics via the high-resolution spherical aberration STEM in University of Tokyo.
- Prepared dense Si-M-N (M=metal) ceramics using SPS (spark plasma sintering) in NIMS.

● 2009-2012, Research Assistant, Xiamen University.

- Synthesized the Si-based polymer precursors with tailored compositions and structures, such as polycarbosilane and polysilazane.
- Prepared the SiBCN precursor by modifying the polysilazane with different boron-containing compounds. Studied the structural evolution of polymer-derived ceramics depending on their unique composition and the high-temperature stability of obtained SiBCN ceramics.
- Prepared iron-modified silicon nitride ceramics via the PDC route, investigated the structural evolution and the magnetic property of the ceramics.

AWARDS & HONORS

- 2012, China Council Scholarship for student study abroad.
- 2011, The Second Prize Scholarship of Xiamen University
- 2010, The First Prize Scholarship of Xiamen University
- 2009, The Second Prize Scholarship of Xiamen University

PUBLICATIONS

1. **Cong Zhou**, Xiang Gao, Yeping Xu, Gerd Buntkowsky, Yuichi, Ikuhara, Ralf Riedel, Emanuel Ionescu. "Synthesis and high-temperature evolution of single-phase amorphous Si-Hf-N ceramics". *Journal of the European Ceramic Society*, 2015, 7(35): 2007-2015.
2. **Cong Zhou**, Claudia Fasel, Ryo Ishikawa, Markus Gallei, Yuichi Ikuhara, Hans-Joachim Kleebe, Ralf Riedel, Emanuel Ionescu. **"**One-pot synthesis of a C/SiFeN(O)-based ceramic paper with *in situ* generated hierarchical micro/nano-morphology"**.** *Journal of the European Ceramic Society*, received: http://dx.doi.org/10.1016/j.jeurceramsoc.2017.03.007.

3. Zhaoju Yu, Le Yang, Hao Min, Pei Zhang, **Cong Zhou** and Ralf Riedel. “Single-source-precursor synthesis of high temperature stable SiC/C/Fe nanocomposites from a processable hyperbranched polyferrocenylcarbosilane with high ceramic yield”. *Journal of Materials Chemistry C*, 2014,2: 1057-1067.
4. **Cong Zhou**, Hao Min, Le Yang, Meiyu Chen, Qingbo Wen and Zhaoju Yu. “Dimethylaminoborane-modified copolysilazane as a novel precursor for high-temperature resistant SiBCN ceramics”. *Journal of the European Ceramic Society*, 2014, 34(15): 3579-3589.
5. **Cong Zhou**, Le Yang, Hao Geng, Qiang Zheng, Hao Min, Zhaoju Yu and Haiping Xia. “Preparation of Si-C-N-Fe magnetic ceramic derived from iron-modified polysilazane”. *Ceramics International*, 2012, 38(8): 6815-6822.
6. Zhaoju Yu, **Cong Zhou**, Ran Li, Le Yang, Siwei Li and Haiping Xia. "Synthesis and ceramic conversion of a novel processible polyboronsilazane precursor to SiBCN ceramic". *Ceramics International*, 2012, 6(38): 4635-4643.
7. Zhaoju Yu, Le Yang, Junying Zhan, **Cong Zhou**, Hao Min, Qiang Zheng and Haiping Xia."Preparation, cross-lingking and ceramization of AHPCS/Cp_2ZrCl_2 hybrid precursors for SiC/ZrC/C composites". *Journal of the European Ceramic Society*, 2012, 32: 1291-1298.
8. Zhaoju Yu, Junying Zhan, **Cong Zhou**, Le Yang, Ran Li and Haiping Xia. "Synthesis and characterization of SiC(Ti) ceramics derived from a hybrid precursor of titanium-containing polycarbosilane". *Journal of Inorganic and Organometallic Polymers and Materials*, 2011, 21: 412-420.
9. Ran Li, **Cong Zhou**, Le Yang, Siwei Li, Junying Zhan, Zhaoju Yu and Haiping Xia. "Synthesis and polymer-to-ceramic conversion of tailorable copolysilazanes". *Journal of Applied Polymer Science*, 2011, 122: 1286-1292.
10. Zhaoju Yu, Ran Li, Junying Zhan, **Cong Zhou**, Le Yang, Guomei He and Haiping Xia. "Synthesis and characterization of a propargyl-substituted polycarbosilane with high ceramic yield". *Journal of Applied Polymer Science*, 2011, 121: 3400-3406.
11. Zhaoju Yu, Junying Zhan, Muhe Huang, Ran Li, **Cong Zhou**, Guomei He and Haiping Xia. "Preparation of a hyperbranched polycarbosilane precursor to SiC ceramics following an efficient room-temperature cross-linking process". *Journal of Materials Science*, 2010, 45: 6151-6158.
12. Zhaoju Yu, Yunhui Fang, Muhe Huang, Ran Li, Junying Zhan, **Cong Zhou**, Guomei He and Haiping Xia. "Preparation of a liquid boron-modified polycarbosilane and its ceramic conversion to dense SiC ceramics". *Polymers for advanced technologies*, 2010, 22: 2409-2414.
13. Ran Li, Junying Zhan, **Cong Zhou**, Zhaoju Yu, Matai Ding and Haiping Xia. "Synthesis and pyrolytic conversion of a hyperbranched liquid polycarbosilane with low oxygen content". *Journal of Functional Materials*, 2010, 12: 2166-2168.
14. Zhaoju Yu, **Cong Zhou**, Ran Li, Junying Zhan, Guomei-He and Matai Ding. "Development of hyperbranched branched polycarbosilanes". *Journal of Functional Materials*, 2010, 7: 1113-1116.

CONFERENCE CONTRIBUTIONS

1. Cong Zhou, X. Gao, Y. Xu, A. Kuwabara, G. Buntkowsky, Y. Ikuhara, R. Riedel and E. Ionescu. Phase separation and crystallization of amorphous SiHfN: evidence for substitutional and interstitial doping of Hf in β-Si_3N_4 in "MES 2014: International Conference Materials Science Engineering", Darmstadt, Germany, Sep. 23-25, 2014.
2. Cong Zhou, R. Ishikawa, Y. Ikuhara, R. Riedel and E. Ionescu. Si-Fe-N(O) based ceramic paper with in-situ generated hierarchical micro/nano-morphology in "IWAC07, the seventh International Workshop on Advanced Ceramics", Limoges, France, Sep. 26-28, 2016.

Eidesstattliche Erklärung

M. Sc. Cong Zhou
Jovanka-Bontschits-Strasse 2
64287 Darmstadt

Eidesstattliche Erklärung

Hiermit erkläre ich an Eides statt, dass ich die vorliegende Dissertation selbstständig und nur mit den angegebenen Hilfsmitteln angefertigt habe. Von mir wurde weder an der Technischen Universität Darmstadt noch einer anderen Hochschule ein Promotionsversuch unternommen.

Darmstadt, den 10. April. 2017

Cong Zhou